

Winter 2014

Multiscale modeling study of methanol oxidation by ion-modified MDH enzymes

Purnima Kharidehal
Louisiana Tech University

Follow this and additional works at: <https://digitalcommons.latech.edu/dissertations>

 Part of the [Other Chemical Engineering Commons](#)

Recommended Citation

Kharidehal, Purnima, "" (2014). *Dissertation*. 275.
<https://digitalcommons.latech.edu/dissertations/275>

This Dissertation is brought to you for free and open access by the Graduate School at Louisiana Tech Digital Commons. It has been accepted for inclusion in Doctoral Dissertations by an authorized administrator of Louisiana Tech Digital Commons. For more information, please contact digitalcommons@latech.edu.

**MULTISCALE MODELING STUDY OF METHANOL
OXIDATION BY ION-MODIFIED MDH ENZYMES**

by

Purnima Kharidehal, B.Tech, M.S.

A Dissertation Presented in Partial Fulfillment
of the Requirements of the Degree
Doctor of Philosophy

COLLEGE OF ENGINEERING AND SCIENCE
LOUISIANA TECH UNIVERSITY

March 2014

UMI Number: 3662203

All rights reserved

INFORMATION TO ALL USERS

The quality of this reproduction is dependent upon the quality of the copy submitted.

In the unlikely event that the author did not send a complete manuscript and there are missing pages, these will be noted. Also, if material had to be removed, a note will indicate the deletion.



UMI 3662203

Published by ProQuest LLC 2015. Copyright in the Dissertation held by the Author.

Microform Edition © ProQuest LLC.

All rights reserved. This work is protected against unauthorized copying under Title 17, United States Code.



ProQuest LLC
789 East Eisenhower Parkway
P.O. Box 1346
Ann Arbor, MI 48106-1346

LOUISIANA TECH UNIVERSITY

THE GRADUATE SCHOOL

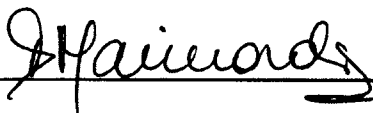
SEPTEMBER 16, 2013

Date

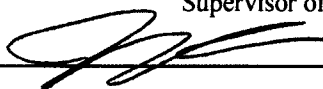
We hereby recommend that the dissertation prepared under our supervision by
Purnima Kharidehal, B.Tech, M.S.

entitled Multiscale Modeling Study of Methanol Oxidation by
Ion-Modified MDH Enzymes

be accepted in partial fulfillment of the requirements for the Degree of
Doctor of Philosophy in Engineering



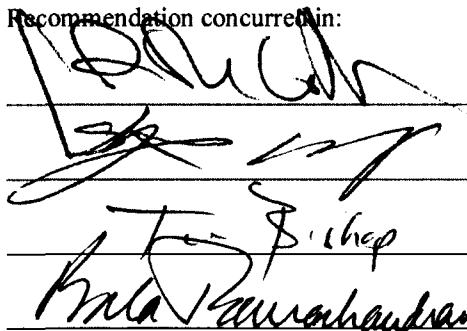
Supervisor of Dissertation Research



Head of Department
ENGINEERING

Department

Recommendation concurred in:



Advisory Committee

Approved:



Director of Graduate Studies



Dean of the College

Approved:



Dean of the Graduate School

ABSTRACT


Enzymes have been considered as molecular electrocatalysts due to their extraordinary characteristics such as their ability to accelerate reactions enormously, to operate under physiological conditions, and to produce fewer by-products during a catalytic reaction. However, enzyme based fuel cells have been reported to have power output and stability limitations, which are restricting the use of this kind of fuel cell to small electronic devices. Methanol dehydrogenase (MDH) is one such enzyme, which oxidizes methanol and other primary alcohols to their corresponding aldehydes. The active site of MDH contains a divalent cation (Ca^{2+}), a co-factor pyrrolo-quinoline quinone (PQQ), several amino acids, and water molecules. Ca^{2+} ion holds the PQQ in place, and also acts as a Lewis acid, contributing to the methanol electro-oxidation reaction mechanism by this enzyme. Among the proposed mechanisms for methanol oxidation by MDH in the literature, the Hydride Transfer (H-T) mechanism seems, to the best of our knowledge, to be the preferred one under normal conditions. Work reported in the literature shows that the binding of the substrate and the reaction energy barrier for substrate oxidation by dehydrogenase enzymes is influenced by the nature of the ion in the enzyme active site. Thus, understanding the role of the ion in the active site of MDH as well as the methanol oxidation mechanism may have major impacts on alternative power sources research as they could lead to the development of new bio-inspired synthetic catalysts that could impact the use of methanol as fuel.

In this study, the binding energy of methanol to the active site models of ion-modified MDH is determined and the effect of ion on methanol oxidation is investigated. It has been observed that the binding affinity of methanol and free energy barrier for the rate determining step of the H-T mechanism decreases as the ionic size increases. This shows that replacing the naturally occurring ion (Ca^{2+}) with Mg^{2+} , Sr^{2+} and Ba^{2+} affect the methanol oxidation process and binding of methanol to the active site of MDH. Density Functional Theory (DFT) calculations at BLYP/DNP theory level are performed using the DMOL³ module of the Materials Studio software to evaluate binding energies and investigate the reaction pathways. Furthermore, polarization curves corresponding to the electrochemical methanol oxidation in biofuel cell anodic chambers when MDH enzymes are used as the anode catalysts are obtained using the kinetic Monte Carlo approach. Microscopic reaction rates, obtained from free energy barriers evaluated using DFT and Transition State Theory (TST), are provided as inputs in a kinetic Monte Carlo (kMC) program (CARLOS 4.1) to model the oxidation process at macroscopic level. These simulations gave a better understanding of the catalytic methanol oxidation mechanism by MDH, helping evaluate the enzyme catalysis and their dependence on various factors like the nature of the ion in the MDH active site.

APPROVAL FOR SCHOLARLY DISSEMINATION

The author grants to the Prescott Memorial Library of Louisiana Tech University the right to reproduce, by appropriate methods, upon request, any or all portions of this Dissertation. It is understood that "proper request" consists of the agreement, on the part of the requesting party, that said reproduction is for his personal use and that subsequent reproduction will not occur without written approval of the author of this Dissertation. Further, any portions of the Dissertation used in books, papers, and other works must be appropriately referenced to this Dissertation.

Finally, the author of this Dissertation reserves the right to publish freely, in the literature, at any time, any or all portions of this Dissertation.

Author 

Date 12/03/2013

DEDICATION

To my dear parents, Jayalakshmi and Ramana Rao Kharidehal,
and my sister, Swati.

TABLE OF CONTENTS

ABSTRACT.....	iii
DEDICATION.....	vi
LIST OF TABLES.....	xi
LIST OF FIGURES	xii
ACKNOWLEDGMENTS	xvi
CHAPTER 1 INTRODUCTION	1
1.1 Enzymes as Catalysts.....	1
1.2 Applications of Enzymatic Catalysts.....	2
1.3 Role of Ion in Enzymes	4
1.4 Methanol as Fuel.....	5
1.5 Methanol Dehydrogenase Enzyme as Anode	7
1.6 Brief Overview of Following Chapters	8
CHAPTER 2 RESEARCH OBJECTIVE AND LITERATURE REVIEW.....	10
2.1 Research Objective	10
2.2 Methanol Dehydrogenase (MDH) Enzyme	11
2.2.1 Active Site.....	11
2.2.2 Methanol Oxidation Mechanisms.....	12
2.2.2.1 Addition-Elimination Mechanism.....	13
2.2.2.2 Hydride-Transfer Mechanisms.....	13
2.2.3 The Role of the Ion in MDH.....	17
CHAPTER 3 MULTI-SCALE SIMULATION TECHNIQUES.....	22

3.1	Multi-Scale Modeling Approach	22
3.2	Enzyme Kinetics.....	26
3.3	Enzyme Modeling and Computational Details.....	28
3.4	Quantum Chemistry	30
3.4.1	Density Functional Theory	33
3.4.2	Basis Sets	35
3.4.3	Transition State Calculations using DMol3.....	36
3.5	Molecular Mechanics.....	38
3.6	Kinetic Monte Carlo	40
CHAPTER 4 MDH ACTIVE SITE MODELS		43
4.1	Enzyme Cluster Models.....	43
4.1.1	MDH Active Site Models	44
4.2	Computational Details	45
4.3	Binding of Methanol to the MDH Active Site Models.....	47
4.3.1	Model I.....	47
4.3.2	Models II and III.....	48
4.4	Structural Effects of Ion-Modified MDH	52
4.4.1	Ion Coordination.....	53
4.4.2	Ion Coordination and Binding Energy.....	57
4.4.3	Substrate Coordination.....	58
4.5	Conclusions.....	60
CHAPTER 5 METHANOL OXIDATION OF ION-MODIFIED MDH ENZYMES		62
5.1	Enzyme Model and Computational Details.....	63
5.2	Local Minima Conformations.....	65
5.3	Structural Effects of Ion in the MDH Active Site	71

5.4	H-T Mechanism by Mg^{2+} -MDH and Sr^{2+} -MDH	73
5.4.1	Step 1: $PQQ \rightarrow PQQH^-$	73
5.4.2	Step 2: $PQQH^- \rightarrow PQQH$	75
5.4.3	Step 3: $PQQH \rightarrow PQQH^*$	76
5.4.4	Step 4: $PQQH^* \rightarrow PQQH_2$	78
5.4.5	Alternate Step: $PQQH \rightarrow PQQH_2$	81
5.5	Conclusions.....	83
CHAPTER 6 KINETIC MONTE CARLO STUDIES		85
6.1	Introduction.....	85
6.2	Input Parameters	86
6.2.1	Lattice Preparation	86
6.2.2	Microscopic Rates.....	88
6.3	Model 1	89
6.3.1	Model Validation	89
6.3.2	Effect of Obstacle Concentration.....	91
6.3.3	Effect of Ion	93
6.4	Model 2.....	95
6.4.1	Lattice Model.....	95
6.4.2	Effect of Substrate Concentration.....	97
6.4.3	Effect of the Ion	101
6.4.4	I-V Curves.....	103
6.5	Conclusions.....	106
CHAPTER 7 CONCLUSIONS AND FUTURE WORK.....		108
7.1	Conclusions.....	108
7.1.1	Binding and Orientation of Methanol.....	108

7.1.2	Methanol Oxidation by Ion-Modified MDH Enzymes.....	110
7.1.3	Enzyme Catalysis by kMC Simulations	112
7.2	Future Work.....	114
REFERENCES		118

LIST OF TABLES

Table 4.1: Ions coordination to the O6, N6 and O5 of PQQ (bond distances in Å) obtained from BLYP/DNP calculations for MDH active site models (Model I, II and III).....	54
Table 6.1: Input microscopic rates of the ion-modified MDH enzymes for the kMC calculations.....	89
Table 6.2: Slope and R ² value for the rate of product formation plots for increasing number of substrate molecules.....	99

LIST OF FIGURES

Figure 2.1 : (a) Structure of MDH obtained from protein data bank (call no 1w6s) (b) α -subunit of MDH enzyme (c) Active site of MDH with PQQ at the center, radially surrounded by 13 amino acid residues.....	12
Figure 2.2 : Addition-Elimination Methanol Oxidation Mechanism.....	13
Figure 2.3 : Hydride Trasfer Methanol Oxidation Mechanisms (a) Classical Hydride-Transfer (b) Alternate Hydride Transfer.....	14
Figure 2.4 : Two-Step Hydride Transfer Mechanism.....	17
Figure 3.1 : Flowchart showing the multiscale modeling approach	23
Figure 3.2 : Schematic free energy profile for uncatalyzed and enzyme catalyzed chemical reactions [76].....	27
Figure 4.1 : MDH Model I consisting of three amino acids (Glu, Asn, Asp) considered for investigation of Binding Energy of Methanol	46
Figure 4.2 : MDH Models II (9AA) and III (13AA) to investigate the Binding Energy of Methanol (Constrained Molecules are shown in Orange).....	46
Figure 4.3 : Methanol binding energies calculated at BLYP/DNP theory level for the 3AA active site models of Mg ²⁺ (\square),Ca ²⁺ (Δ), Sr ²⁺ (\diamond) and Ba ²⁺ (\circ) containing MDH.	48
Figure 4.4 : Methanol binding energies calculated at the BLYP/DNP theory level for the 3AA (Model I), 9AA (Model II) and 13AA (Model III) active site models of Mg ²⁺ (\square), Ca ²⁺ (Δ), Sr ²⁺ (\diamond) and Ba ²⁺ (\circ) containing MDH.....	50
Figure 4.5 : The nature of the ion in the active site of MDH modifies the binding and orientation of methanol	53
Figure 4.6 : Bond lengths (Ion – O6, N6 and O5) obtained from BLYP/DNP calculations for Mg ²⁺ (\square),Ca ²⁺ (Δ), Sr ²⁺ (\diamond) and Ba ²⁺ (\circ) containing MDH active site models (Model I, II and III).	56

Figure 4.7 : Binding Energy versus Average values of Ion Coordination lengths (Ion – O6, N6 and O5) obtained from BLYP/DNP calculations for Mg^{2+} (\square), Ca^{2+} (Δ), Sr^{2+} (\diamond) and Ba^{2+} (\circ) containing MDH active site models (Model I, II and III)	57
Figure 4.8 : Bond distance H17-C5 compared for Ion-Modified MDH active site models (Model I, II and III). (Top left Figure insert shows the distance in consideration).....	58
Figure 4.9 : Bond distance H16-O14 compared for Ion-Modified MDH active site models (Model I, II and III). (Top left Figure insert shows the distance in consideration).....	59
Figure 5.1 : Active site model selected for Mg^{2+} -MDH	63
Figure 5.2 : Best three minima configurations for the reactant, intermediates, and product of the Hydride-Transfer methanol oxidation mechanism by for Mg^{2+} -MDH obtained at the BLYP/DNP theory level.....	67
Figure 5.3 : Structural variations in selected bond lengths for the three best conformations shown in Figure 5.2	68
Figure 5.4 : Bond length differences obtained from BLYP/DNP calculations for Ion-Modified MDH active site models.....	71
Figure 5.5 : Optimized structures obtained at BLYP/DNP theory level involved in Step 1 of the H-T mechanism for Mg^{2+} -MDH (Top Set) and Sr^{2+} - MDH (Bottom Set).....	73
Figure 5.6 : TS1 bond distances comparison between the Mg^{2+} -MDH, Ca^{2+} -MDH and Sr^{2+} -MDH active site models at BLYP/DNP theory level	74
Figure 5.7 : Optimized structures obtained at BLYP/DNP theory level involved in Step 2 of the H-T mechanism for Mg^{2+} -MDH (Top Set) and Sr^{2+} - MDH (Bottom Set).....	75
Figure 5.8 : TS2 bond distances comparison between the Mg^{2+} -MDH, Ca^{2+} -MDH and Sr^{2+} -MDH active site models at BLYP/DNP theory level.....	76
Figure 5.9 : Optimized structures obtained at BLYP/DNP theory level involved in Step 3 of the H-T mechanism for Mg^{2+} -MDH (Top Set) and Sr^{2+} - MDH (Bottom Set).....	77
Figure 5.10: TS3 bond distances comparison between the Mg^{2+} -MDH, Ca^{2+} -MDH.....	78
Figure 5.11: Optimized structures obtained at BLYP/DNP theory level involved in Step 4 of the H-T mechanism for Mg^{2+} -MDH (Top Set) and Sr^{2+} - MDH (Bottom Set).....	79

- Figure 5.12: TS4 bond distances comparison between the Mg^{2+} -MDH, Ca^{2+} -MDH and Sr^{2+} -MDH active site models at BLYP/DNP theory level..... 79
- Figure 5.13: Potential Energy Surface corresponding to the four step H-T mechanism by MDH active site models with Mg^{2+} (solid), Sr^{2+} (dashed) and Ca^{2+} (dotted). Reactant-relative free energies calculated at the BLYP/DNP theory level are in kcal/mol. Free energies corresponding to the Ca^{2+} -MDH case were taken from Idupulapati *et al.*[49, 62]. 81
- Figure 5.14: Optimized structures obtained at BLYP/DNP theory level involved in Alt-Step of the H-T mechanism for Mg^{2+} -MDH and Sr^{2+} - MDH. 82
- Figure 5.15: Alt-TS bond distances comparison between the Mg^{2+} -MDH, Ca^{2+} -MDH and Sr^{2+} -MDH active site models at BLYP/DNP theory level..... 82
- Figure 6.1 : Ca^{2+} -containing Methanol Dehydrogenase enzyme (**top-right**) and view of its binding pocket and active site (**left**). Projection of active site components (green) and other residues (black) according to their center of masses (and plotted as dots), onto a 2-D lattice representing the biocatalytic surface (**right**). Red and blue dots represent substrate (methanol) and product (formaldehyde) molecules [116] 88
- Figure 6.2 : A typical progress curve for enzyme [144]..... 90
- Figure 6.3 : Concentration profiles of substrate and product molecules formed for MDH active site models with respect to time..... 91
- Figure 6.4 : Lattice configurations showing the Substrate (Methanol molecules) as red dots and Product (Formaldehyde Molecules) as blue dots with increasing Obstacle concentration (other amino acids in MDH) for Ca^{2+} -containing MDH, and the green dots represent the active site cluster. 92
- Figure 6.5 : Final lattice configurations showing the effect of ion in the product formation.Green dots represent the active site amino acids and the red and blue dots represent substrate (methanol) and product (formaldehyde) molecules 94
- Figure 6.6 : Plot showing product (Formaldehyde Molecules) formation for the different ions MDH active site models with respect to time. 95
- Figure 6.7 : Two-dimensional enzyme structures of MDH as lattice in CARLOS program as input structure (a) X axis negated (b) Y axis negated (c) Z axis negated..... 96
- Figure 6.8 : Three dimensional enzyme structure from the PDB database (left). Y-axis neglected two-dimensional enzyme structure of MDH as input structure (right) 96

Figure 6.9 : Rate of Product Formation with respect to increasing substrate concentration.....	98
Figure 6.10: Plot showing the reaction rate with respect to number of substrate molecules	100
Figure 6.11: Rate of Product Formation for Ion modified MDH enzymes with respect to increasing substrate concentration	101
Figure 6.12: Lattice configurations showing the effect of ion in the product formation. Green dots represent the active site amino acids and the red and blue dots represent substrate (methanol) and product (formaldehyde) molecules	102
Figure 6.13: I-V curves obtained for both the models and compared to experimental obtained curve	104
Figure 6.14: I-V curves obtained for Ion-Modified MDH enzymes.....	105

ACKNOWLEDGMENTS

I would like to take this opportunity to thank my advisor Dr. Daniela Mainardi for her support, patience and insightful advice throughout my research work and my academic pursuit at Louisiana Tech University. I would also like to especially acknowledge Dr. Ramachandran for his guidance and support throughout my study. I thank my committee members Dr. Decoster, Dr. Wang, and Dr. Bishop for their advisory role in my research. Also, I want to acknowledge Dr. Jansen for his input and suggestions and for providing the CARLOS 4.1 program to run the kMC simulations.

I would like to express my appreciation to my past group members Dr. Phani Dathar, the late Dr. Nagesh Idupulapati, Dr. Ancy Kunjumon, Dr. Katie Bearden, King Ki, and my current group members, especially Fernando Soto, for their valuable input and help.

I'd like to specially thank my grandparents and parents for their blessings and best wishes. Most of all, I would like to thank Aditya for his invaluable support and faith that helped me through the tough times and kept me moving forward towards accomplishing this goal. A special thank you goes out to my sister, my uncle, my family, my roommates, and friends for their unyielding support while I have been working towards my degree.

CHAPTER 1

INTRODUCTION

1.1 Enzymes as Catalysts

With increasing challenges in creating alternative fuels, reducing harmful by-products in manufacturing, and preventing pollution, highly active and efficient catalysts could be a viable way to meet these challenges [1]. Biocatalysts, in particular enzymes, have gained much attention because they are sustainable, accelerate reactions enormously (with turnover frequencies of a few to thousands per second), and are endowed with high stereo-, regio- and chemoselectivity [2, 3]. Enzymes, also known as Nature's catalysts, have been used in various fields such as biomedical, chemical, pharmaceuticals, food industry, textile manufacturing, and in the production of over 500 commercial goods [4, 5] because they operate most effectively under physiological conditions at low concentrations and produce few by-products during the catalytic reaction, unlike conventional catalysts.

Enzyme based fuel cells generate power outputs in the range of micro- to milliwatts, compared to the kilowatt outputs from conventional, i.e. chemical fuel cells. It is observed that enzyme based fuel cells operate close to ambient temperature and pressure [6], as most proteins are unstable above ambient temperatures and at high ranges of pH. For instance, enzymatic fuel cells operate between pH 4-8 and around

temperatures 20-50° C, unlike the conventional Pt-catalyzed PEM fuel cells that are typically operated at 80-100° C and need either strong acidic or alkaline electrolytes to operate [6]. These features have led to the use of enzymes as bio-electro catalysts [7].

1.2 Applications of Enzymatic Catalysts

Since the 1960s, with advancements in technology and science, enzymes have been used as catalysts for biofuel cells applications. In 1964, the first enzyme-based biofuel cell was reported, which used glucose as the fuel and glucose oxidase (GOx) as the anodic catalyst [8]. Since then different enzymes have been used as catalysts for various special applications such as implantable devices, sensors, drug delivery, micro-chips, and portable power supplies [9]. In order to monitor some specific pollutants, enzymes such as horse radish peroxidase (HRP) and acetylcholinesterase have been used on environmental sensors [10, 11], and a biofuel cell using sugar as the fuel and enzymes as catalysts was developed by Sony to power a Walkman® [12].

In general, redox enzymes such as alcohol dehydrogenase (ADH), aldehyde dehydrogenase, glucose oxidase (GOx), glutaminase, horse radish peroxidase (HRP), catalase, xanthine oxidase, choline oxidase, urease, and lactate oxidase are considered as bio-electrodes [13]. For example, most oxidases have been used as catalysts for biosensors; however, their response depends upon the oxygen concentration and this limitation causes trouble in designing the sensors for undiluted blood, microbiological media, and other biological samples with unstable oxygen concentration [14]. To overcome this problem of oxygen dependency, nicotinamide adenine dinucleotide (NAD)-dependent dehydrogenases have been considered. Because large overpotentials are required for the direct electrochemical oxidation of NAD, the practical application of

these biosensors is restricted [15]. There have been reports that hydrogenases can replace Pt electrodes and they suggested that the active sites of hydrogenases are comparable in activity to Pt [6, 7].

Alcohol dehydrogenases (ADH) produced by several aerobic bacteria and containing pyrroloquinoline quinone (PQQ) as the prosthetic group have achieved significant consideration as bio-electrocatalysts, replacing oxidases and NAD dependent catalysts. PQQ enzymes transfer electrons from the substrate to an electron acceptor other than oxygen, and additionally, they can transfer electrons directly to the solid or electrode surface making it more efficient as an electrocatalyst [14]. Also, in PQQ-enzymes, the cofactor (PQQ) is bound to the enzyme and avoids the addition or generation of a separate cofactor, like NAD or FAD; hence, it has gained much more importance as biofuel cell catalysts [14, 16].

The first methanol-oxidizing fuel cell was reported by Hill and coworkers [17], which used a PQQ containing bacterial methanol dehydrogenase as an anodic catalyst with phezanine ethosulfate mediating electron transfer to a Pt electrode, which had an ability to catalyze the oxidation of methanol. For this fuel cell, an open current voltage of 0.3 V was recorded with a maximum current density of 0.5 mA/cm² based on the anode dimensions [17]. Later in 1986, a better fuel cell was reported by Yue and Lowther [18] that used two immobilized enzymes in the anode compartment, namely, methanol dehydrogenase and formate dehydrogenase to catalyze the complete oxidation of methanol to CO₂. This device recorded a current density of 0.02 mA/cm² at a cell voltage of 65 mV [18]. To state another example, electrochemical glucose test strips that use gene engineered apo-PQQ-dependent glucose dehydrogenase (PQQ-GDH) have been

employed successfully. However, it was found that the PQQ cofactor bonds very weakly and that these were single-use test strips. Later, using redox mediators, which help transfer the electrons from the enzyme active region to the electrode, have increased the efficiency of such systems [14, 19]. Another study by Lapénaité *et al.* reported that PQQ-dependent glucose dehydrogenase can be employed in the design of enzymatic biosensors that can be used for detection of heavy metals such as Cd^{2+} and Pb^{2+} ions in a concentration range of 15×10^{-5} mol/l [20].

1.3 Role of Ion in Enzymes

Metal ions, like Zn^{2+} , Mg^{2+} , Ca^{2+} , Mn^{2+} , Fe^{2+} , Cu^{2+} , Mo^{4+} (or Mo^{6+}), and W^{4+} (or W^{6+}) act as cofactors for many enzymes activity and more than half of all enzymes associate with a particular metal to function [21-23]. Some of the most complex and important processes in nature, such as photosynthesis and water oxidation, are catalyzed by metalloproteins [24]. Metal ion sites in proteins play multiple roles; they either act as cofactors in catalytic and regulatory processes or contribute towards the structural stability of the system [23].

In order to explore the mechanism action of metalloenzymes thoroughly, understanding the chemical consequences of metal binding is important because the metal ion nature and the surrounding environment determine the reactants and mechanism for the specific enzyme. They act as catalysts by binding the reactants (substrates) to the metal center(s) and the amino acid groups coordinated to the ion. These binding sites are generally centered in a hydrophilic ligand shell which is surrounded by a hydrophobic region [4, 22, 25].

Metal ions assist in binding the substrate to the enzyme active site in such a way that a transition state of the catalytic reaction is readily formed, and a product is easily released. They participate in catalysis by either changing their oxidation states or acting as electrophiles, often with positive charges greater than one, and they have a large ionic volume so that they can accommodate many ligands. They also offer steric selection between metals and substrates [4, 22, 25].

The most prominent alkaline earth metals in biological systems are magnesium and calcium [26]. Magnesium mostly increases the enzyme's functionalities or stabilizes their structures. For example, to stabilize structures, such as cell membranes, proteins, DNA, and RNA, magnesium is used. Moreover, it also plays a catalytic role in many enzymes, for instance, assists hydrolysis and condensation reactions to occur at biologically relevant pH values that normally occur at extremes levels of pH. Calcium is generally involved in the structural stability of the enzyme. It has also been seen in nucleic acids complexation, carbohydrate metabolism, and other biological activities such as nerve impulse transmission and muscle contraction that these two metal ions (Mg^{2+} and Ca^{2+}) play an important role [27].

1.4 Methanol as Fuel

Methanol is considered as one of the best fuels in conventional direct fuel cells, which can be used as power supplies for small-scale portable applications. Methanol is the simplest alcohol, and industrially, an important chemical. It has unique properties and characteristics such as being produced from both fossil and renewable sources, thus, making it useful as an alternative fuel. It is easy to store and transport as it is a liquid at ambient temperature [28]. Methanol releases six protons and electrons per molecule

during its oxidation. These features have made methanol a suitable fuel for fuel cells, and Direct methanol fuel cells (DMFC) have been shown to work at low and intermediate temperatures (up to 150° C) [29].

Biological systems (microbes or enzymes) furnish an attractive strategy for power generation. Unlike conventional fuel cells which utilize sources like oil, bio fuel cells use renewable resources such as alcohols, sugars and fats as fuels to generate electric energy. Bio-processes chemically transform carbon-based molecules (ethanol or methanol) that not only produce energetic fuel but also mitigate problems associated with the accumulation of greenhouse gases in the environment [28, 30, 31].

Numerous fuels such as sugars and aliphatic alcohols have been employed in enzymatic fuel cells. Glucose is the most common and intuitive fuel for enzymatic biofuel cells due to its high abundance in nature and essential role in human metabolism. Fructose, which is a structural isomer of glucose and disaccharides as lactose, and cellobiose are the other sugars that have been employed as fuels. Aliphatic alcohols such as methanol, ethanol, and glycerol are the other common fuels that have been used in enzymatic fuel cells. These three alcohols can be regarded as renewable fuels that can be produced from biomass, and their use in enzymatic fuel cells could offer new types of miniature portable power sources [30, 31].

Mostly, the fuels for biofuel cells are chosen based on their application. For implantable applications, glucose and lactase are considered logical choices because these fuels are found in the blood stream. For portable electronic devices, glycerol, ethanol and methanol seem more practical as they are liquid fuels that are easy to package and can be produced in large quantities [30, 31].

1.5 Methanol Dehydrogenase Enzyme as Anode

A PQQ dependent enzyme Methanol Dehydrogenase (MDH), which contains a calcium ion in its active site with an ability to oxidize methanol, has been used as an anode for a methanol-fed bio-catalytic fuel cell. Zhang *et al.* [32] developed this bio-fuel cell by immobilizing MDH on N,N,N',N'-tetramethyl-p-phenylenediamine (TPMD)-functionalized carbon paste electrode and used it as the anode catalyst. This fuel cell produced a continuous power output of 0.25 milli-Watts/cm² for 2 weeks of continuous operation. It is believed that the major factor that affects this fuel cell performance by limiting the power output (expected (theoretical) output is 100 milli-Watts/cm²) is the TPMD mediator, which is responsible for the electron transfer to the electrode from the fuel oxidation by the enzyme [32]. This is believed to be due to the oligomerization (the forming of polymers by the combination of relatively few monomers) of the mediator molecules, which seem to increase when stimulating the fuel cell operating conditions by subjecting the mediator to repeated charge-discharge cycles. This oligomerization causes the fuel cell performance to be deteriorated due to reduced electron transfer from the enzyme to the electrode [32]. Additionally, the accumulation of the by-product formaldehyde (formic acid) as result of methanol (fuel) oxidation by MDH in the bio-fuel cell may slowly reduce the activity of the enzyme, thus limiting the overall power output [32].

Various studies on methanol oxidation by ion-modified MDH have shown that the activation energy for the oxidation reaction is altered. For example, it was reported that when the naturally occurring Ca²⁺ ion was replaced with Ba²⁺ and Sr²⁺, respectively, in the MDH active site, the activation energy for the reaction decreased in both the Sr²⁺-

and Ba²⁺-modified MDH [33, 34]. To state another example, when the Ca²⁺ ion in the Glucose Dehydrogenase (GDH) active site was replaced with Ba²⁺, the energy barrier corresponding to the rate-determining step for the glucose oxidation mechanism was lower in the case of Ba²⁺-GDH than that for Ca²⁺-containing GDH [35]. One more instance where Membrane-integrated quinoprotein glucose dehydrogenase (mGDH) was reconstituted in the presence of Mg²⁺ instead of Ca²⁺ ion showed that Mg²⁺ anchors PQQ to mGDH protein better and activates the cofactor for glucose oxidation [36]. Therefore, these numerous studies indicate that the type of metal ion in the enzyme active site indeed alters the energetics of the oxidation process.

Enzymatic fuel cells using ion-modified MDH might offer potentially attractive power sources for some small electronic devices. Thus, for its better usefulness, it is important to increase the stability/activity of this enzyme; hence, understanding the mechanism behind enzyme catalysis and the role of the ion in the enzyme catalysis becomes significant. With the use of effective computational chemistry tools such as Density Functional Theory and other multi-scale modeling approaches in general, the functioning of enzymes has been unfolded substantially. Thus, such multi-scale studies can help design bio-inspired synthetic catalysts.

1.6 Brief Overview of Following Chapters

In Chapter 2, the objective of this research and a detailed description of the MDH enzyme are given and the present state of art knowledge about the effect of the ion in MDH is discussed. Chapter 3 will provide the theory behind the computational methods used in this multiscale modeling study.

In Chapter 4, investigations on the binding of methanol to the ion-modified MDH active site models and the effect of the amino acid's nature in the active site models of MDH are presented. In Chapter 5, investigations of methanol oxidation mechanisms by Mg^{2+} and Sr^{2+} containing MDH are presented.

In Chapter 6, a kinetic Monte Carlo (kMC) approach for modeling methanol oxidation by ion-modified MDH is discussed. Finally, conclusions and suggestions for future work are presented in Chapter 7.

CHAPTER 2

RESEARCH OBJECTIVE AND LITERATURE REVIEW

2.1 Research Objective

As reviewed in Chapter 1, enzymes have been considered as biomolecular electro-catalysts due to their extraordinary characteristics. However, enzymatic fuel cells have been reported to have power output and stability limitations, which are restricting the use of this kind of fuel cell. Methanol dehydrogenase (MDH) is one such enzyme, which oxidizes methanol and other primary alcohols to their corresponding aldehydes [37]. The active site of MDH contains a divalent cation (Ca^{2+}), a co-factor pyrrolo-quinoline quinone (PQQ), several amino acids and water molecules. It is believed that the Ca^{2+} ion holds the PQQ in place, and also acts as a Lewis acid, contributing to the methanol electro-oxidation reaction mechanism by this enzyme.

It was also demonstrated that the divalent cation has a central role in the proton abstraction catalysis, and replacing Ca^{2+} with other divalent ion could modify the methanol oxidation pathways. Work reported in the literature shows that the binding of the substrate and the reaction energy barrier for substrate oxidation by dehydrogenase enzymes is influenced by the nature of the ion in the enzyme active site [34, 38, 39].

The first main goal of this study is to carry out a detailed theoretical investigation of substrate binding and oxidation mechanism on ion-modified active site models of MDH enzyme. This goal is accomplished by first building representative models of the

active site of MDH to investigate the binding and coordination of the substrate molecule, and then the effect of the ion in the binding of methanol to these active site cluster models of MDH is carried out by replacing the Ca^{2+} ion in the active with Mg^{2+} , Sr^{2+} and Ba^{2+} ions. Furthermore, the oxidation mechanisms proposed for Ca^{2+} -MDH (naturally occurring MDH) are investigated for these ion-modified enzymes, and the reaction barriers are evaluated. The next major goal is to study the enzyme kinetics at a macroscopic level and to calculate the I-V Curves using a kinetic Monte Carlo (kMC) approach. In order to accomplish this objective, an approach to model enzyme kinetics at the macroscopic level using a kinetic Monte Carlo code has been established. Understanding the role of the ion in the active site of MDH, as well as the methanol oxidation mechanism, may have major impacts on alternative power sources research which could lead to the development of new bio-inspired synthetic catalysts that could impact the use of methanol as fuel.

2.2 Methanol Dehydrogenase (MDH) Enzyme

2.2.1 Active Site

The structure of MDH from *Methylobacterium extorquens* and from *Methylophilus W3A1* has been characterized using X-ray crystallographic methods [40-46]. It has been determined that the enzyme has an $\alpha_2\beta_2$ tetrameric structure with two subunits (Figure 2.1a), α (66 kDa) and β (8.5 kDa), and that each heavy unit (α) has an active site that contains a pyrrolo-quinoline quinone (PQQ) molecule that acts as the MDH co-factor, a Ca^{2+} ion, several amino acids, and water molecules (Figure 2.1b). The subunit α is surrounded by the smaller unit, β . It has been found that the Ca^{2+} ion in the MDH active site is electrostatically bonded to the nitrogen atom (N6) of the PQQ

molecule, the C5 quinone oxygen (O5), the oxygen (O10) of the carboxylate of PQQ, the oxygen atoms (O12 and O13) of the carboxylate of Glu-177, and the oxygen atoms O11 and O14 of Asn-261 and Asp-303, respectively (Figure 2.1c) [40-43]. From X-ray studies, distances from the Ca^{2+} ion to the N6, O5, and O10 atoms of PQQ are in the 2.32–2.47, 2.25–2.77, and 2.30–2.44 Å range, respectively [40]. Apart from holding the PQQ in place, the calcium ion is also believed to act as a Lewis acid, contributing to the methanol electro-oxidation reaction mechanism by this enzyme [40-46].

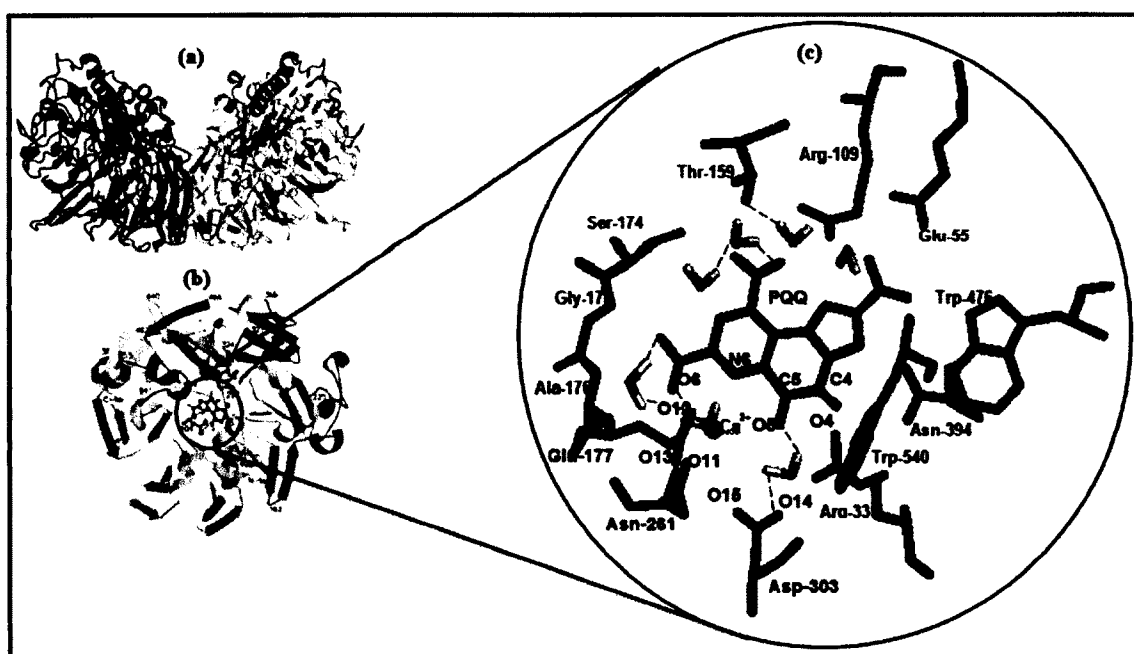


Figure 2.1: (a) Structure of MDH obtained from protein data bank (call no 1w6s) (b) α -subunit of MDH enzyme (c) Active site of MDH with PQQ at the center, radially surrounded by 13 amino acid residues.

2.2.2 Methanol Oxidation Mechanisms

In the literature, four possible mechanisms for the oxidation of methanol by the naturally occurring Ca^{2+} -containing MDH have been proposed, the three-step Addition-

Elimination [47], the Hydride Transfer (“four-step” and “alternate”) [47], the addition-elimination-protonation [48], and the modified hydride transfer [49].

2.2.2.1 Addition-Elimination Mechanism

In the first step of the addition-elimination (A-E) mechanism (Figure 2.2), a proton (H16) is abstracted from methanol and added to Asp-303; thus, a hemiketal intermediate is formed with C5 of PQQ. The second step involves the H16 proton elimination from the active site base (Asp-303) and its transfer to the oxygen O5 of PQQ. In the final step, a second proton (H17) transfer occurs from the remains of the methanol molecule to the O4 of PQQ, resulting in the formation of formaldehyde [47].

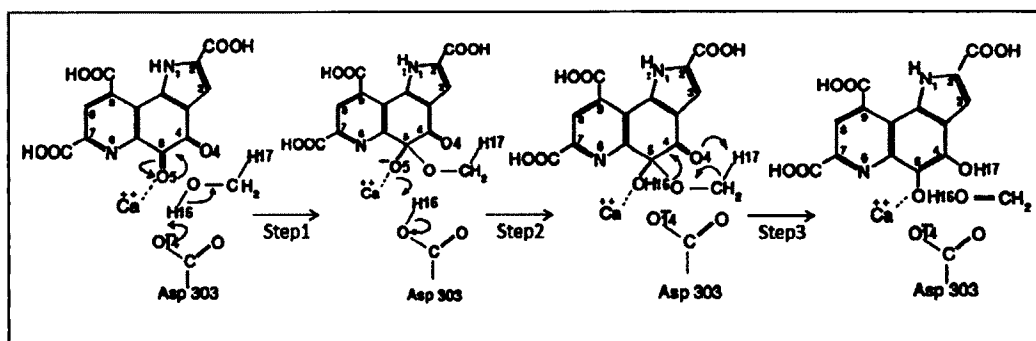


Figure 2.2: Addition-Elimination Methanol Oxidation Mechanism.

2.2.2.2 Hydride-Transfer Mechanisms

The four-step H-T mechanism (Four-step H-T) (Figure 2.3) shows the simultaneous transfer of two protons (H16 and H17) from methanol to the active site base (H16) and to the carbon C5 of PQQ (H17), leading to the formation of formaldehyde in the very first step of the mechanism (Figure 2.3a). In the second step, H16 is transferred from the active base to the oxygen O5 of PQQ. The third step involves the transfer of H17 from C5 of PQQ to the active site base, and finally in the last step, H17 is transferred

from the active site base to the oxygen atom O4 of PQQ [47]. There is also an alternative step leading to the “alternate” hydride transfer mechanism (Alternate H-T), in which the pyrrole nitrogen contributes to the ionization of the O4 of PQQ, possibly contributing to the tautomerism of the intermediate by not involving the ASP-303 catalytic base (Figure 2.3b) [47]. According to this alternate mechanism, after the formation of the formaldehyde, the active base plays no role in the oxidation mechanism. The transfer of the H17 from C5 of PQQ to the O4 of PQQ takes place directly due to the pyrrole nitrogen (Figure 2.3b).

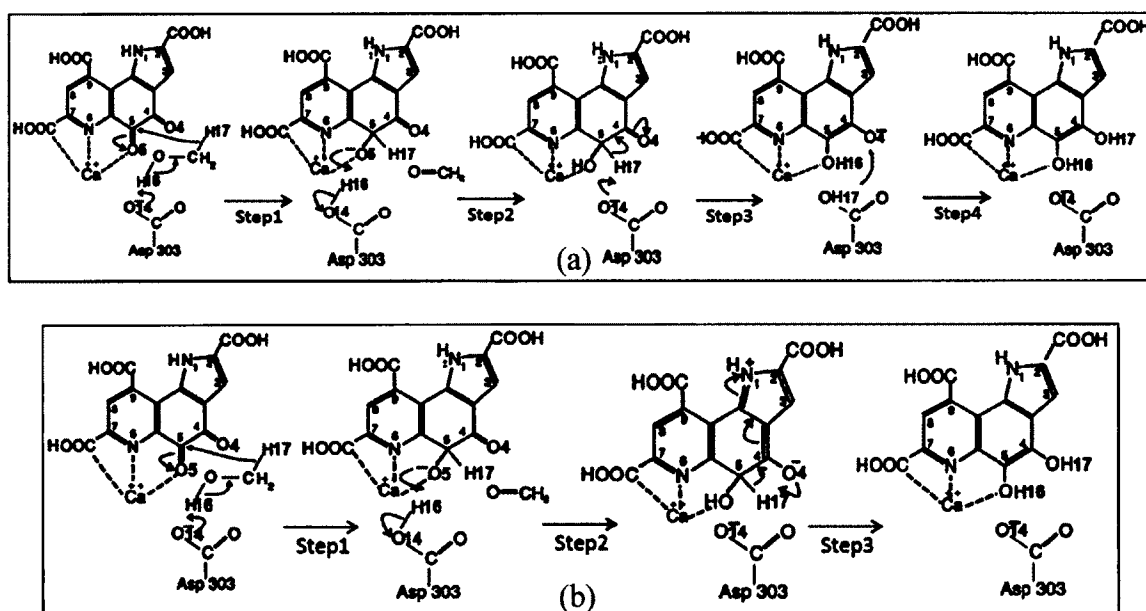


Figure 2.3: Hydride Transfer Methanol Oxidation Mechanisms (a) Classical Hydride-Transfer (b) Alternate Hydride Transfer.

Several experimental and theoretical studies were conducted to elucidate/support the methanol oxidation mechanism by Ca^{2+} -MDH. Frank *et al.* [50, 51] and Itoh *et al.* [39, 52] supported the A-E mechanism by showing that PQQ systems can oxidize methanol, ethanol, and 2-propanal to their corresponding aldehydes via the formation of hemiketal adducts bound to C5 of PQQ in organic solution, thus suggesting that a

covalent PQQ-substrate complex would be possible. However, crystallographic studies of soluble glucose dehydrogenase at 1.9 Å resolution by Oubrie *et al.* [53, 54], quantum mechanics/molecular mechanics and molecular dynamics calculations by Reddy *et al.* [55, 56], and conformational variation calculations of the active site residues of the MDH enzyme by Zhang *et al.* [55] favor the H-T mechanism. The Electron Paramagnetic Resonance studies of Kay *et al.* [57] on substrate binding in ethanol dehydrogenase, eliminated the possibility of the A-E mechanism, as that process is an energetically expensive pathway leading to the breaking of the strong coordination of the substrate and the calcium cation, which is energetically very expensive to be broken (50 Kcal/mol), thus eliminating the possibility of A-E processes. The investigations by Li *et al.* [58], conclude that the C5-reduced PQQ intermediate is produced during oxidation reaction. Hence, these studies lend more support towards the H-T mechanism.

Leopoldini *et al.* [48] performed theoretical calculations at the B3LYP theory level on the MDH active site and obtained the energy barriers for the rate-determining steps of the A-E and H-T methanol oxidation mechanism by MDH to be 34.6 and 32.3 kcal/mol, respectively. In their calculations, however, only the reactive groups (CH_3COO^- and NH_3COCH_3) of the amino acids having coordination with the calcium ion and the PQQ molecule were considered, and hydrogen atoms of each reactive group were frozen during their simulations. No water molecules near the catalysis area were considered by those authors, and also the by-product formaldehyde formed during the reaction mechanism(s) was excluded from the calculations performed. The energy barriers Leopoldini *et al.* [48] found for the methanol oxidation mechanisms by Ca^{2+} -MDH were well above the general kinetic requirements of an enzymatic catalytic process. Hence,

these authors postulated an alternative mechanism: the “addition-elimination-protonation” (not shown) for the methanol oxidation by MDH [37, 47].

Following the most recent and popular procedure for investigating several enzyme reaction mechanisms, the A-E and H-T for methanol oxidation by Ca^{2+} -MDH were explored by Idupulapati *et al.* [49, 59] using Density Functional Theory on a model representing the active site of MDH. When the protein environment (with a dielectric solvation of 4) is considered in the model, two rate-determining steps for the A-E (steps 1 and 3) with free energy barriers of 18.9 and 20.8 kcal/mol, respectively, and one rate-limiting step for the H-T mechanism (step 1) with a barrier of 19.7 kcal/mol were predicted at the BLYP/DNP density functional theory level by Idupulapati *et al.* The free energy barriers for these rate-limiting steps of both methanol oxidation mechanisms did not compare well with the experimental free energy barrier for methanol oxidation by Ca^{2+} -MDH (8.5 kcal/mol), suggesting that a different mechanism may exist for this reaction [33].

According to the proposed two-step H-T methanol [49] oxidation by MDH, the hydride (H17) transfers directly to O4 instead of C5 of PQQ (Figure 2.4). This transfer allows the possibility to eliminate Steps 3 and 4 of the Four-step H-T (Figure 2.3a), which involves the transfer of H17 from C5 to O14 of ASP303 and from ASP303 to O4 of PQQ. The initial proton abstraction (H16 to O14 of ASP303), which occurs in concert with the hydride transfer, remains the same for Step 1. This transfer also allows the possibility for a two-step mechanism, where the second step involves the proton transfer (H16) from O14 of ASP303 to O5 of PQQ, thus getting PQQ reduced in this final step (Figure 2.4).

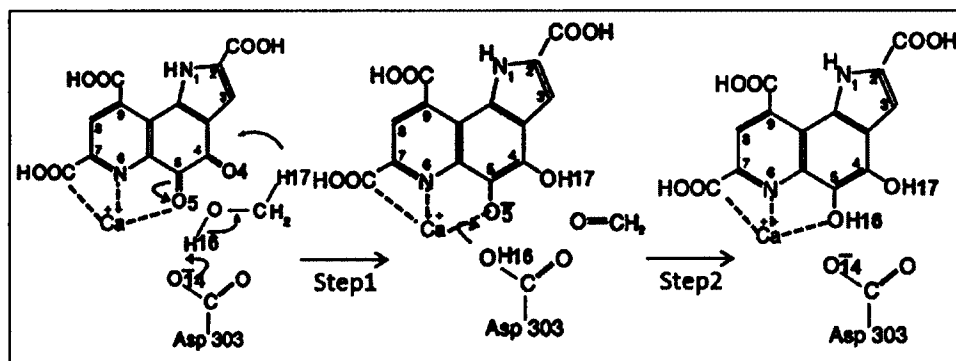


Figure 2.4: Two-Step Hydride Transfer Mechanism.

2.2.3 The Role of the Ion in MDH

More than one third of enzymes require metal ions for their catalytic activity. Apart from controlling the enzyme-catalyzed reactions, metal ions also help orient or bind the substrate in the enzyme active site in such a way that it provides a site for catalytic activity. These metal ions act as electrophiles as they are mostly positively charged and often have a charge greater than one. In order to understand the role of other bivalent metal ions in the active site of MDH, several experimental and theoretical studies were conducted [60]. It was proposed, for instance, that calcium cation in MDH from *Methylobacillus glycogens* can be replaced by strontium without losing enzyme activity [61]. That study showed that the specific activity of Sr^{2+} -containing MDH was over ten times higher than that of Ca^{2+} -containing MDH and it was observed that the methanol dehydrogenase activity increased in the cells that cultured in a Sr^{2+} medium.

Other spectroscopic and semi-empirical calculations on MDH have also shown that the binding constant of Sr^{2+} and Ba^{2+} to PQQ are weaker than that of Ca^{2+} , which can be attributed to the size of the calcium ion as it best fits in the binding pocket of PQQ in the MDH active site [52]. It has been found that the binding of the larger metal ions to the PQQ co-factor cause a distortion, making the coordination smaller when the calcium ion

is present [39, 62]. In order to observe the structural variations of the MDH active site and its kinetics on methanol oxidation, the naturally occurring Ca^{2+} ion was replaced with Ba^{2+} or Sr^{2+} respectively in the MDH active site. It was reported that there are no major differences between these ion-modified enzymes regarding the interactions between PQQ and the metal ion in the active site [33]; however, when tested upon methanol oxidation, the activation energy for the reaction decreased in both the Sr^{2+} - and Ba^{2+} -modified MDH. Sr^{2+} -MDH showed a decrease in activation energy (7.6 kcal/mol) with respect to that for Ca^{2+} -MDH (8.5 kcal/mol), the lowest activation energy was found in the case of Ba^{2+} -MDH (3.5 kcal/mol). These results were unexpected since the Ba^{2+} ion, a weaker Lewis acid than Ca^{2+} , should decrease the activity of the enzyme and hence the energy of activation should be larger [33]. Thus, those results showed that as the ionic radii increase ($\text{Ba}^{2+}(1.35\text{\AA}) > \text{Sr}^{2+}(1.12\text{\AA}) > \text{Ca}^{2+}(0.99\text{\AA})$), the activation energy for methanol oxidation decreases ($E_{\text{act}}(\text{Ba}^{2+}\text{-MDH}) < E_{\text{act}}(\text{Sr}^{2+}\text{-MDH}) < E_{\text{act}}(\text{Ca}^{2+}\text{-MDH})$).

In another study, the Ca^{2+} ion in the Glucose Dehydrogenase (GDH) active site was replaced with Ba^{2+} and the enzyme was tested for glucose oxidation [35]. From the spectral and kinetic studies performed, the energy barrier corresponding to the rate-determining step for the glucose oxidation mechanism was lower in the case of Ba^{2+} -GDH than that for Ca^{2+} -containing GDH, indicating that the type of metal ion in the enzyme active site indeed affects the formation rate of intermediates. Reconstitution of Membrane-integrated quinoprotein glucose dehydrogenase (mGDH) from *Acinetobacter calcoaceticus* with PQQ in the presence of Mg^{2+} showed that Mg^{2+} anchors PQQ to mGDH protein and activates the cofactor for glucose oxidation [36].

Buurman *et al.*[63] further investigated the role of magnesium and calcium ions in the GDH activity of *Klebsiella pneumonia* NCTC 418, and concluded that magnesium-limited growth conditions containing high Ca^{2+} concentrations resulted in high GDH activities. However, no conclusive evidence was stated in order to determine which ion (Mg^{2+} or Ca^{2+}) is the most preferred ionic species for the binding of the GDH PQQ cofactor. Along those lines, these authors concluded that calcium and magnesium ions are interchangeable.

On the other hand, there could be some limitations associated when the naturally occurring ion is replaced by other ions in the active site of the enzyme. For instance, a study by Okajima *et al.* [64] on the investigation of metal ion specificity for quinone cofactor biogenesis in bacterial copper amine oxidase showed that the other divalent ions (Co^{2+} , Ni^{2+} and Zn^{2+}) are capable of forming topa quinone (TPQ) but less efficiently than Cu^{2+} . They have shown that the high Lewis acidity of Cu^{2+} ion in cooperation with the coordination structure in the protein favors the presence of Cu^{2+} in the active site than other metal ions. To state another example, the quantum mechanical calculations performed by Topol *et al.* [65] have postulated that when iron (Fe^{2+}) was replaced by cobalt (Co^{2+}) and nickel (Ni^{2+}) in the active site of FIH enzyme, the reaction may occur very slowly as the reaction barrier for the Co and Ni containing enzyme were very high compared to the native iron-containing enzymatic system.

Thus, the various studies on ion-modified dehydrogenase enzymes indicate that ions play a vital and diverse role in enzyme catalysis. In order to fully understand the role of the ion in the Methanol Dehydrogenase enzyme active site, the investigation of Mg^{2+} and Sr^{2+} as the MDH active site metal ion is needed to complete these studies. Mg^{2+} is a

smaller ion than Ca^{2+} (naturally occurring ion in MDH) and therefore its insertion in the MDH active site may cause none or minimal distortion. The small atomic radius (0.72 Å) and being a harder metal ion makes it suitable for coordination to hard ligands like oxygen atoms.

For example, a study on the crystal structures of human hematopoietic prostaglandin D synthase (H-PGDS) by Tsuyoshi Inoue *et al.* [66] reported that Ca^{2+} and Mg^{2+} ions increase the activity of human prostaglandin D synthase (H-PGDS) by decreasing the K_m value for the substrate or cofactor glutathione (GSH), and as for the isomerization of PGH_2 to PGD_2 , prostaglandin D synthase uses GSH as a cofactor and since the structure of the enzyme is homodimer, Ca^{2+} or Mg^{2+} increases its activity. It was observed that due to the small size of the Mg^{2+} ion, it could accommodate more water molecules in the dimer interface, and this effect decreased the K_m value by four-fold for GSH and in turn increased the activity of H-PGDS [66].

Moreover, the unusual chemistry associated to Mg^{2+} has led to its usefulness in enzyme activation and catalysis. It is also considered the most commonly found metal ion cofactor in enzymatic systems. For instance, all enzymes utilizing or synthesizing ATP require the presence of magnesium ions for their catalytic activity [67]. Also, Mg^{2+} binds to essential biomacromolecules such as DNA and RNA efficiently to participate in neutralization of the polyanionic charge of these nucleic acids. Until date, no theoretical investigations are reported in the literature concerning methanol oxidation by Mg^{2+} -containing MDH.

On the other hand, Sr^{2+} is considered a more efficient ion than Ca^{2+} for catalyzing methanol by MDH since upon exposure to air and at high temperatures, the activity of

Sr^{2+} -MDH was more stable than Ca^{2+} -containing MDH. Experimental activation energy values for methanol oxidation by Ca^{2+} and Sr^{2+} -containing MDH were in the same range, with a slight decrease in the case of Sr^{2+} -MDH which could be attributed to an increased stability of the transition state, and considering the fact that Sr^{2+} ion is larger than Ca^{2+} , and their electronegativity values are almost the same ($\text{Sr}^{2+} = 0.95$ and $\text{Ca}^{2+} = 0.99$) [68]. However, there is no theoretical information reported so far in regard to methanol oxidation by Sr^{2+} -containing MDH and this is directed to study Sr^{2+} -containing MDH.

To state another example, in order to understand the thermal stability of bromoperoxidase (BPO), the effect of metal ions on the enzyme stability was studied by Rodriguez *et al.* [69]. It was confirmed that the addition of calcium ion to apo-enzyme increased the stability and other divalent ions such as Sr^{2+} and Mg^{2+} enhanced the thermostability and activity of the enzyme. It is believed that other alkaline-earth group metal ions can be incorporated into the normal binding site of calcium in the enzyme [69], and on these terms, studying the replacement of Ca^{2+} ion by Sr^{2+} and Mg^{2+} ions in the MDH enzyme active site will provide more information about the functioning of MDH enzyme.

CHAPTER 3

MULTI-SCALE SIMULATION TECHNIQUES

To study how proteins and biomolecules function, molecular modeling and simulation techniques have proven to be powerful tools and applying these methods to understand enzymatic reactions is a particularly challenging application because enzyme catalysis involves processes of differing length and time scales. Even though experimental techniques such as X-ray crystallography, Nuclear Magnetic Resonance, and other spectroscopic methods provide explicit information about the enzyme structure, details about the catalytic mechanisms are not sufficient enough to clearly understand the reactivity of the enzyme. Insights into these mechanisms have potential applications in the design of new catalysts. In these developments, computational modeling has an important role to play as it can provide information about the unstable species such as transition states and reaction intermediates that cannot be studied directly by experiments in systems as complex as enzymes. Thus, computer simulation can provide important information that is complementary to experiments.

3.1 Multi-Scale Modeling Approach

Using multi-scale modeling is an effective way to deal with such biochemical processes by integrating various physical techniques ranging from atomistic to coarse-grained simulations. A combination of various computational tools is usually required in order to model an entire biological system effectively, which can be treated as a cascade

of individual subsystems as shown in Figure 3.1. Classification of these subsystems is based on their different body interactions which depend on magnitudes of time and length.

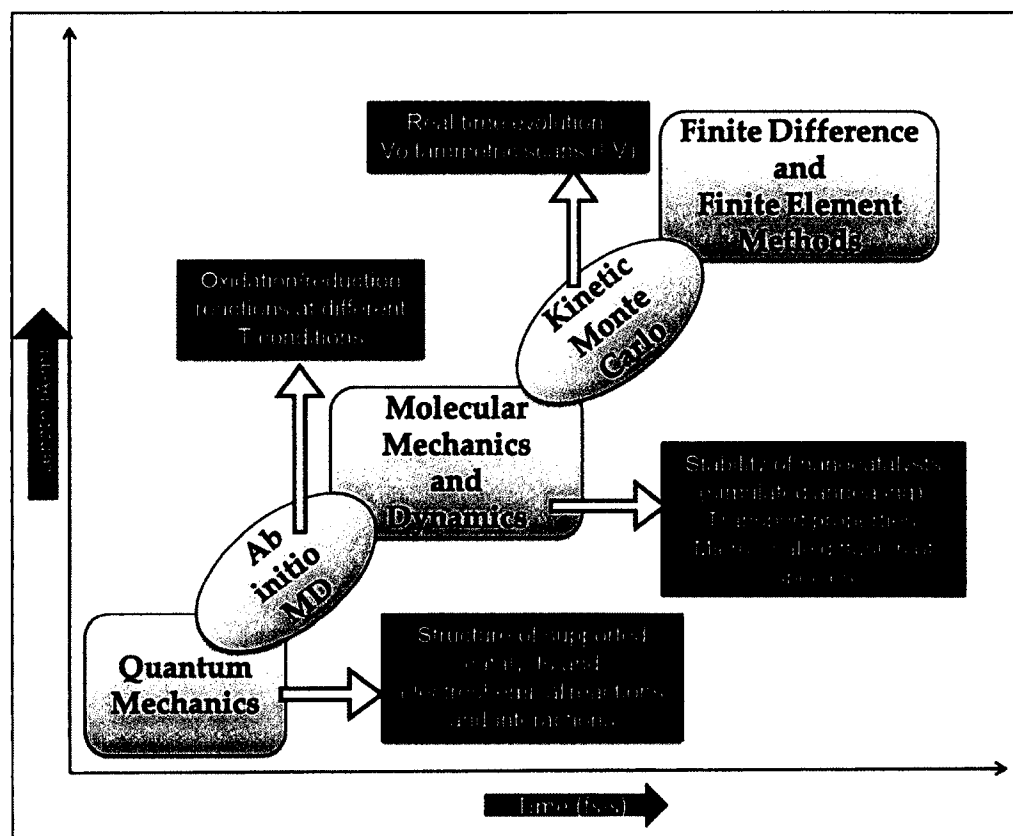


Figure 3.1 Flowchart showing the multiscale modeling approach.

Quantum mechanical (QM) methods such as *ab initio*, semiempirical, and density functional theory (DFT) [70] are used to study the structural and energetic information in molecular systems containing less than one hundred atoms which belong to the microscopic regime (picometers to angstrom length scale). These atomistic simulations provide parameters for larger time and length scales. DFT methods have become a powerful tool in calculating not only structural and energetic molecular information but also other quantities such as the activation energies of chemical and biological reactions

as DFT is computationally cheaper than correlated *ab initio* methods like the configuration interaction and Møller–Plesset perturbation theory, thus reducing the many-body electron problem treated by the wave function to a single electron problem dealt with the electron density instead [71].

In general, QM methods are useful in modeling smaller site-specific systems like reactions at a small region within an enzyme active site (limited to a few hundred of atoms). Molecular mechanics (MM) and molecular dynamics (MD) are used for larger systems (containing more than hundreds of atoms) and these techniques rely on the parameterization of bonding and nonbonding interactions via force fields [72]. These methods are operative over wide length- and time-scale ranges while still dealing with individual atoms. Classical MD simulations have been employed in the literature for the determination of enzyme mechanisms and/or support for a particular one from two or three already proposed. MD studies enhance the understanding of the role of the active site residues that are of fundamental importance for a better description of the catalytic mechanism.

Finite element analysis (FEA), finite difference methods (FDM) and Monte Carlo methods are used to model simulations in the macroscopic spatial regime (millimeters to meters length scale) [73]. In particular, kinetic Monte Carlo (kMC) methods are designed to deal with a large range of scales and require parameters that can be obtained from experiments or simulations from smaller scales. In a typical kMC simulation, the short time dynamics and the interactions between species are represented by discrete hops from one position to another based on random probabilities. These simulations are usually conducted on a grid that acts as a platform for the species to interact and these

interactions are dependent on a set of predefined rules and the initial and final atomic configurations [74].

In this study, DFT techniques are used to optimize the MDH active site models to understand the substrate binding and orientation and to calculate the activation energy barriers for methanol oxidation according to a given mechanism. Transition State Theory (TST) is used to obtain the reaction rates for the oxidation mechanism and these microscopic rates are used as inputs for the kMC simulations to obtain the macroscopic rates of the reaction. Thus, to model enzyme kinetics a combination of tools involving Density Functional Theory, Transition State Theory, and Molecular Mechanics were combined in a Kinetic Monte Carlo approach. Information regarding microscopic energy barriers and pre-exponential factors needed to determine reaction rates involved in each step of the methanol oxidation mechanisms by MDH was obtained from DFT and TST, respectively. This microscopic reaction rates were then provided as inputs in the kMC program, and the methanol oxidation process was modeled on a 2-D reactive surface representing the enzyme active site.

The 2-D surface was determined using MM simulations by exploring the enzyme binding pocket and the projection of enzyme residues seen by the substrate molecules (methanol) as they approach the enzyme active site, thus reducing, in a first approximation, the complexity of the problem. A grid representing possible methanol adsorption, diffusion and reaction sites was mapped onto the projected biocatalyst image in a 2-D surface for a random substrate approach onto the reactive enzyme surface. kMC simulations will then predict information on the macroscopic rates for methanol oxidation

by MDH enzymes, which in turn will provide information on the polarization curves (I-V curves) when MDH is used in the fuel cell anodic chambers.

The main focus of this chapter is to describe each method used in this study and the integration of QM, MM information on a kMC method, leading to a proposed multiscale approach to study MDH-assisted methanol oxidation.

3.2 Enzyme Kinetics

Fundamental knowledge and understanding of experimental enzyme kinetics is essential for simulating enzyme reactions. Here, a brief review of the concepts necessary for enzyme simulation is presented. Typically, an enzymatic reaction under steady-state conditions is often written as Equation 3.1.



where E represents the enzyme, S is the substrate, ES is the enzyme-substrate complex, and P is the product; k_1 and k_{-1} are the rates of association and dissociation of the ES complex, respectively; and k_{cat} is the apparent first-order rate constant, also called the turnover number [75].

An important quantity in enzyme kinetics is k_{cat}/K_m , which is an apparent second-order rate constant that describes the specificity of an enzyme for a given substrate. Here, K_m is the Michaelis constant ($K_m = (k_{-1} + k_{\text{cat}})/k_1$) and it is a measure of the concentration of substrate at which the rate of an enzymatic reaction is one half its maximum, V_{max} [75]. However, K_m is more difficult to calculate than k_{cat} , so k_{cat}/K_m is not typically computed. The general procedure is to compute relative free energies in simulations of enzyme catalysis and these computed activation free energies are usually compared to

experimental values derived from k_{cat} using Transition State Theory (TST), which provides a connection between k_{cat} and the free energy of activation (ΔG), (Equation 3.2)

$$k_{cat} = \frac{k_B T}{h} \exp\left(-\frac{\Delta G}{RT}\right), \quad \text{Eq. 3.2}$$

where k_{cat} is the rate constant (s^{-1}), k_B is the Boltzmann's constant (3.29×10^{-24} cal/K), h is the Planck's constant (6.626×10^{-34} Js), T is the absolute temperature (298.15 K at room temperature), and R is the universal gas constant (8.314 J/Kmol). TST is expected to be a good approximation for energy barriers above ~ 10 kcal/mol, which includes essentially all enzyme-catalyzed reactions. A reaction rate determines how fast particular reaction takes place i.e., how quickly reactants change into products. Enzymes have an ability to stabilize the ground state of a reaction relative to the ground state and this principle is shown in Figure 3.2.

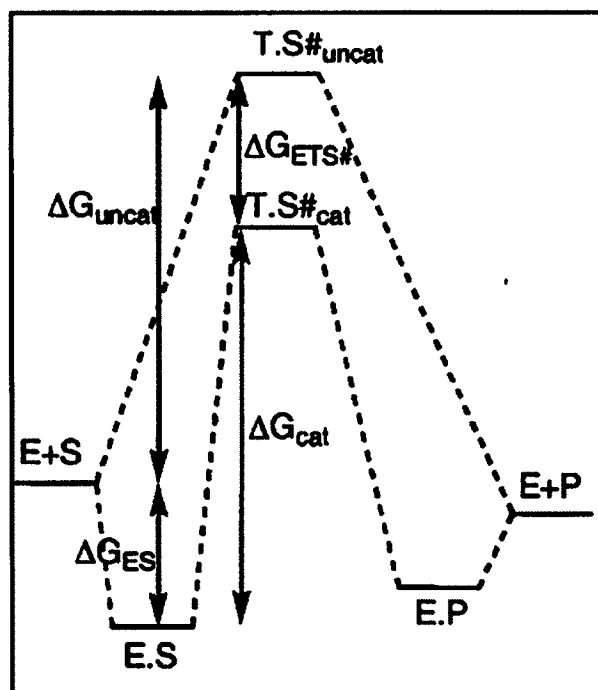


Figure 3.2: Schematic free energy profile for uncatalyzed and enzyme catalyzed chemical reactions [76].

The activation barrier of a reaction is represented by ΔG_{cat} and ΔG_{uncat} for the catalyzed and uncatalyzed reactions, respectively. In the case of uncatalyzed reaction, the relative free energy is between the transition state ($\text{T.S}_{\text{uncat}}$) to the reactant. In the corresponding enzymatic reaction, the substrate first binds to the enzyme to form an enzyme-substrate complex (E.S), and then react via one (or several) transition state(s), resulting in an enzyme-product complex (E.P) from which the product (P) is finally released and the enzyme is set free again. In this case, the reaction barrier (ΔG_{cat}) is the relative energy between the E.S complex and the transition state (T.S_{cat}) [76].

3.3 Enzyme Modeling and Computational Details

In order to model the enzyme catalysis, first, an active site model is constructed where the actual reaction takes place. The remaining protein that is not explicitly included in the model can affect the reaction model in two main ways, by steric and polarization effects. By locking certain atoms, typically where the truncations are made to their crystallographic positions, the steric effects can be taken into account. This way, very large and unrealistic movements of the various groups can be avoided. In the case of metalloenzymes, where the ion coordinates with the important residues to keep them in place and presence of bonding and/or hydrogen bonding between residues, steric effects is less important. Therefore, in our active site models for studying methanol oxidation mechanism, no atoms were constrained [77-82].

Accordingly, for treating the neglected surrounding enzyme environment, a homogeneous polarizable medium with a continuum solvation model such as COSMO [83, 84] (conductor-like screening model) is used to estimate solvation effects of the rest of the enzyme that is not included in the active site model. This model works in such a

way that the solute molecule forms a cavity within the dielectric continuum of permittivity that represents the solvent [83, 84]. The charge distribution of the solute polarizes the dielectric medium. The response of the dielectric medium is described by the generation of screening (or polarization) charges on the cavity surface. The standard value for the dielectric constant ϵ was chosen to be 4 [79-82] to model the protein's surroundings. Hence, all geometry optimizations were performed in the presence of this solvation model [85] and Density Functional Theory calculations are then performed at $\epsilon=4$ to obtain reaction free energy barriers.

All the geometry optimizations, binding energy and reaction energy barrier simulations in this dissertation were carried out using DMOL³ module[86] of Materials Studio 4.4 and 6.0 [87]. Gradient Approximation Method (GGA) was employed with Becke exchange, plus Lee-Yang-Parr (BLYP) [88-90] correlation functional and DNP basis set. The errors in energies are expected to be in the order of 2-5 (kcal/mol) and to the second decimal place for calculated bond lengths (angstroms) when the theory level BLYP/DNP is used [90-92]. In these simulations, Harmonic vibrational frequencies are also calculated in order to confirm that the stationary points on the potential energy surface are either all local minima or transition state. In the case of local minima, all the frequencies are real, and for the transition state, there is one imaginary frequency [49].

The reaction barrier height is a property derived from the Born-Oppenheimer electronic energies and the vibrational zero point energies (ZPE), which are not affected by temperature, whereas the so called Arrhenius activation energy, E_{act} , depends on the temperature [93]. Hence, the energy barrier is not the same as the Arrhenius activation energy E_{act} , and their connection may not be straight forward [94, 95]. In this work, we

provide information on the calculated free energy barrier (that is, the actual (with ZPE) reaction barrier for the forward reaction with the thermal corrections to the Gibbs Free energy at 298.15 K included) for each step of the methanol oxidation mechanisms by ion-modified MDH.

In order to evaluate the free energy barriers, quantum mechanical calculations have proven to be appropriate. The following session reviews the theories behind quantum mechanics.

3.4 Quantum Chemistry

To study the molecular level chemistry, for instance, the motion of electrons in a molecule, quantum mechanical calculations have proven to be the most powerful approach. The time-dependent Schrödinger equation (Equation 3.3) is the governing equation in quantum mechanics and solving this can in principle provide all the properties of a system like energy.

$$\hat{H}(r)\psi(r)=E\psi(r). \quad \text{Eq. 3.3}$$

In Equation 3.3, \hat{H} is the Hamilton operator for the total energy of a molecular system as given in Equation 3.4, ψ is the wave function in the i -th state of the system which depends on the $3M$ spatial coordinates of the nuclei, the $3N$ spatial coordinate of the electrons, and the N spin coordinates of the electrons, which are collectively described by the term \mathcal{P}_i , and E_i is the spatial energy of the system described by the wave function.

$$\hat{H} = \sum_i^{\text{electrons}} \frac{-\hbar^2}{2m_e} \nabla_A^2 + \sum_A^{\text{nuclei}} \frac{-\hbar^2}{2m_A} \nabla_A^2 - \sum_i^{\text{electrons}} \sum_A^{\text{nuclei}} \frac{-e^2 Z_A}{r_{iA}} + \sum_{i \rightarrow j}^{\text{electrons}} \frac{e^2}{r_{ij}} + \sum_{A \rightarrow B}^{\text{nuclei}} \frac{e^2 Z_A Z_B}{r_{AB}}. \quad \text{Eq. 3.4}$$

The Hamiltonian operator \hat{H} (Equation 3.4) is the sum of the kinetic energy of electrons and nuclei, potential energy of attractive forces between nuclei and electrons, electron-electron repulsive force, and nucleus-nucleus repulsive force. Equation 3.4 when written in atomic units (Planck's constant $\hbar = 1$, $m_e = 1$, $e = 1$) is shown in Equation 3.5 [96].

$$\hat{H} = -\frac{1}{2} \sum_{i=1}^N \nabla_i^2 - \frac{1}{2} \sum_{A=1}^M \frac{1}{M_A} \nabla_A^2 - \sum_{i=1}^N \sum_{A=1}^M \frac{Z_A}{r_{iA}} + \sum_{i=1}^N \sum_{j \neq i}^N \frac{1}{r_{ij}} + \sum_{A=1}^M \sum_{B \neq A}^M \frac{Z_A Z_B}{R_{AB}}, \quad \text{Eq. 3.5}$$

where ∇^2 is the Laplace operator, M_A is the mass of the nucleus A , Z is the charge and r is the distance between the particles. Solving the Schrödinger equation involves finding the values of E_i and Ψ_i so that when the wave function is operated upon by the Hamiltonian, it returns the wave function multiplied by the energy [96]. Only for one electron system like the hydrogen atom the exact solution for Schrödinger's equation is obtained [97].

To solve the equation for the many-particle systems, i.e. beyond the hydrogen atom, some simplifications have to be introduced. One of the most fundamental approximations, known as the Born-Oppenheimer approximation or clamped nuclei approximation, helps in simplifying the calculations for multi-scale molecular systems. According to this, since the nuclei have much more mass than the electrons, their motions can be separated. The kinetic energy of nuclei and the nucleus-nucleus repulsion can be considered as an effective potential. Therefore, Equation 3.5 reduces to electronic Hamiltonian as shown in Equation 3.6.

$$\hat{H} = \frac{1}{2} \sum_{i=1}^N \nabla_i^2 - \sum_{i=1}^N \sum_{A=1}^M \frac{Z_A}{r_{iA}} + \sum_{i=1}^N \sum_{j \neq i}^N \frac{1}{r_{ij}} = \hat{T} + \hat{V}_{Ne} + \hat{V}_{ee}. \quad \text{Eq. 3.6}$$

The solution of Equation 3.6 is given by Equation 3.7

$$\hat{H}_{elec}\Psi_{elec}=E_{elec}\Psi_{elec}, \quad \text{Eq. 3.7}$$

where Ψ_{elec} is the electronic wave function and E_{elec} is the electronic energy term as given in Equation 3.8.

$$E_{tot}=E_{elec}+E_{nuc}. \quad \text{Eq. 3.8}$$

The wave function Ψ term by itself is not of much significance, but the square of the wave function represents the probability of finding electrons within a certain volume and its integral, as represented by Equation 3.9, which gives the total number of electrons (N) in the system.

$$N=\int |\Psi(x_1, x_2, \dots, x_N)|^2 dx_1 dx_2 \dots dx_N. \quad \text{Eq. 3.9}$$

Electrons are fermions with a spin equal to $1/2$; therefore, an anti-symmetric wave function is applied with respect to the interchange of the spatial and spin coordinates of any two electrons (Equation 3.10).

$$\Psi(x_1, x_2, \dots, x_i, x_j, \dots, x_N) = -\Psi(x_2, \dots, x_j, x_i, \dots, x_N). \quad \text{Eq. 3.10}$$

The solution to the electronic Schrödinger equation, i.e. calculating the electronic energies for different nuclear arrangements, leads to a potential energy surface (PES), the minima of which determine the ground state geometries of a molecule [98-100]. *Ab-initio* methods such as Hartree-Fock (HF), Configuration Interaction (CI), and the Local Spin Density and the Generalized Gradient approximations within the Density Functional Theory (DFT) do not rely on empirical data or use experimental parameters in their computations. The DFT technique has been employed in this research, and in the next session, a detailed summary of its principles is discussed.

3.4.1 Density Functional Theory

DFT is based on the Hohenberg-Kohn theorem [101], according to which the ground-state energy is a functional of the electron density of the system, namely, $E = E[\rho(r)]$ [101]. The wave function of an N -electron system contains $3N$ coordinates, whereas the electron density is independent of the number of electrons as it is the square of the wave function, integrated over $N-1$ electron coordinates. However, a problem arises here, that is, the connection between the electron density with the energy. The aim of DFT methods is to design the functional connecting these two quantities. The energy functional is divided into three parts, kinetic energy $T[\rho]$, the nuclei-electron attraction $E_{ne}[\rho]$, and the electron-electron repulsion $E_{ee}[\rho]$, as expressed in Equation 3.11, can be expressed as follows [91]:

$$E[\rho] = T[\rho] + E_{ee}[\rho] + E_{ne}[\rho]. \quad \text{Eq. 3.11}$$

The introduction of the orbital-based scheme by Kohn and Sham (KS) laid the foundation for the use of DFT methods in computational chemistry [102]. The basis of KS formalism is dividing the total kinetic energy (T) into two parts, the kinetic energy of N electrons of non-interacting system (T_s), and a missing fraction (T_c) relative to the real interacting system as shown in Equation 3.12 [102]:

$$T[\rho] = T_s[\rho] + T_c[\rho]. \quad \text{Eq. 3.12}$$

Furthermore, the electron-electron repulsion ($E_{ee}[\rho]$) functional can be divided into the classical Coulomb interaction (J) and a non-classical part containing correlation and exchange ($E_{ncl}[\rho]$). So the total new energy can now become (Equation 3.13) [102]:

$$E[\rho] = T_s[\rho] + T_c[\rho] + J[\rho] + E_{ncl}[\rho] + E_{ne}[\rho]. \quad \text{Eq. 3.13}$$

Next, an exchange-correlation functional ($E_{xc}[\rho]$) is formed (Equation 3.14) by combining the missing fraction of the kinetic energy ($T_c[\rho]$) and the correlation and exchange part ($E_{nc}[\rho]$).

$$E_{xc}[\rho] = T_c[\rho] + E_{nc}[\rho]. \quad \text{Eq. 3.14}$$

Thus, finally the total energy can be written as (Equation 3.15) [102]:

$$E[\rho] = T_s[\rho] + J[\rho] + E_{ne}[\rho] + E_{xc}[\rho]. \quad \text{Eq. 3.15}$$

The first three terms ($T_s[\rho]$, $J[\rho]$, $E_{ne}[\rho]$) can be calculated explicitly. How accurately the exchange-correlation term $E_{xc}[\rho]$ is described, which incorporates all unknown contributions to the total energy, will determine the effectiveness of the DFT method.

The way the kinetic energy, the exchange and correlation terms are described, differentiates the various DFT methods [103, 104]. Three types of functionals are used for computing the electron correlation with the electron density [92, 105]. Local spin density approximation (LSDA) functional is the first type, which uses only the values of electron spin densities. The second type involves both values of the electron spin density and its gradient and is known as the Generalized Gradient Approximation (GGA) functional. These functionals are also referred to as non-local functionals. The hybrid functional is the third kind of functional, which describes the exchange function as a linear combination of Hartree-Fock, local and gradient-corrected exchange term [92, 105]. This exchange term is then combined with local or gradient corrected correlation term [91, 92, 105].

The GGA functionals are widely used for modeling enzymatic reactions and the most extensively used GGA exchange-correlation combinations in various atomic

calculations are BP86, BLYP and BPW91 [96, 106]. To perform optimization and transition state calculations in this project, the BLYP exchange-correlation functional as employed in the DMOL³ module [86] of Materials Studio[®] software is used. A BLYP functional is the combinations of Becke's (B) GGA exchange function and Lee, Yang and Parr (LYP) correlation function [88-90].

3.4.2 Basis Sets

To represent the atomic or molecular orbitals, a set of functions known as basis sets are used [96]. In order to express the unknown molecular orbitals (MO), quantum mechanical calculations use a basis set expansion which are commonly expressed as linear combination of atomic orbitals (LCAO) as shown in Equation 3.16 [96, 99],

$$\psi_i = \sum_{\mu=1}^K C_{\mu} \varphi_{\mu} , \quad \text{Eq. 3.16}$$

where Ψ_i is a spatial molecular orbital MO, and φ_{μ} is one of K atomic orbitals (H-like functions; these are the basis functions), and C_{μ} are coefficients. Basis functions φ_{μ} need not be H-alike always. To approximate the orbitals accurately, they are represented by larger basis sets which impose fewer restrictions on the locations where an electron can be present; however, they require higher computational power and a longer time to perform the calculations [96, 99].

The basis functions are based on either analytical or numerical functionals. The two types of analytical basis functions are the Slater Type Orbitals (STO) and the Gaussian Type Orbitals (GTO). In the case of a numerical basis function, it consists of a table of the values that an atomic orbital wavefunction has at many points around the nucleus, with empirical functions fitted to pass through these points. In most calculations, empirical functions are used instead of the analytical Gaussian-type functions because the

molecule can be dissociated exactly to its constituent atoms. It minimizes the basis set superposition effects and an accurate description is possible even if the bonds are weak [99, 107].

For our calculations, one such numerical basis set used is Double Numerical plus Polarization (DNP) basis set [108]. According to this basis set, a polarization d function on heavy atoms and a polarization p function on hydrogen atoms is considered. This DNP basis can be compared to the split-valence double zeta 6-31G** in size; however, it is more accurate than the Gaussian basis sets of the same size [85, 109]. For systems consisting of ions, this basis set is most suitable in conjunction with Density Functional Theory calculations in this work.

3.4.3 Transition State Calculations using DMol3

To perform the transition state calculations as a part of this dissertation work, the DMOL³ module of the Materials Studio[®][85, 109] software is used along with the synchronous transit methods (Linear Synchronous Transit, LST and Quadratic Synchronous Transit, QST [110, 111]). Reactants and products involved in each reaction step are considered for defining atom pairing according to Equation 3.17 [110, 111], so that a 3D trajectory file representing the reaction path is generated with the Reaction Preview tool of the Materials Studio[®] software.

$$r_{ab}^i(f) = (1 - f)r_{ab}^R + fr_{ab}^P, \quad \text{Eq. 3.17}$$

where r_{ab}^R and r_{ab}^P are the inter-nuclear distances between the pair of atoms a and b in the reactant and the product respectively, and f is an interpolation parameter which varies between 0 and 1 [110, 111]. For molecules with N atoms, the number of distinct inter-nuclear separations is $N(N-1)/2$ by which Equation 3.17 over specifies the geometry.

All the reactant, intermediates, and product were optimized. Atom pairing of the reactant and the product involved in each step is done in order to generate a 3D trajectory file to represent the reaction path preview. Then, these 3D trajectory files are used as inputs to obtain the corresponding transition states, using the linear synchronous transit and quadratic synchronous transit (LST/QST) calculation with conjugate gradient minimization [111] within the Transition State search tool in DMOL³. This methodology starts with a LST/optimization (bracketing the maximum between the reactant and the product and performing energy minimization of the obtained maximum in the reaction pathway). The Transition State obtained is used as a starting point for performing a finer search with the QST/optimization followed by a conjugate gradient minimization. This cycle is repeated until a stationary point with only one imaginary frequency (transition state) is found [111], since in many cases, several imaginary frequencies are found. In the later situation, the corresponding (imaginary) modes of vibrations are animated in order to visualize the mode that would eventually follow the intended step from a particular reactant to the product. That particular mode is then selected to perform the transition state optimization to verify whether the obtained geometry is indeed a transition state.

The transition state finally obtained by the LST/QST/conjugate gradient method may not be the transition state connecting the intended reactant and product for a particular reaction step. Therefore, in order to thoroughly investigate the reaction paths, the intrinsic reaction coordinate (IRC) analysis is performed. In DMOL³, the IRC calculations are included in the Transition State Confirmation tool [109]. This tool starts at the transition state and locates successive minima in the direction of the reactant and product paths. This path is known as the minimum energy path, which should connect the

supposed transition state to the presumed reactants and products [110]. It uses the nudged elastic band method to validate a transition state by introducing a fictitious spring force which connects the neighboring points to ensure continuity of the path, and then it projects the force so that the system converges to the minimum energy path [110].

3.5 Molecular Mechanics

For larger systems with more than 100 atoms, quantum mechanical calculations may not be feasible because they (QM) are performed to deal with the electronic motion present in the system. For such bigger systems, molecular mechanics (MM) is suitable because it considers the position of the nucleus on an atom to calculate the energy of a large atomic system also known as the force field method, by ignoring the electronic motion of a system [112]. Simple algebraic expressions are used in the case of MM for computing the total energy of a molecular system without solving a wave function or total electron density. The fundamental tool of MM is the empirical forcefield (EFF or FF) which is the extrapolation of the experimental data obtained for small molecules to larger molecules. For larger systems, it quickly provides energetically favorable conformations [112].

MM method takes into consideration the following principles to model a molecular system:

1. Electrons and nuclei are treated as unified atom-like particles and these particles are considered as spherical balls.
2. The bonds between the particles are viewed as springs.
3. Potential energy functions derived from classical mechanics that rely on empirical parameters are used to treat the interactions between the atom-like

particles. These functions (Forcefield) describe the interactions between the sets of atoms.

4. The sum of interactions determines the conformation of these particles.

Forcefields can be obtained for various functional forms such as to account for the accurate prediction of properties which are bond stretching, angle bending, bond rotation, non-bonded electronic, and Van der Waal's interactions. The general forcefield equation is given in Equation 3.18, which represents the bonded interactions of bond stretching (E_r), angle bending (E_θ), and torsion (E_\square) in the first three terms [112].

$$E_{\text{total}} = E_r + E_\theta + E_\phi + E_{\text{nb}} + [\text{special terms}]. \quad \text{Eq. 3.18}$$

The internal energy terms given in Equations 3.19, 3.20, and 3.21 are similar for most FF.

$$E_r = \sum K_r (r-r_0)^2, \quad \text{Eq. 3.19}$$

$$E_\theta = \sum K_\theta (\theta-\theta_0)^2, \text{ and} \quad \text{Eq. 3.20}$$

$$E_\square = \sum K_\square [1 + \cos(n\phi-\phi_0)], \quad \text{Eq. 3.21}$$

where, K_r , K_θ , and K_\square are force constants for bond, angle and dihedral angle, and r_0 , θ_0 , and \square_0 define the equilibrium distance, angle and phase angle, respectively. The periodicity of the Fourier term is represented by n . These parameters values are derived from model molecules and vary for different FF [96, 112].

The non-bonded interactions (E_{nb}) such as Van der Waal's interactions are represented in the fourth term of Equation 3.19. Lennard-Jones potential given in Equation 3.22 is commonly used for Van der Waals interactions.

$$E_{\text{vdW}} = \sum_{i=1}^N \sum_{j=i+1}^N \left(4\epsilon_{ij} \left[\left(\frac{\sigma_{ij}}{r_{ij}} \right)^{12} - \left(\frac{\sigma_{ij}}{r_{ij}} \right)^6 \right] \right). \quad \text{Eq. 3.22}$$

Special terms need to be added for biochemical systems, and because biochemical molecules are often charged, an electrostatic energy term as given in Equation 3.23 is added to E_{nb} [96, 112].

$$E_{elec} = \frac{q_i q_j}{4\pi\epsilon_0 r_{ij}}. \quad \text{Eq. 3.23}$$

Different forcefields are used for different systems and purposes. For example, MM2/MM3 forcefields are used for small molecule systems. OPLS is used for liquid systems, while CHARM, AMBER, and GROMOS are used for proteins and nucleic acids. COMPASS (Condensed-phase Optimized Molecular Potentials for Atomic Simulation Studies) is used for organic and inorganic materials. In this research, COMPASS (Condensed phase optimized *ab initio* forcefield) forcefield is used for running the calculations as it is considered one of the advanced forcefields with very accurate predictions of structural, vibrational, and thermo-physical properties at various experimental conditions [87, 113, 114]. Minimization is done using Smart Minimizer which uses Steepest descent algorithm, followed by Conjugate gradient method, and finally quasi-Newton methods for optimizing the enzyme models available in MS4.4

3.6 Kinetic Monte Carlo

The kinetic Monte Carlo (kMC) methods are designed to deal with a large range of scales and require parameters that can be obtained from experiments or simulations from smaller scales. In a typical kMC simulation, the short time dynamics and the interactions between species are represented by discrete hops from one position to another based on random probabilities. These simulations are usually conducted on a grid that acts as a platform for the species to interact, and these interactions are dependent on

a set of predefined rules and the initial and final atomic configurations [74]. kMC methods yield time evolution of individual reaction rates (difficult to determine experimentally), which compete with each other as a function of external variables such as pressure and temperature. The rates are specified as probabilities and the time evolution of surface configuration is given by a Master Equation [115] (Equation 3.24), which is derived from first principles, as Monte Carlo is a probabilistic approach.

$$\frac{dP(c,t)}{dt} = \sum_{c' \neq c} [P(c',t)r_{c',c} - P(c,t)r_{cc'}], \quad \text{Eq. 3.24}$$

where $P(c,t)$ is the probability of finding the system in configuration c , at time t , and $r_{cc'}$ is the microscopic rate of the reaction that transfer c into c' . There are methods which are used internally by the CARLOS program to solve this equation: First-Reaction Method (FRM), Variable Step Size Method (VSSM), Random Selection Method (RSM) [115]. The First-Reaction Method (FRM) [115] is used here, which is appropriate for cases where reaction constants vary with time. According to this method, when the system is in a given configuration c , the set of all possible reactions is determined, and a time of occurrence $t_{c'c}$ is generated for each reaction i compatible with configuration c , according to Equation 3.25 [116].

$$\exp\left[-\int_t^{t_{c'c}} r_{c'c}^i(t') \cdot dt'\right] = \delta. \quad \text{Eq. 3.25}$$

In Equation 3.25, $r_{c'c}^i$ is the time dependent rate of reaction i , and δ is a random number selected uniformly in the interval (0,1). Then, the reaction with the smallest time is selected, the configuration is changed accordingly, and the time is incremented to t . Finally, the set of possible reactions is generated according to the new configuration c' ,

and the procedure is repeated. The microscopic rate r_i are related to macroscopic parameters as stated by Equation 3.26 [116]:

$$r_i = \nu_i \exp\left[-\frac{E_{ai}}{RT}\right], \quad \text{Eq. 3.26}$$

where ν_i is the prefactor, and E_{ai} is the activation energy of reaction i . In the case of electrochemical reactions, it is necessary to introduce the potential dependence of the reaction rate. In the presence of an overpotential V (defined as the difference between the actual and the equilibrium potential), the microscopic rate of a reaction r_i [117] is given by Equation 3.27.

$$r_i = \nu_i^0 \exp\left(-\frac{(E_{ai} + \alpha e_0 V)}{K_B T}\right), \quad \text{Eq. 3.27}$$

where e_0 is the charge of an electron, V is the overpotential, and α is the transfer coefficient ($\alpha = 0.5$ if the reaction consumes electrons, and $\alpha = -0.5$ if it produces) [117]. By taking the difference between the rates of reactions (reactions/unit cell/sec in our kMC output) for the reactions that produce electrons and those for the ones that consume electrons, the net electrode currents can be evaluated. From these, the polarization curves can be obtained for the fuel cell.

CHAPTER 4

MDH ACTIVE SITE MODELS

Typically, enzymes contain thousands of atoms, and studying the reactivity of enzymes using small quantum chemical clusters of say 100 atoms is one major issue in modeling enzymes [118-122]. It is considered that the catalysis occurs at the reactive cleft known as the active site of the enzyme. In order to represent this reactive portion of the enzyme, a proper model of the enzyme active site has to be chosen first [118-122]. Normally, these models start from a crystal structure of the enzyme, available from the Protein Data Base (PDB), and most computational studies are based on these structures. As a large number of calculations are involved in studying the reaction pathways, it is extremely important to keep the size of the quantum chemical model as small as possible. Also, it is crucial to choose the model in such a way that it accurately represents the chemistry taking place at the active site and no essential groups are left out [118-122].

4.1 Enzyme Cluster Models

With the aim to reduce the size of the model, the cluster approach for modeling enzymes has been employed effectively, where the residues of the active site are truncated in such a way that their side chains or important backbones are only included in the model. Especially in metalloproteins, the amino acids that bind the cofactor are essential for structure and function [123]. Both the protonated and unprotonated states of amino acids should be considered in calculations, depending on their role in the catalytic

mechanism. [118-122]. Additionally, based on available structures of enzyme-substrate complexes, several possible binding modes have to be considered. In metalloenzymes, a large part of the catalysis is influenced by the electronic structure of the metal ion and its immediate environment. To represent the correct model of a metal active site, the coordination shell of the metal ion should be included appropriately. In most instances, the first coordination shell of the metal with a solvation environment is adequate enough, but in circumstances where some second shell residues are known to affect the reactions, they are included explicitly [79, 122, 124]. The importance of a second coordination sphere of metal ion in catalytic metalloproteins lies in tuning the substrate specificity and participation in the substrate turnover. However, for simple reactions such as electron and metal transfer, the second coordination sphere is less obvious [123].

For the model to be a good representation of the enzyme and act like the actual system, two approximations are used, namely the polarizable continuum model and a coordinate-locking scheme as discussed in Chapter 3. From systematic cluster size investigations by Himo *et al.* [119-122, 124], it is clearly understood that as the model size increases, the solvation effects are reduced and a more realistic system is possible. This implies more advanced applications will be feasible. In these lines, cluster model studies have been conducted by the Mainardi group at Louisiana Tech to represent the quantum chemical model for MDH [49, 62].

4.1.1 MDH Active Site Models

Different active site models were considered with relevant amino acids to shed light on which amino acid acts as the most active catalytic base for methanol oxidation to proceed. From these methanol binding energy calculations, it was reported that Asp303

plays a key role, and a representative MDH model should contain this amino acid. Also, it was concluded that additional amino acids and water molecules in the active site model need to be included for studying the oxidation mechanism by MDH. Accordingly, the best active site model for MDH was determined as PQQ + Ion + Asp303 + Glu177 + Asn261+ 3 nearby water molecules (Figure 4.1) to provide accurate information about the reaction mechanisms [49, 62]. To validate if this active site model is sufficient enough in order to study the enzyme kinetics, larger active site models (effect of other distal amino acids) need to be studied. Essentially, the actual active site of MDH consists of 13 amino acids (Model III in this study), and comparing the binding and structural details to the smaller models to this actual active site model will provide information about the appropriate active site cluster model for studying the reaction pathways.

Taking into account these points, three models have been investigated here. To the best of our knowledge, no information has been reported so far, regarding the binding energy of methanol to these ion-modified MDH active site models. Hence, in this chapter the binding energy of methanol to the active site models is evaluated, and these binding energy calculations will provide insight into the stability of the cluster model system.

4.2 Computational Details

For evaluating the binding energy of methanol, the structure of MDH was obtained from the protein data bank (PDB) (Call No. 1w6s for MDH, respectively) [41, 43, 125, 126]. The active site of MDH is believed to consist of 13 amino acids among which 9 are polar (hydrophilic) amino acids and 4 are non-polar (hydrophobic) amino acids [37, 43, 127]. In order to understand how the binding of methanol is affected by the nature of amino acids in the active site of the MDH, in this study we have chosen the

active site models accordingly. As shown in Figures 4.1 and 4.2, Model I consists of three amino acids (Glu, Asn, Asp), Model II consists of the polar residues (Glu, Asn, Asp, Arg, Ser, Thr), and Model III consists of all 13 amino acids (polar and non-polar residues). In all the three models, the surrounding water molecules are included.

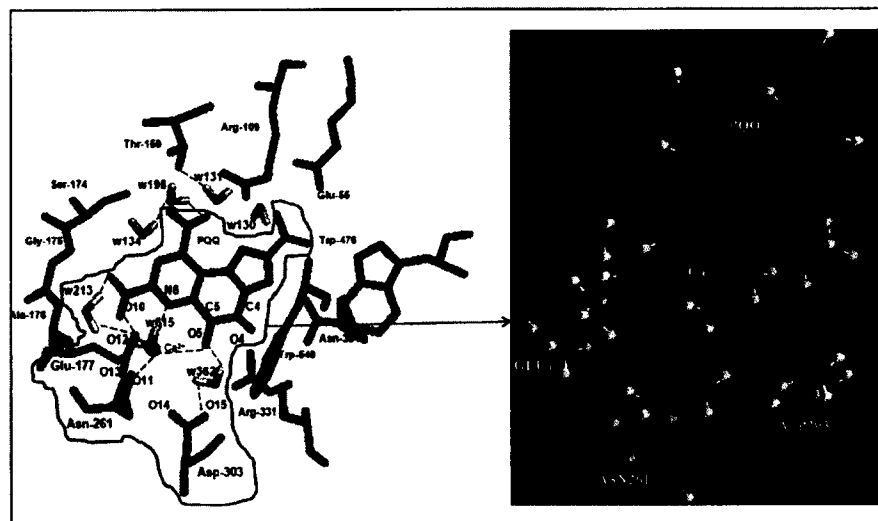


Figure 4.1: MDH Model I consisting of three amino acids (Glu, Asn, Asp) considered for investigation of Binding Energy of Methanol.

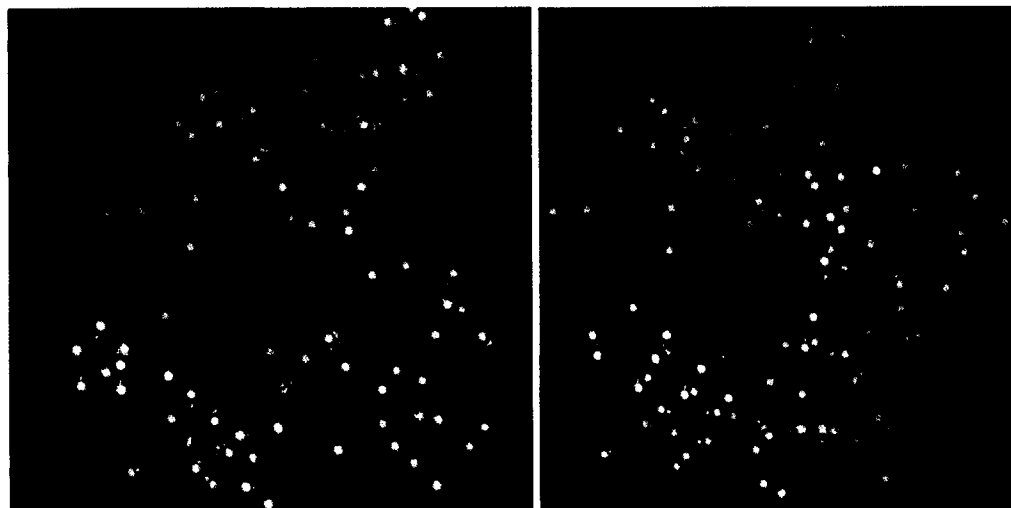


Figure 4.2: MDH Models II (9AA) and III (13AA) to investigate the Binding Energy of Methanol (Constrained Molecules are shown in Orange).

In the case of Model I, no constraints (frozen atoms) were imposed during geometry optimizations. For the other two models, few atoms were constrained to avoid unrealistic movements of the various groups in accordance with previous studies on cluster size modeling. These models are optimized using the Generalized Gradient Approximation (GGA) within the Density Functional Theory formalism as mentioned in Chapter 3 (Section 3.3) [85] to obtain the structure and energetics of MDH active site models.

To evaluate the binding energy of methanol, Equation 4.1 was applied, which is based on previous studies on substrate binding [42, 62]. According to this equation, stable systems have more negative binding energies.

$$\text{BE}(\text{Methanol}) = \text{E}(\text{Model}+\text{Methanol}) - [\text{E}(\text{Methanol})+\text{E}(\text{Model})] \quad \text{Eq. 4.1}$$

4.3 Binding of Methanol to the MDH Active Site Models

4.3.1 Model I

For the binding energy calculations, the first active site model considered is the three amino acid (3AA) model or Model I (Figure 4.1), as this active site model was sufficient enough to study the methanol oxidation mechanism, and it completes the first coordinate shell of calcium ion [49]. It can be observed from Figure 4.3 that the binding of methanol is stronger in the case of Mg^{2+} -MDH (-1.6eV) and weaker in the case of Ba^{2+} -MDH (-0.4 eV), indicating that the smaller the size of the ion, the greater the affinity for the substrate.

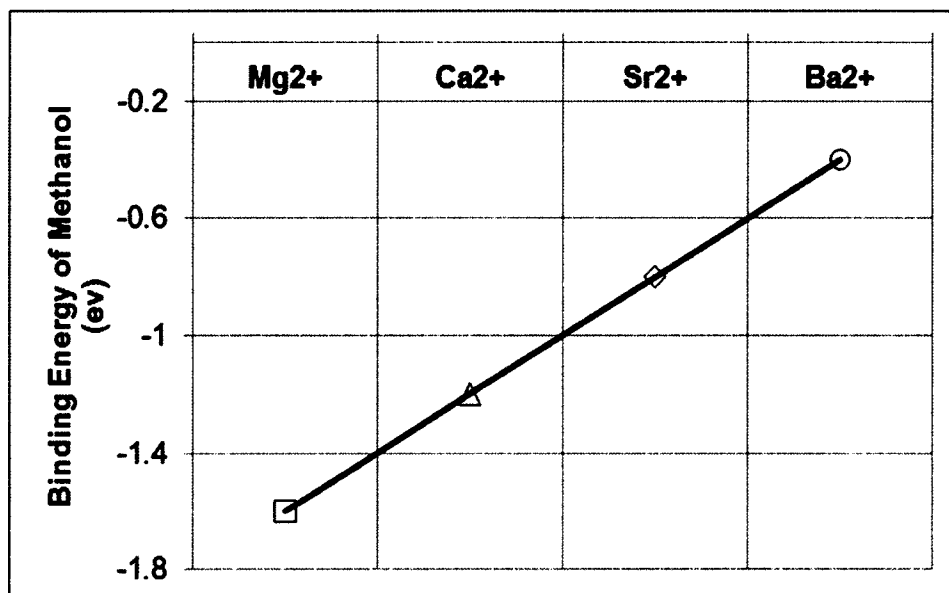


Figure 4.3: Methanol binding energies calculated at BLYP/DNP theory level for the 3AA active site models of Mg²⁺(□), Ca²⁺(Δ), Sr²⁺ (◇) and Ba²⁺ (○) containing MDH.

These results show that the affinity of Ba²⁺, Sr²⁺ and Ca²⁺ for methanol is less stable when compared to that of Mg²⁺, which is in agreement with Goodwin *et al.* [33], who suggested that replacement of Ca²⁺ with Ba²⁺ (a larger ion) in the MDH enzyme caused a decrease in the affinity for methanol. This also implies that the stability of the system depends on the Lewis acidic nature of the ion. Weaker Lewis acid (Ba²⁺) binds methanol poorly and stronger Lewis acid (Mg²⁺) binds methanol tightly. To investigate how the other residues play a role in the binding energy of the substrate (methanol), the polar and non-polar amino acids were added to this 3AA active site model and the binding energy was calculated.

4.3.2 Models II and III

It is essential to study the effect of the nature of the amino acids in the active site as these modify the orientation and binding of the substrate. For instance, in order to determine the frequency distribution of enzyme's catalytic residues, a dataset of 178

enzymes was used by Bartlett *et al.* [128]. From their study, it was observed that 65% of catalytic residues are provided by the charged amino acids (His, Arg, Lys, Glu, Asp), while 27% of catalytic residues are provided by the polar group of residues (Gln, Thr, Ser, Asn, Cys, Tyr, Trp), and just 8% are provided by the other non-polar (hydrophobic) group of residues. This trend was expected as the catalysis involves the movement of protons and electrons and charge stabilization, which require electrostatic forces provided by charged and/or polar residues [128].

In another study by Silberstein *et al.* [129] regarding the identification of the substrate binding sites in enzymes, it was believed that the presence of polar residues in the active site of an enzyme is of importance, as they facilitate the ligand to bind in different rotational/translational states. This feature also distinguishes the active site from the other regions of the enzyme because these polar groups are required for the catalytic activity and aid in providing a binding site for the substrate [129]. It is considered that the hydrophobic residue side-chains help in the catalytic activity of the enzyme by providing a neutral environment to increase the relative catalytic power of the charged functional group in the same region, or to exert the steric strain on substrates which lowers the energy of the transition state of a reaction.

In a more recent study by Kumar *et al.* [130] on the analysis of the frequency distribution of enzyme's catalytic residues belonging to different organisms and localizations, they have reported that Histidine and Aspartic acid have the highest probability occurrence as a catalytic residue among all the 13 frequently distributed amino acids, thus indicating its multiple roles at the enzymatic active site such as nucleophilic and electrophilic agent, acid and base, and stabilization of enzyme-substrate

transition state complex. In these terms, the active site residues for MDH were included accordingly and the binding energy calculations were evaluated as shown in Figure 4.4. The polar amino acids surrounding the cofactor (PQQ) and metal ion were taken into account, and the 9 AA active site model was built. Next, the complete active site amino acids, i.e. including the non-polar (hydrophobic) amino acids, 13 AA active site model was built.

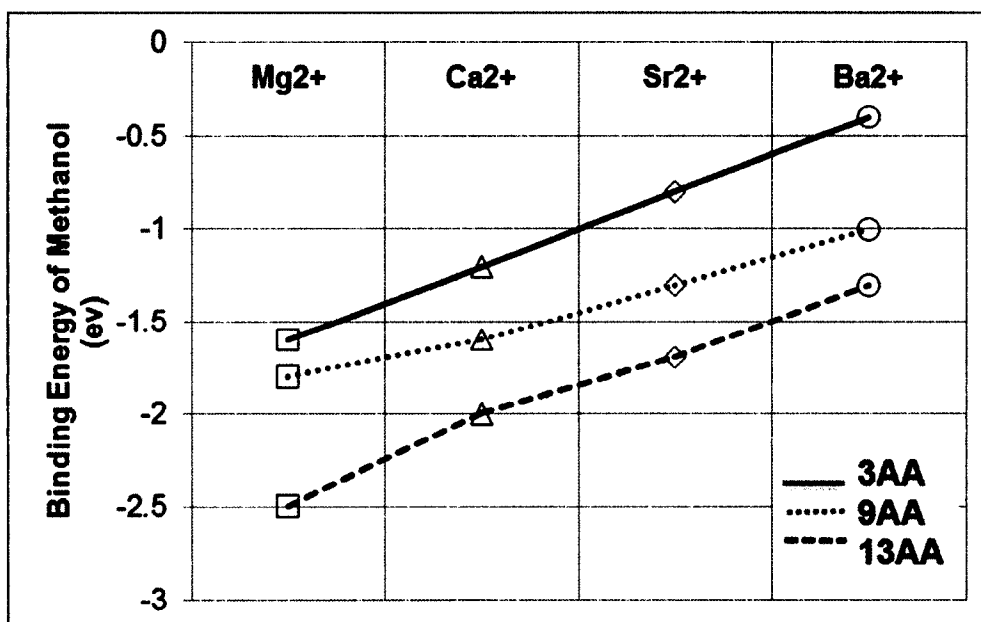


Figure 4.4: Methanol binding energies calculated at the BLYP/DNP theory level for the 3AA (Model I), 9AA (Model II) and 13AA (Model III) active site models of Mg²⁺(□), Ca²⁺(Δ), Sr²⁺(◇) and Ba²⁺(○) containing MDH.

It was observed that there is a similar trend as in the case of 3AA (Figure 4.3). The larger ion (Ba²⁺-MDH) is weakly bonded to methanol, and as the size of the ion decreased, the affinity towards methanol increased. Another study on the effect of metal ion on physicochemical properties and redox reactivity of Phenolates and Phenoxy Radicals by Itoh *et al.* [131] illustrates that the stronger the Lewis acidity of cationic species, the stronger the oxidation ability. In these terms, Mg²⁺ being a stronger Lewis

acid than Ca^{2+} may be more efficient in oxidizing methanol, or as the binding of methanol is stronger in the case of Mg^{2+} -MDH, it can be difficult to oxidize methanol. From another point of view, by experimental studies by Goodwin et al. [33], the decrease in activation energy for methanol oxidation in the case of Ba-MDH was unexpected as barium ion, being a weaker acid, was supposed to decrease the activity of MDH. These findings suggest that the Lewis acidity of the ion plays a role in the affinity and oxidation of methanol by MDH. Thus, Sr^{2+} is a slightly weaker Lewis acid than Ca^{2+} and as the binding of methanol is weak when compared to Ca^{2+} -MDH, Sr^{2+} -MDH might increase the activity of MDH by decreasing the activation energy for the methanol oxidation process.

When comparing the three active site models, the 13AA (Model III) active site is the most stable as the binding energy of methanol is around 1 eV and 0.5 eV more stable than Model I (3AA) and Model II (9AA). These results show that when the Model I active site model (3AA) consisted of only the two acidic amino acids (Asp and Glu) and a polar residue (Asn), the binding of methanol to the active site region is greater compared to that of Model II (9AA) which includes the remaining polar amino acids, and Model III (13AA) which also includes the non-polar amino acids. Model III has the lowest methanol binding energy in all the active site models (Mg^{2+} , Ca^{2+} , Sr^{2+} and Ba^{2+} - containing MDH), indicating that the hydrophobic residues (Gly, Ala and Trp) side chains enable a steric strain on substrate affinity, and provide a neutral environment to increase the catalytic power of the charged moieties, in turn aiding in the catalytic activity of the enzyme.

4.4 Structural Effects of Ion-Modified MDH

Even though the standard 20 amino acids give rise to an enormous variety of protein frameworks to promote varied chemical transformations, they cannot do everything. Many enzymes use nonstandard amino acids, either through ribosomal incorporation (such as selenocysteine or pyrrolysine) or post-translational modification (formation of pyrroloquinoline quinone, oxidation of thiols to disulfides, etc.) to increase the possibility of better chemistry at the active site [132]. In the case of cofactor-dependent enzymes, the protein scaffold provides a binding pocket with reactive residues that binds the substrate in a specific orientation with respect to the cofactor. These features promote a reaction along a particular manifold and minimize the occurrence of side reactions [132].

Similarly, in MDH (which is a PQQ dependent dehydrogenase enzyme) the molecular cleft surrounded by the quinone carbonyl at C5 (O5), the pyridine nitrogen N6, and the carboxylate group oxygen O6 of the PQQ (Figure 4.5) is considered the most suitable place for metal ion coordination in the enzyme [49, 62]. Thus, the coordination of the ions with the selected N6, O5 and O6 atoms of the PQQ are noted from the obtained minimum energy structures.

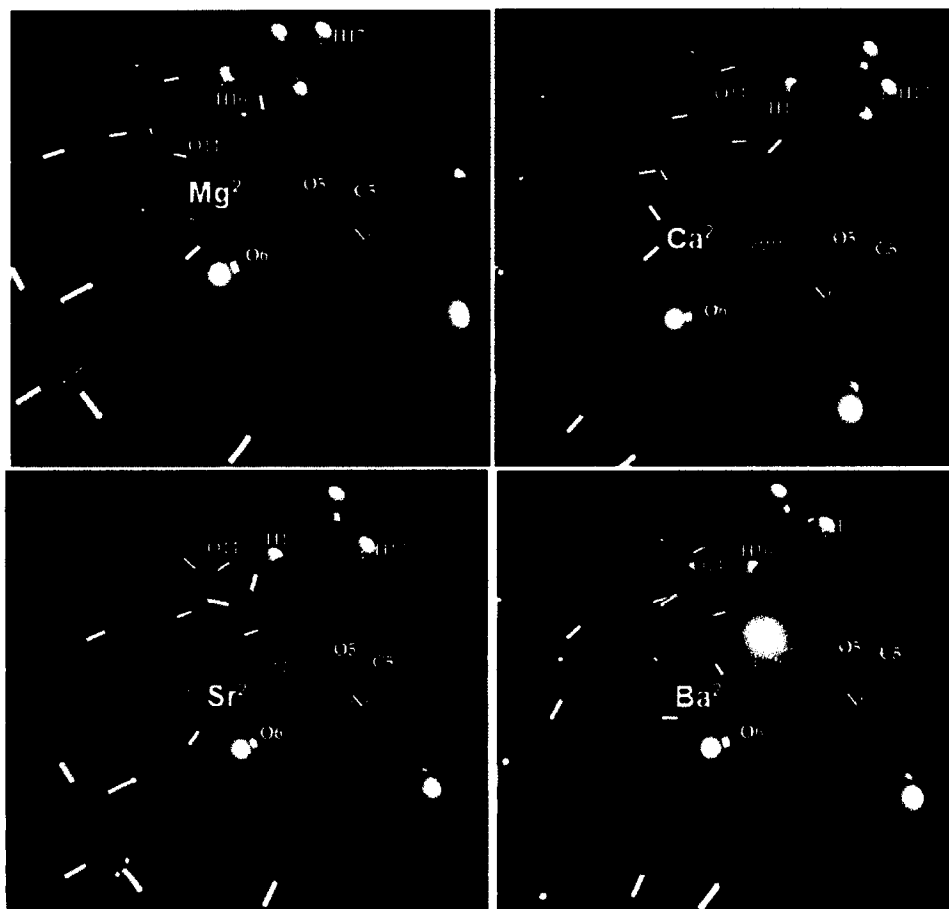


Figure 4.5: The nature of the ion in the active site of MDH modifies the binding and orientation of methanol.

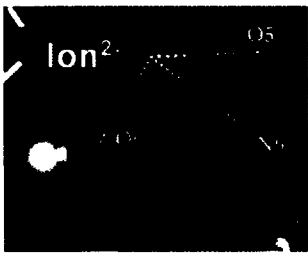
4.4.1 Ion Coordination

It is identified that there are three main functions for metals in enzymes: 1) the metal site is the actual catalytic center, 2) the metal acts as a binding group to bring the enzyme and substrates in a productive connection, and 3) the metal provokes the effects of another metal in an enzyme system [133, 134]. It is believed that metal ions contribute to orient the substrates in the active site but do not directly play a catalytic role [133, 134]. In the case of the MDH enzyme, the coordination of the ions with the selected N6, O5 and O6 atoms of the PQQ are noted from the obtained active site models (optimized

structures) and compared in order to clearly understand the contribution of these ions in the coordination of the substrate (methanol).

The bond distances of the Mg^{2+} ion to O5, O6 and N6 atoms of the PQQ have decreased from (0.1-0.4 Å) and the bond distances of the Sr^{2+} and Ba^{2+} ion to O5, O6 and N6 atoms of the PQQ have increased (0.08-0.5 Å) when compared to distances of the calcium ion to these atoms of PQQ (Table 4.1). The coordination of the ion to the O5 of PQQ is an important distance to take into account as it is considered that during the oxidation mechanism, Ca^{2+} ion acts as a Lewis acid by way of its coordination to the C5 carbonyl oxygen of PQQ. In particular, when the bond distance (Ion-O5) was compared between the three models (for all the four ions), it was witnessed that this coordination increased as the ionic size increased.

Table 4.1: Ions coordination to the O6, N6 and O5 of PQQ (bond distances in Å) obtained from BLYP/DNP calculations for MDH active site models (Model I, II and III).

	ACTIVE SITE MODELS		Mg^{2+}	Ca^{2+}	Sr^{2+}	Ba^{2+}
		3AA	O6	2.267	2.570	2.650
N6			2.141	2.603	2.767	3.057
O5			2.097	2.456	2.674	2.846
9AA		O6	2.534	2.637	2.825	3.166
		N6	2.524	2.65	2.858	3.209
		O5	2.111	2.459	2.618	2.826
13AA		O6	2.315	2.585	2.760	2.913
		N6	2.383	2.546	2.742	2.908
		O5	2.195	2.401	2.536	2.757

As shown in Figure 4.6, the decrease and the increase in distances can be attributed to the difference in the ionic radii of these ions (Mg^{2+} - Ca^{2+} = -0.27 Å, Sr^{2+} - Ca^{2+} = 0.13Å and Ba^{2+} - Ca^{2+} = 0.36Å). The same trend was observed when all three models were compared. This shows that replacement of the naturally occurring calcium ion with magnesium, strontium and barium affects the atom coordination, creating structural distortion in all three models. These results are in agreement with previous studies by Idupulapati *et al.* [62] on the MDH active site models, where coordination and binding effects by replacing calcium ion by barium ion at B3PW91/6-311+G** theory level were studied. It was reported that the bond lengths Ba^{2+} -O5, Ba^{2+} -O6 and Ba^{2+} -N6 were 0.37, 0.40 and 0.53 Å larger than the corresponding ones in the Ca^{2+} -MDH models, and it was concluded that the increase in bond distances is mainly due to the ionic size of Ba and that the nature of ion modifies the orientation and binding of methanol to MDH active site.

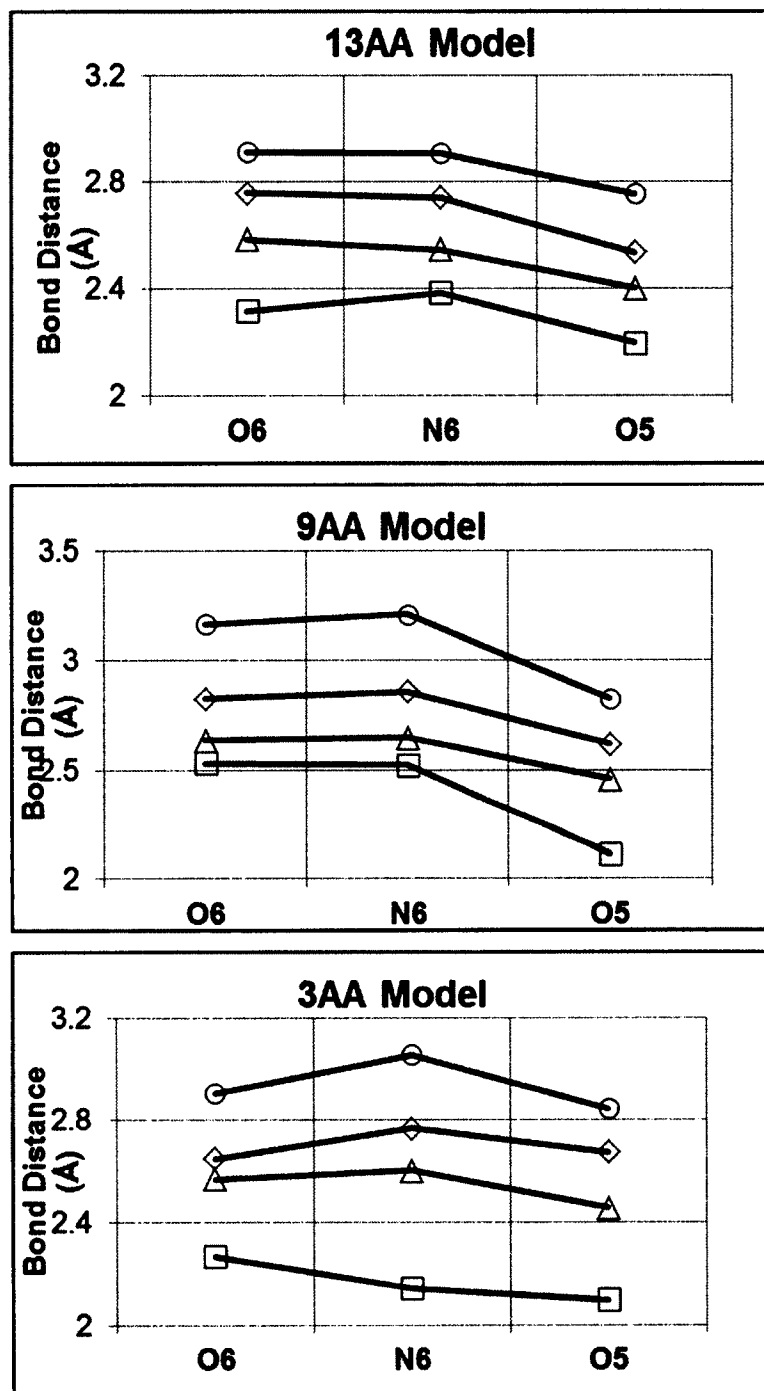


Figure 4.6: Bond lengths (Ion – O6, N6 and O5) obtained from BLYP/DNP calculations for Mg²⁺ (□), Ca²⁺ (△), Sr²⁺ (◇) and Ba²⁺ (○) containing MDH active site models (Model I, II and III).

4.4.2 Ion Coordination and Binding Energy

To verify that the 3AA model is an appropriate cluster model to study the methanol reaction pathways, it is important to understand the ion coordination with respect to the binding of the substrate to the three active site models in consideration. Taking into account this point, a plot between the average bond distances noted in Table 4.1 for each ion-modified enzyme versus the binding energies calculated for the three active site model is shown in Figure 4.7.

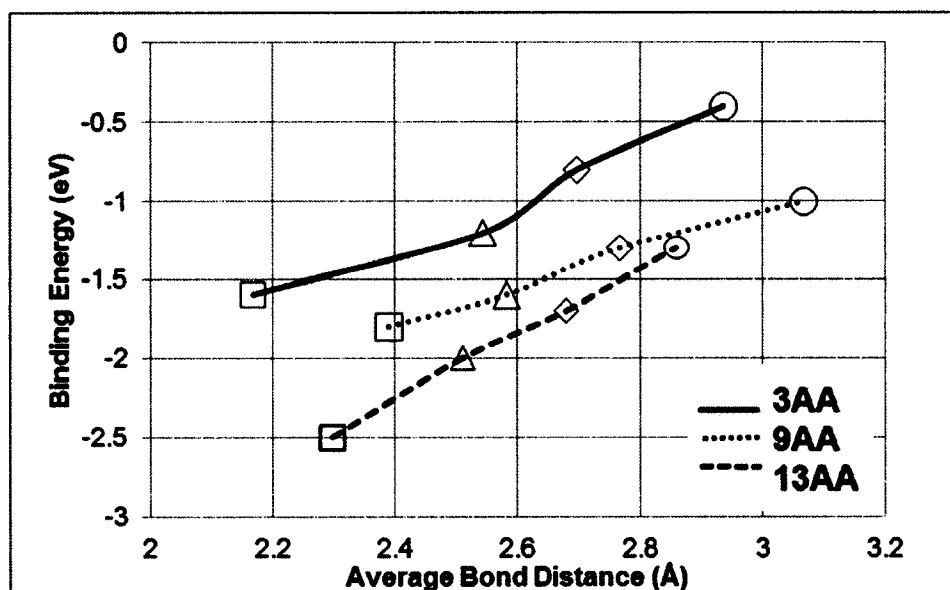


Figure 4.7: Binding Energy versus Average values of Ion Coordination lengths (Ion – O6, N6 and O5) obtained from BLYP/DNP calculations for Mg^{2+} (\square), Ca^{2+} (Δ), Sr^{2+} (\diamond) and Ba^{2+} (\circ) containing MDH active site models (Model I, II and III).

From the graph (Figure 4.7), we can interpret that the 3AA model average bond distances is in close correlation with the 13AA model with respect to the binding energy values. Even though the binding of methanol is weaker in the case of 3AA cluster model, the ion coordination average distances follow a similar trend as seen in the 13AA active site model and are within the experimental range. This shows that the 3AA active site

model is appropriate to study the methanol oxidation reaction mechanisms. The major difference is in the case of the 9AA model, which does not follow the complete active site model (13AA) trend. There is a shift in this case which could be due to the fact just the polar residues do not enable a steric effect to hold the ion in place for a better coordination and causes distortion.

4.4.3 Substrate Coordination

As it is considered that the orientation of the substrate is also affected by replacing the naturally occurring ion, the bond lengths H17-C5 and H16-O14 are noted for the modified MDH active site models (Figure 4.8 and Figure 4.9).

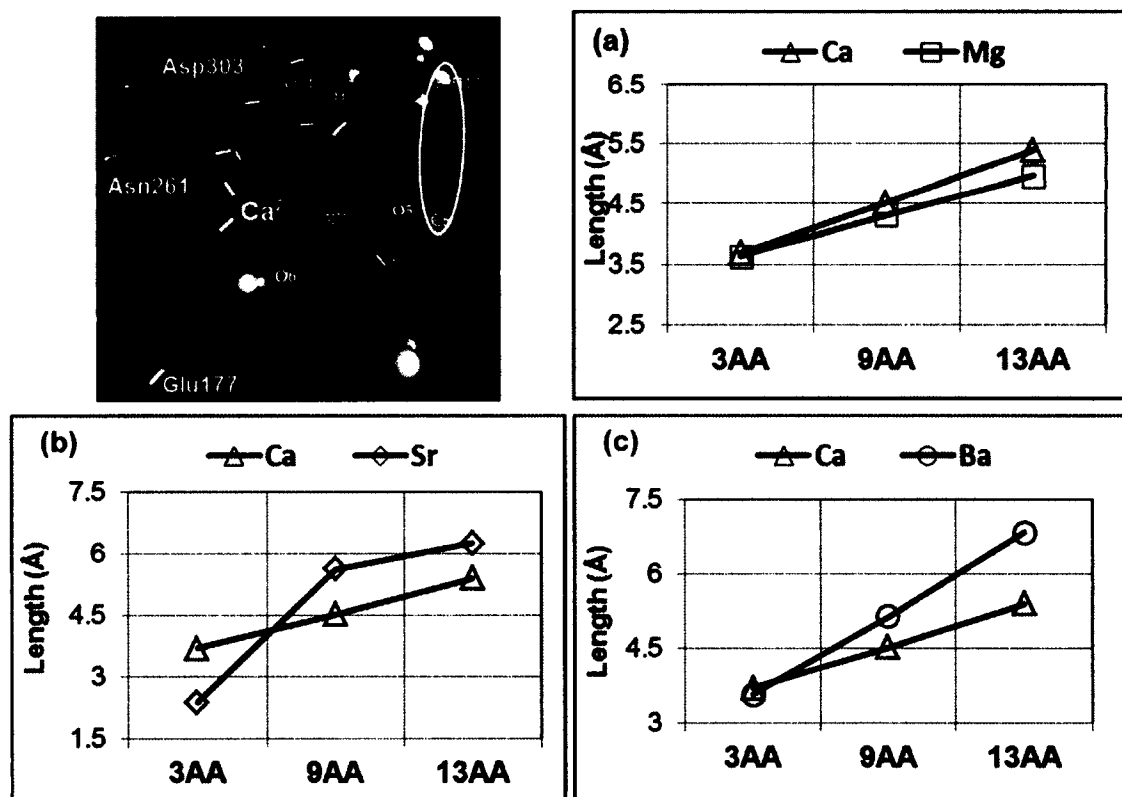


Figure 4.8: Bond distance H17-C5 compared for Ion-Modified MDH active site models (Model I, II and III). (Top left Figure insert shows the distance in consideration)

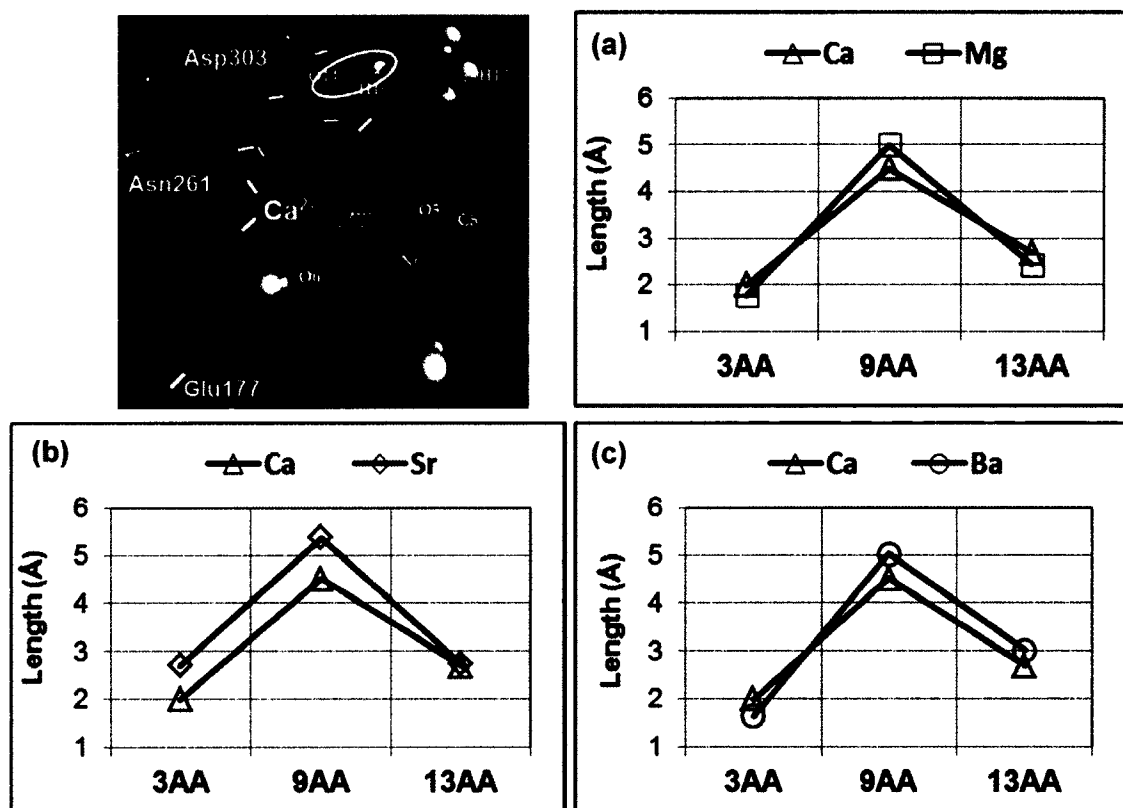


Figure 4.9: Bond distance H16-O14 compared for Ion-Modified MDH active site models (Model I, II and III). (Top left Figure insert shows the distance in consideration)

These two bond distances were considered in particular, as the experimental results predict that hydroxyl of methanol is close enough to be hydrogen bonded to the side chain of Asp303, and the methyl group is near to the C5 of PQQ. In our models, H17 and H16 are the two protons being transferred in the first step of the H-T mechanism (Figure 2b).

Understanding the effect of the ion on these distances will provide insight into the proton abstraction, and which ion facilitates the oxidation mechanism efficiently. From Figure 4.8, it can be seen that the distance H17-C5 is less (1.31Å) in Sr²⁺-MDH for Model I (Figure 4.8b), indicating that the proton, H17, is transferred easily to C5 than in the case of Ba²⁺, Ca²⁺ and Mg²⁺-MDH. When these distances (H17-C5 and H16-O14)

were compared for the three models (Model I, Model II and Model III), it was observed that the main differences between these models lies in the H16-O14 distance (Figure 4.9).

Especially in Model II (9AA), the H16-O14 bond distance is higher by almost 2-3 Å than the other two models (Model I and Model III) irrespective of the ion present in the active site. This implies that the nature of amino acids also plays a major role in the orientation of the substrate (methanol). The Model I configuration is the one for which these distances are the lowest and these distances are close (~ 0.04 - 1.0 Å) to the case of Model III. These structural effects analysis shows that Model I is an appropriate active site cluster model to further study the methanol oxidation mechanism as the distances are in close correlation with the 13 AA model, which is considered the real active site from experimental studies.

4.5 Conclusions

From the binding energy values and analysis on the coordination of the methanol, it is observed that as the size of the ion increases ($Mg^{2+} < Ca^{2+} < Sr^{2+} < Ba^{2+}$), the binding of methanol becomes weaker, indicating that the oxidation of methanol can be facilitated when a larger ion is present in the active site of MDH. This trend is in accordance with earlier studies on affinity and binding of methanol to the MDH active site [33, 62].

By exploring the structural effects of the ion-modified MDH active sites, it can be concluded that the replacement of the naturally occurring calcium ion with magnesium, strontium and barium affects the atom coordination, creating structural distortion in all the three MDH active site models. Also, it ascertains that Model I is an appropriate active site cluster model to investigate the methanol oxidation pathway as the ion first-shell coordination sphere is complete in the case of Model I.

To understand thoroughly what is happening during the methanol oxidation by replacing the naturally occurring ion, these binding energy calculations have given insight about the affinity of the substrate to these MDH active site models. These aspects will help investigate the methanol oxidation mechanism with Sr^{2+} and Mg^{2+} -containing MDH, and thus, it is studied next.

CHAPTER 5

METHANOL OXIDATION OF ION-MODIFIED MDH ENZYMES

In this chapter, the methanol oxidation by the ion-modified MDH enzymes is studied. As the first step is to build an enzyme cluster model to study the reaction pathways, Model I active site model is considered based on previous chapter result analysis, where it was established that Model I is an appropriate active site cluster model. It was shown from those results that the structural variations in the case of Model III (complete active site) and Model I are in close correlation. Especially the ions coordinated with the N6, O6 and O5 atoms of PQQ and H16-O14 (methanol orientation) distances in both the models are in close range and can be concluded that 3AA model can represent the actual active site model (13AA) to explore the methanol oxidation mechanism.

Also, based on previous studies on MDH active site by Idupulapati *et al.* [49, 135], who reported that the three amino acids (Glu, Asn and Asp) and the surrounding water molecules' active site cluster (Model I) was considered acceptable for the methanol oxidation mechanism calculations as the ion first-shell coordination sphere is complete in this case. Thus, in order to investigate the proposed H-T methanol oxidation mechanism by Mg^{2+} and Sr^{2+} -containing MDH and to compare with the theoretical studies on Ca^{2+} -containing MDH by Idupulapati *et al.* [49,135], Model I's MDH active site model as

shown in Figure 5.1 is considered to reduce the number of atoms to conduct accurate electronic structure calculations.

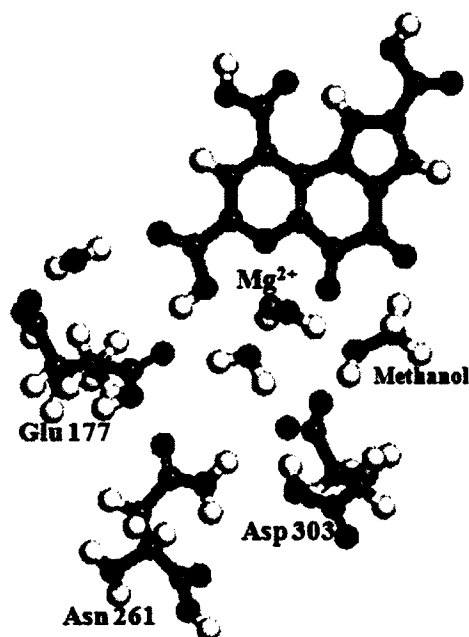


Figure 5.1: Active site model selected for Mg^{2+} -MDH.

5.1 Enzyme Model and Computational Details

According to the approach presented by Himo *et al.*[118, 136], unprotonated (charged) amino acids can be modeled by their corresponding protonated (neutral) amino acids. This approach has been tested by Himo *et al.*, and well justified by the fact that proteins and enzymes have low dielectric constants ($\epsilon \sim 4$), indicating that charge separation, if present, should be very small. These authors have shown that by using these charge-neutral models, accurate enzymatic reaction energies and barriers were yielded [118, 136].

The role of Glu177 in the methanol oxidation mechanism is unclear; thus, to shed light into the role of Glu177, quantum mechanical calculations on models representing the active sites of Ca^{2+} - and Ba^{2+} -containing MDH in the presence of methanol at the

B3PW91/6-311+G** theory level were performed by Idupulapati *et al.* [62]. They have reported that there is a need for the presence of Asp303 in the active site model for aiding as a base catalyst for methanol oxidation, and they also emphasized the necessity of additional neighboring amino acids, such as Asn261 and Glu177, in the active site model to be considered for better ion coordination; the results provided extra confidence for fully protonating Glu177 and Asn261 in this study. On the other hand, in the case of Asp303, aspartic acid was used, but the carboxylic group (the one facing the Ca^{2+} ion in Figure 5.1) was kept as such, COO^- , since this group is indeed involved in the proposed proton transfer reactions.

However, a more detailed assessment of all protonation states of the charged active site model residues (Glu and Asp) was made using PROPKA program (a protein pKa predictor) [137]. The analysis showed that Asp303 has a pKa value of 3.4 and Glu177 has a value of 6.3. In principle, it is considered that when the pH of the system is higher than the pKa value of a residue, the unprotonated form of the amino acids should be used. In the case of MDH, the enzyme is active in the pH range of 8-9. Thus, Asp303 and Glu177 should be in their charged form. However, to reduce the complexity of the system and considering the fact that Asp303 is the catalytic base for initiating the proton transfer, Glu177 is assumed to be in its protonated form. Asn261 is an uncharged polar amino acid, so it is assumed to be in its normal state.

The active site model corresponding to Mg^{2+} and Sr^{2+} ions instead of the naturally occurring Ca^{2+} in the MDH active site was tested upon the methanol oxidation mechanism (shown for Ca^{2+} -MDH in Figure 2.3a and Figure 2.3b). The reactant, intermediates, and product for all the steps of the mechanisms were optimized at the

BLYP/DNP theory level and solvation effects were included with a dielectric constant of 4 to represent the protein environment. The transition states were obtained for each step of the mechanism and the energies, representative bond distances, and free energy barriers were compared to the ones obtained for the naturally occurring Ca^{2+} -MDH. The computational details mentioned in Chapter 3 (Section 3.3) to study the H-T methanol oxidation mechanisms by Mg^{2+} and Sr^{2+} containing MDH.

5.2 Local Minima Conformations

Once the active site model of the enzyme is prepared, the next step is to study the enzyme reaction in this model. As mentioned in Chapter 3, one of the main reasons to computationally study enzyme reactions is that they provide information about the transition state complex that is not accessible by experiments due to their short lifetime and complexity involved, but they are very important for understanding the reactivity of the enzyme. To model the reaction pathways in enzymes, various simulation techniques have been applied. To obtain the potential energy profile or minimum energy pathway (MEP), the energy of the system should be minimized at several points along the reaction coordinate. The highest energy point on this MEP represents the TS structure. It is preferred that multiple enzyme-substrate conformations be considered when MEPs are calculated because TS structures and the barriers for different starting conformations can differ significantly [138].

Thus, in order to obtain accurate results, diverse possible arrangements of the reactant, intermediates, and product were investigated, and several optimized energy configurations along the real potential energy surface of the molecular system were found. The best three minima configurations for reactant, intermediates, and product are

reported in Figure 5.2. The free energies obtained for the different minima were compared and only the ground state conformations (Figure 5.2 *a*, *d*, *g*, *j*, and *m*) were considered for calculating transition state structures. Plots shown in Figure 5.3 illustrate variations in selected bond lengths for the three best conformations reported for reactant, intermediates, and product.

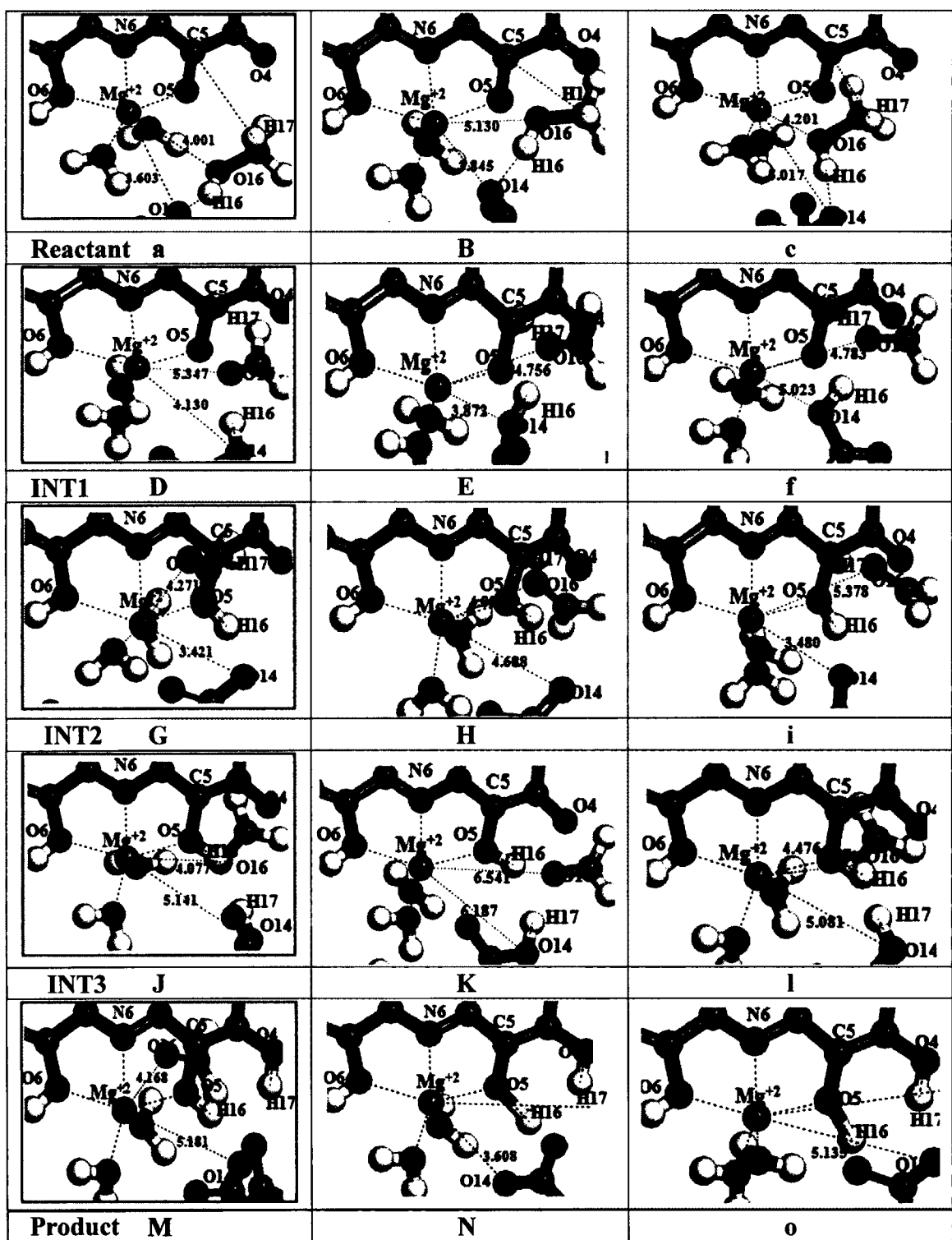


Figure 5.2: Best three minima configurations for the reactant, intermediates, and product of the Hydride-Transfer methanol oxidation mechanism by for Mg^{2+} -MDH obtained at the BLYP/DNP theory level.

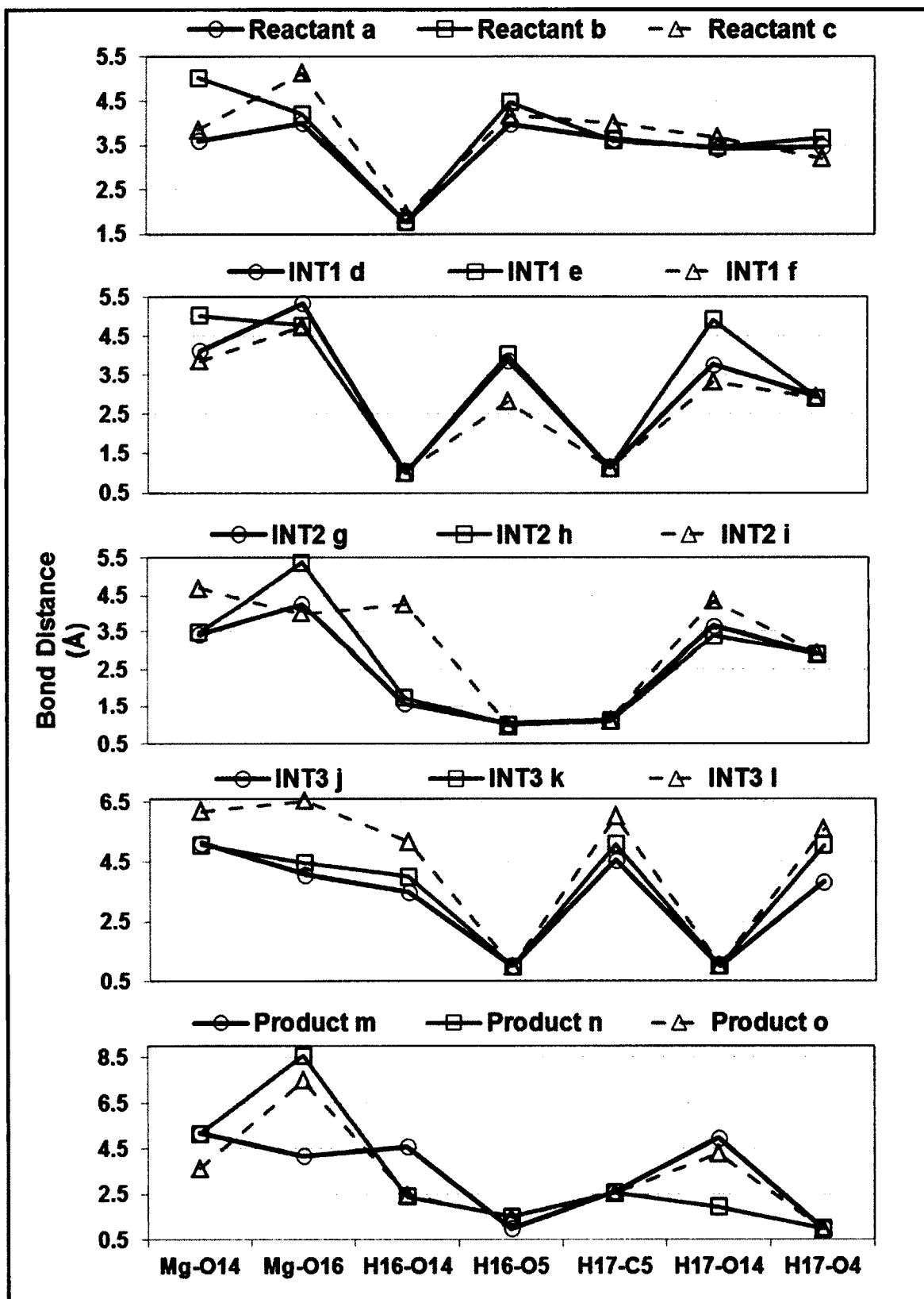


Figure 5.3: Structural variations in selected bond lengths for the three best conformations shown in Figure 5.2.

The best three stable Reactant conformations are shown in Figure 5.2*a-c*. The Reactant shown in Figure 5.2*a* is the most stable Reactant configuration when compared to the other two isomers (Figure 5.2*b* and *c*), which are 2.4 and 3.7 Kcal/mol less stable than the Reactant (Figure 5.2*a*), respectively. The main differences between configurations *a*, *b* and *c* lie in the Mg²⁺-O14 and Mg²⁺-O16 distances (Figure 4). The most stable Reactant configuration (Figure 5.2*a*) is the one for which those distances are the lowest (Figure 5.3) with values of 3.60 and 4.00 Å, respectively.

In the case of Intermediate 1, among the three stable conformations (Figure 5.2*d-f*), the intermediate structure shown in Figure 5.2*d* (INT1) is the most stable configuration compared to its other two conformers (Figure 5.2*e* and *f*), which are 0.9 and 3.4 Kcal/mol less stable than the most stable case. These configurations show differences for several distances, and particularly for Mg²⁺-O14, Mg²⁺-O16, H16-O5, and H17-O14 (Figure 5.3).

For Intermediate 2 (Figure 5.2*g-i*), the most stable configuration is INT2 (*g*) when compared to the other two isomers (Figure 5.2*h* and *i*), which are 0.1 and 7.5 Kcal/mol less stable than that of Figure 5.2*g*, respectively. The main differences between configurations *g*, *h* and *i* lie in the distances Mg²⁺-O14, Mg²⁺-O16, H16-O14, and H17-O14 (Figure 5.3).

From the best three configurations found for Intermediate 3 (Figure 5.2*j-l*), the most stable configuration (INT 3) is the one shown in Figure 5.2*j*. The other two isomers (Figure 5.2*k* and *l*) are 0.2 and 4.6 Kcal/mol less stable than INT3. The differences between these configurations are significant, particularly for Mg²⁺-O14, Mg²⁺-O16, H16-

O14, H17-C5, and H17-O4 (Figure 5.3). The most stable conformation of INT 3 is the one for which those distances are the smallest.

In the case of the product, among the three stable conformations (Figure 5.2m-o), the structure shown in Figure 5.2m has the most stable configuration compared with the other two conformers (Figure 5.2n and o), which are 5.2 and 5.3 Kcal/mol less stable than that in Figure 5.2m. Structural differences are very significant for these three structures (Figure 5.3), particularly for Mg^{2+} -O16 and H17-O14. The most stable conformation of INT 3 is the one for which those distances are the smallest and largest, respectively. Mg^{2+} -O16 is 4.17, 8.57, and 7.47 Å, and H17-O14 is 4.96, 1.93, and 4.27 Å for the configurations of Figure 5.2m, n, and o in that order.

In the case of the product, among the three stable conformations (Figure 5.2m-o), the structure shown in Figure 5.2m has the most stable configuration compared with the other two conformers (Figure 5.2n and o), which are 5.2 and 5.3 Kcal/mol less stable than that in Figure 5.2m. Structural differences are very significant for these three structures (Figure 5.3), particularly for Mg^{2+} -O16 and H17-O14. The most stable conformation of INT 3 is the one for which those distances are the smallest and largest, respectively. Mg^{2+} -O16 is 4.17, 8.57, and 7.47 Å, and H17-O14 is 4.96, 1.93, and 4.27 Å for the configurations of Figure 5.2m, n, and o in that order.

In the same way as in Mg^{2+} -MDH, to obtain accurate results, diverse possible arrangements of the reactant, intermediates and product were investigated for Sr^{2+} -MDH, and several optimized energy configurations along the real potential energy surface of the molecular system were found. The ground state configurations were used to investigate the transition states.

5.3 Structural Effects of Ion in the MDH Active Site

The geometries of the reactant, intermediates and product of Mg^{2+} and Sr^{2+} containing MDH models are within the experimentally observed configurations of Ca^{2+} -MDH [39]; however, structural distortion is observed by the replacement of the metal ion in the MDH active site (Figure 5.4). The molecular cleft surrounded by the quinone carbonyl at C5 (O5), the pyridine nitrogen N6 and the carboxylate group oxygen O6 of the PQQ (Figure 5.1) is considered the most suitable place for metal ion coordination in the enzyme [49, 62]. Thus, the coordination of the ions with the selected N6, O5 and O6 atoms of the PQQ are noted from the obtained minimum energy structures and compared to Ca^{2+} -MDH coordination. The bond distances of the Mg^{2+} ion to O5, O6 and N6 atoms of the PQQ has decreased ($\sim 0.33 \text{ \AA}$) and the bond distances of the Sr^{2+} ion to O5, O6 and N6 atoms of the PQQ has increased ($\sim 0.24 \text{ \AA}$) when compared to distances of the calcium ion to these atoms of PQQ (Figure 5.4).

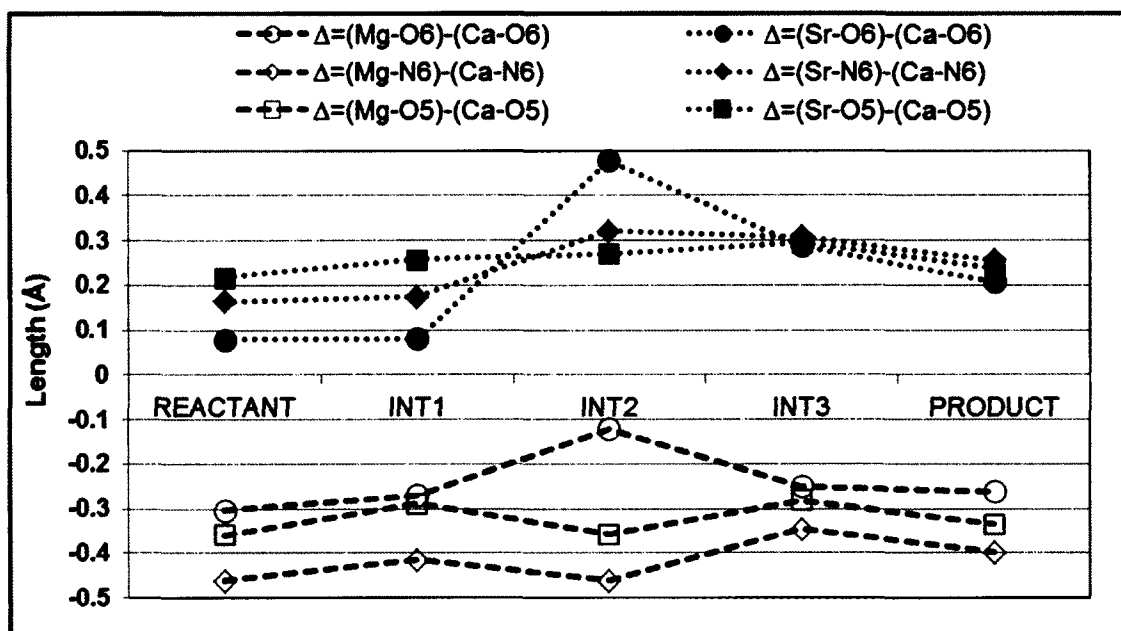


Figure 5.4: Bond length differences obtained from BLYP/DNP calculations for Ion-Modified MDH active site models.

As magnesium has an ionic radius of 0.66 Å which is smaller than the Calcium ion radius (0.99 Å) and strontium has an ionic radius of 1.13 Å, which is greater than the Calcium ion. As shown in Figure 4, the decrease and the increase in distances can be attributed to the difference in the ionic radii of these ions ($Mg^{2+} - Ca^{2+} = -0.27$ Å, $Sr^{2+} - Ca^{2+} = 0.13$ Å). This shows that replacement of the naturally occurring calcium ion with magnesium and strontium affects the atom coordination, creating structural distortion (as discussed in Chapter 4).

In order to shed light into the methanol oxidation mechanism that actually operates at the active site of Ca^{2+} -MDH, several experimental and theoretical studies have been conducted as mentioned earlier in Chapter 2 [33, 39, 50, 51]. To state the examples, Kay *et al.* [57], from their electron paramagnetic resonance studies on substrate binding in ethanol dehydrogenase, eliminated the possibility of the A-E mechanism, because that process is an energetically expensive pathway leading to the breaking of the strong coordination of the substrate and the calcium cation. Also, considering the conformational variations of the active site residues of the MDH enzyme, recent studies have supported the hydride transfer mechanism [53-56], as shown by Zheng *et al.*[139] using crystallographic and theoretical studies favor the H-T mechanism. In a more recent (2011) study by Li *et al.* [58], show that the possibility of the C5-reduced PQQ intermediate is more likely during the methanol oxidation reaction by MDH. Hence, this lends support to the hydride transfer mechanism. Thus, in the present study, we have considered the H-T mechanism and the alternate H-T mechanism.

5.4 H-T Mechanism by Mg^{2+} -MDH and Sr^{2+} -MDH

The ground state conformations corresponding to the reactant, intermediates and product of the Hydride transfer methanol oxidation mechanism by Mg^{2+} -MDH and Sr^{2+} -MDH were next considered for calculating transition state structures along the reaction pathway. Free energy barriers were calculated and compared to those reported in the literature for the H-T methanol oxidation mechanism by Ca^{2+} -MDH [49, 62].

5.4.1 Step 1: $PQQ \rightarrow PQQH^-$

In this step, PQQ oxidized form is converted to $PQQH^-$ by the hydride (H17) transfer from methanol to the C5 of PQQ, and the H16 proton abstraction from methanol to Asp-303 occur simultaneously forming formaldehyde. Thus, the intermediate (INT1) is evolved through the first transition state, TS1 (Figure 5.5).

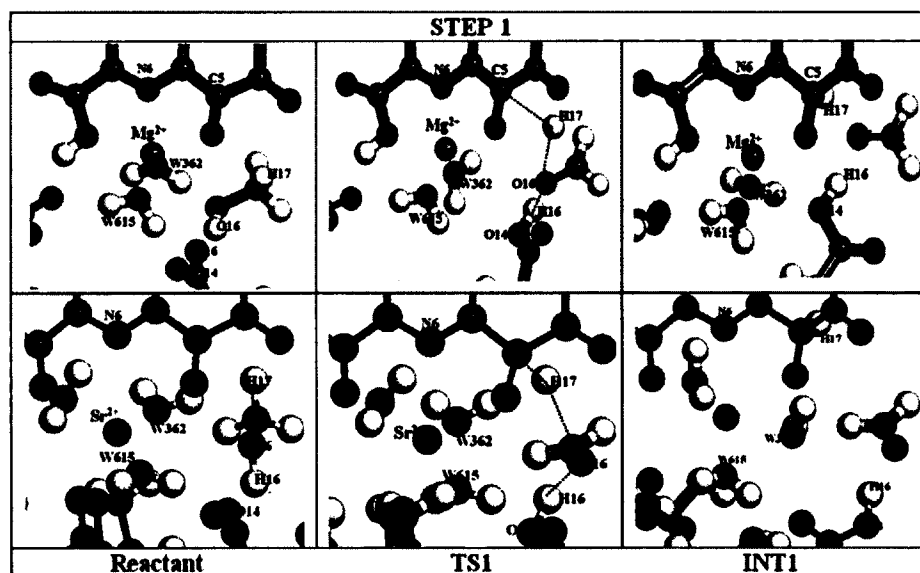


Figure 5.5: Optimized structures obtained at BLYP/DNP theory level involved in Step 1 of the H-T mechanism for Mg^{2+} -MDH (Top Set) and Sr^{2+} -MDH (Bottom Set).

The C5-H17 bond length was reduced from Reactant to TS1 and finally to INT1, and the bond length O14-H16 evolved from the Reactant to TS1, and finally to INT1, showing the abstraction of the proton H16 by Asp-303 (Figure 5.5). The relevant bond distances for the TS1 are noted and compared (Figure 5.6).

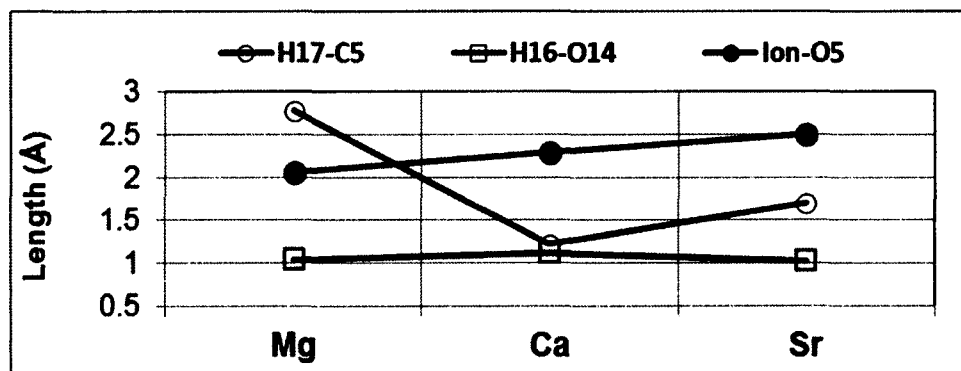


Figure 5.6: TS1 bond distances comparison between the Mg^{2+} -MDH, Ca^{2+} -MDH and Sr^{2+} -MDH active site models at BLYP/DNP theory level.

The H17-C5 is higher by 1.5 Å in the case of Mg-MDH when compared to Ca^{2+} -MDH and higher by 1.1 Å when compared to Sr^{2+} -MDH, suggesting that it takes greater energy for the proton to transfer to C5 of PQQ. Also, noting the distance Ion-O5 (Figure 5.6), it indicates that as the size of ion increases ($Sr^{2+} > Ca^{2+} > Mg^{2+}$), the Ion-O5 bond length increases, implying that the smaller ion (Mg^{2+}) attracts the oxygen O5 of PQQ closer to form a strong bond, and this in turn affects the transfer of H17 to C5 of PQQ.

As the proton transfer from methanol becomes difficult, this influences the energy barrier and for Mg^{2+} -MDH the free energy barrier for step 1 was calculated to be 22.2 kcal/mol, which is 2.5 kcal/mol higher than the corresponding barrier obtained for the case of Ca^{2+} -MDH (19.7 kcal/mol for Ca^{2+} -MDH) [62]. In the case of Sr^{2+} -MDH, the free energy barrier for this step was calculated to be 6.8 kcal/mol (12.9 kcal/mol) lower than the Ca^{2+} -MDH and close to the experimental activation energy (7.6 kcal/mol) value for

Sr^{2+} -MDH. The reason the free energy barrier is higher for Mg^{2+} -MDH and is lower for Sr^{2+} -MDH compared to that of the naturally occurring MDH (Ca^{2+} -MDH) can also be due to the fact that Mg^{2+} could not polarize the C5-O5 bond as Sr^{2+} and Ba^{2+} [49], thus resulting in less negative charge on the oxyanion O5 of PQQ and effecting the proton abstraction process.

5.4.2 Step 2: $\text{PQQH}^- \rightarrow \text{PQQH}$

According to this step, a proton is transferred from Asp-303 to O5 of PQQ resulting in the formation of the second intermediate (INT2) and semi quinone (PQQH) form of PQQ. The transition state (TS2) for this step showed that the proton is still attached to the O14 of the Asp-303 with $\text{H16-O5} = 2.09 \text{ \AA}$ and $\text{H16-O14} = 1.00 \text{ \AA}$ in the case Mg^{2+} -MDH. For Sr^{2+} -MDH, the H16 proton is in an intermediate position with $\text{H16-O5} = 2.76 \text{ \AA}$ and $\text{H16-O14} = 2.47 \text{ \AA}$ (Figure 5.7).

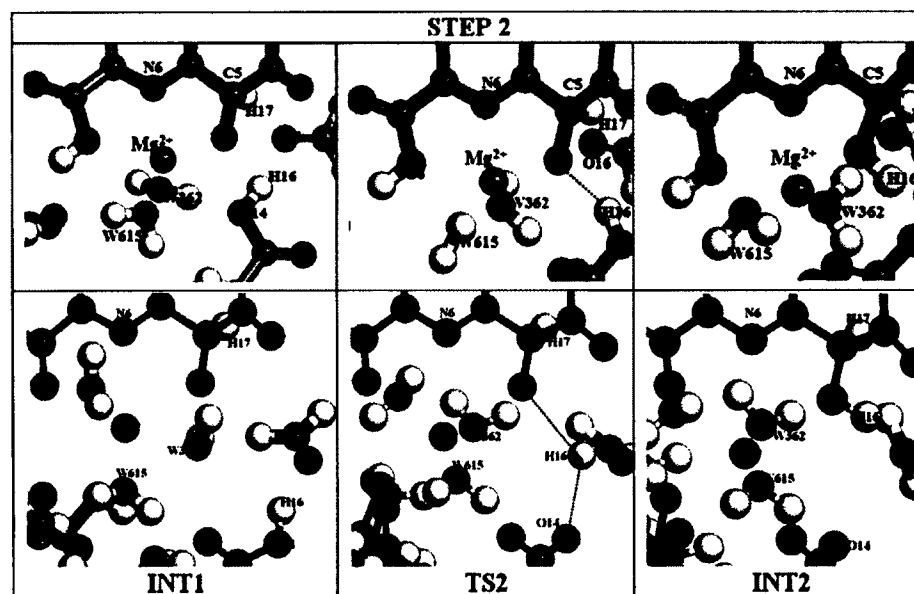


Figure 5.7: Optimized structures obtained at BLYP/DNP theory level involved in Step 2 of the H-T mechanism for Mg^{2+} -MDH (Top Set) and Sr^{2+} -MDH (Bottom Set).

These distances are compared to Ca-MDH in Figure 5.8. In the case Mg^{2+} -MDH and Sr^{2+} -MDH, the free energy barrier for this step is 8.0 kcal/mol and 8.6 kcal/mol, which is 5.1 kcal/mol and 5.7 kcal/mol higher than the corresponding barrier obtained for the case of Ca^{2+} -MDH [49].

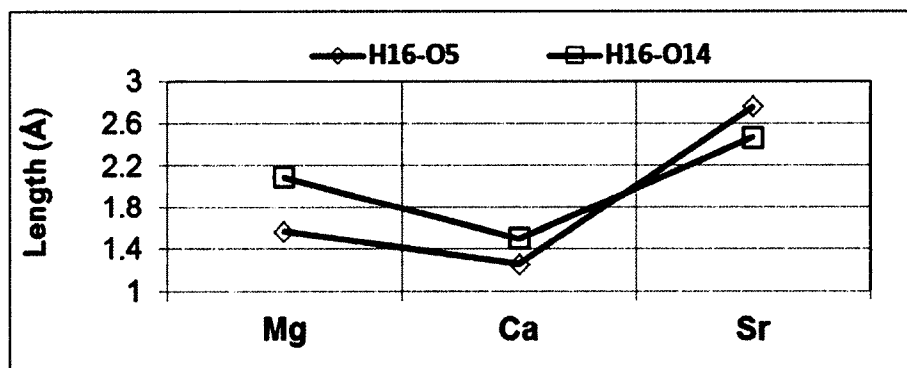


Figure 5.8: TS2 bond distances comparison between the Mg^{2+} -MDH, Ca^{2+} -MDH and Sr^{2+} -MDH active site models at BLYP/DNP theory level.

5.4.3 Step 3: PQQH → PQQH^{-*}

The third step involves the transfer of H17 proton from C5 of PQQ to O14 of Asp-303 and the formation of PQQH^{-*} complex (*implies that this complex is not similar to the PQQH⁻ complex as in Step 1 and that in this case it is in its semiquinone form). The transition state for this step showed an intermediate location of H17 from the C5 of PQQ to the O14 of Asp-303, with H17-O14 bond length decreasing from INT 2 to TS3 to INT3, and the H17-C5 distance increasing from INT 2 to TS 3 to INT 3 for both cases (Mg^{2+} and Sr^{2+} -MDH) as shown in Figure 5.9. For this step, the free energy barrier obtained for Mg^{2+} -MDH was 36.6 kcal/mol and for Sr^{2+} -MDH was 28.0 kcal/mol, showing that this step may be the rate determining step as the energy barrier is highest, but this is kinetically not feasible as the barrier value is above the general kinetic requirements of an enzymatic catalytic process (energy barriers are expected to be less than or around 18 kcal/mol [48]). Additionally, the free energy barrier for this step are

higher than the corresponding barrier obtained for the case of Ca^{2+} -MDH [49] at the theory level of this work.

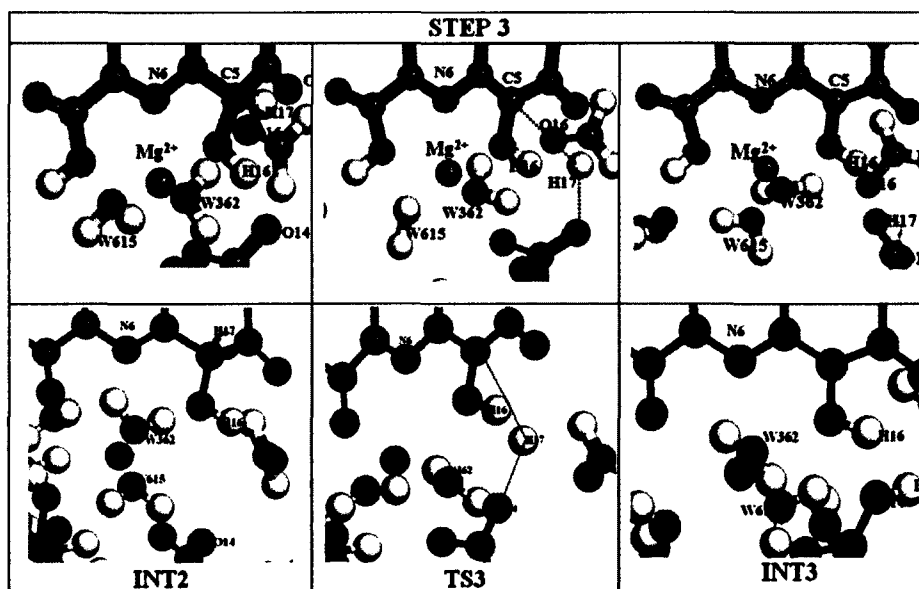


Figure 5.9: Optimized structures obtained at BLYP/DNP theory level involved in Step 3 of the H-T mechanism for Mg^{2+} -MDH (Top Set) and Sr^{2+} -MDH (Bottom Set).

It is interesting to notice that the energies of INT 2 and INT 3 are practically the same for both the modified MDH models, considering the typical error when BLYP is used in combination with DNP (first decimal place in kcal/mol), and therefore, these results indicate that the second proton (H17) transfer of the H-T methanol oxidation mechanism by Mg^{2+} and Sr^{2+} containing MDH is not taking place, since it might be unnecessary due to the closer proximity of the ion and other MDH active site components. The comparison of the H17-O14 and H17-C5 distances are shown in Figure 5.10.

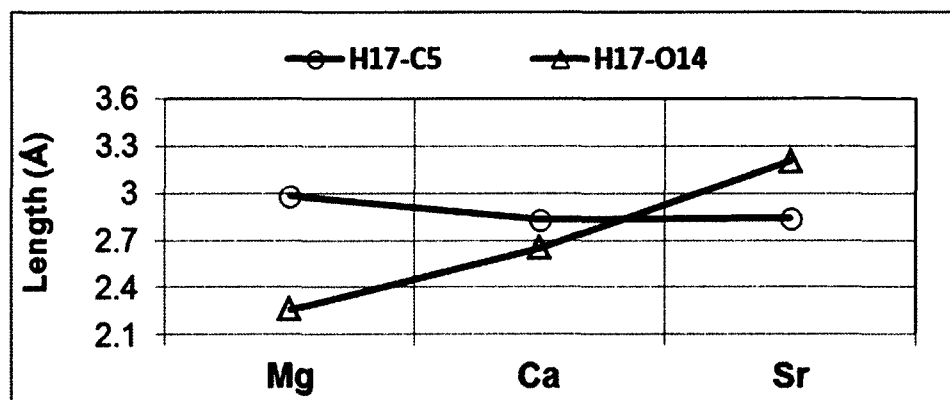


Figure 5.10: TS3 bond distances comparison between the Mg^{2+} -MDH, Ca^{2+} -MDH and Sr^{2+} -MDH active site models at BLYP/DNP theory level.

5.4.4 Step 4: $\text{PQQH}^{-*} \rightarrow \text{PQQH}_2$

Step 4 involves the transfer of proton H17 from Asp-303 to the O4 of PQQ, thus forming a stable product and reduced form of PQQ (PQQH_2). Unlike for Ca^{2+} -MDH, this step is barrierless for Mg^{2+} -MDH at the BLYP/DNP theory level of this work, as a transition state (“TS4”) could not be identified as such, even though the proton H17 was found at an intermediate location on its way from O14 of Asp-303 to O4 of PQQ with $\text{O14-H17} = 2.19 \text{ \AA}$ and $\text{O4-H17} = 2.59 \text{ \AA}$ in the final product, finally reducing PQQ (Figure 5.11).

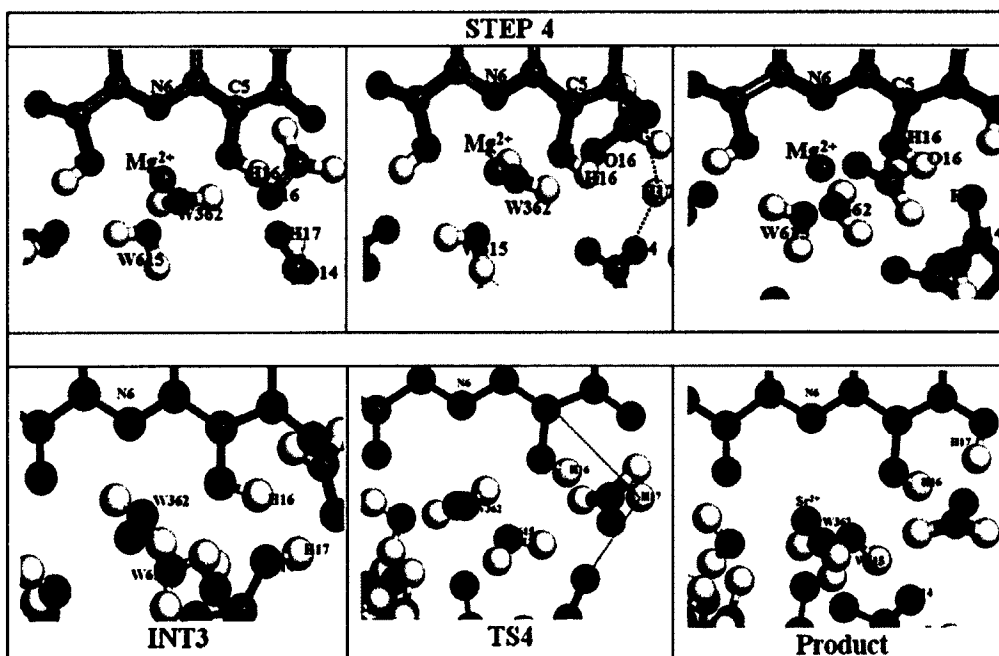


Figure 5.11: Optimized structures obtained at BLYP/DNP theory level involved in Step 4 of the H-T mechanism for Mg^{2+} -MDH (Top Set) and Sr^{2+} -MDH (Bottom Set).

In the case of Sr^{2+} -MDH, the transition state for this step also showed an intermediate location of H17 from the O14 of Asp-303 to the O4 of PQQ, with H17-O14 bond length increasing from 0.99 Å (INT 3) to 2.73 Å (TS4) to 4.53 Å (Product), and the H17-O4 distance decreasing from 4.46 Å (INT3) to 2.31 Å (TS4) to 0.98 Å (Product) (Figure 5.11). These distances are compared to the Ca^{2+} -MDH in Figure 5.12.

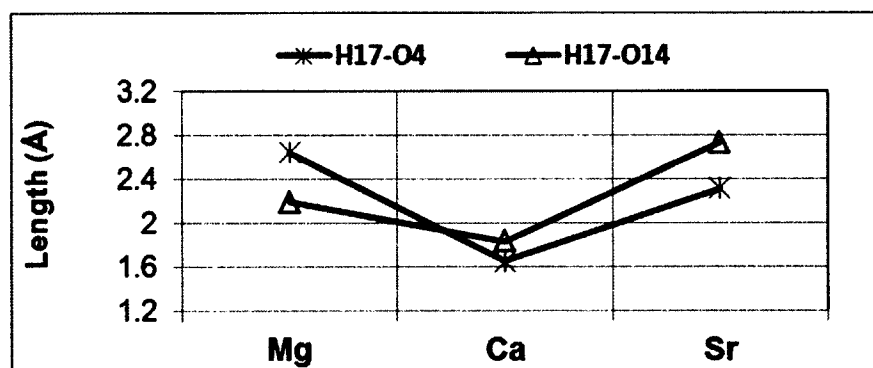


Figure 5.12: TS4 bond distances comparison between the Mg^{2+} -MDH, Ca^{2+} -MDH and Sr^{2+} -MDH active site models at BLYP/DNP theory level.

Steps 3 and 4 of the methanol H-T oxidation mechanism as applied to a Mg^{2+} -MDH model (Figure 1b) at the BLYP/DNP theory level show significant differences with respect to the ones corresponding to that of Ca^{2+} -MDH. This variation can be attributed to the small size of Mg^{2+} ion, and due to the fact that it could not polarize the bond (C5-O5) as it is well coordinated to the other surrounding active site residues. Also, these findings might be in line with the fact that Mg^{2+} does not stabilize the semiquinone form of PQQ as confirmed from the spectro-electrochemical studies on the stability of PQQ by Mg^{2+} instead of Ca^{2+} in soluble glucose dehydrogenase by Sato *et al.* [140]; thus, this suggests that the binding of Mg^{2+} to PQQ in this enzyme and in its free state are indeed different as there is negligible spectral effect on the reduced and oxidized forms PQQ.

This also suggests that there is a probability of an alternative step taking place for the second proton transfer. In this alternate step, the pyrrole nitrogen contributes to the ionization of the O4 of PQQ and the catalytic base does not play any role. This reduces the four step hydride transfer mechanism into a three step mechanism. In order to understand why the last two steps of the four step HT mechanism are kinetically not feasible for these ion-modified MDH, the alternate step was tested.

The relative free energy barriers for the H-T mechanism were compared to the Ca^{2+} -MDH as shown in Figure 5.13.

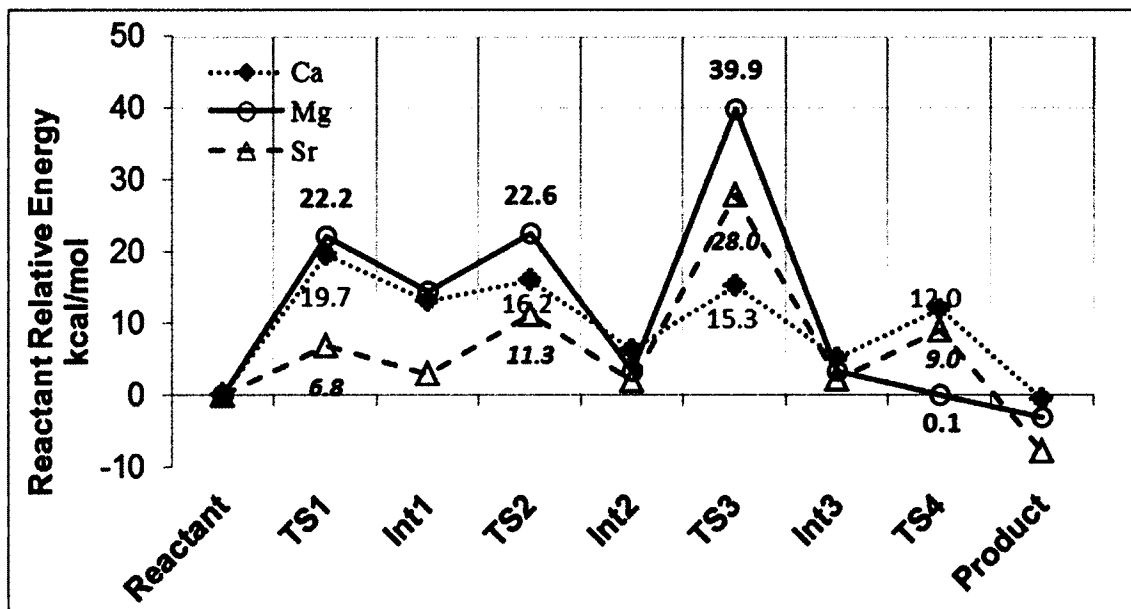


Figure 5.13: Potential Energy Surface corresponding to the four step H-T mechanism by MDH active site models with Mg^{2+} (solid), Sr^{2+} (dashed) and Ca^{2+} (dotted). Reactant-relative free energies calculated at the BLYP/DNP theory level are in kcal/mol. Free energies corresponding to the Ca^{2+} -MDH case were taken from Idupulapati *et al.*[49, 62].

5.4.5 Alternate Step: $\text{PQQH} \rightarrow \text{PQQH}_2$

In this alternate step, a direct transfer of H17 proton from C5 of PQQ to O4 of PQQ occurs, thus forming the product. In other words, the semiquinone form of PQQ is reduced to PQQH_2 directly without the involvement of the catalytic base (Asp303). The transition state (Alt-TS) showed an intermediate location of H17 from the C5 of PQQ to the O4 of PQQ in the case of Mg^{2+} -MDH, with H17-C5 bond length increasing from 1.11 Å (INT 2) to 1.91 Å (Alt-TS) to 2.60 Å (Product), and the H17-O4 distance decreasing from 2.90 Å (INT 2) to 1.81 Å (Alt-TS) to 0.99 Å (Product) (Figure 5.14).

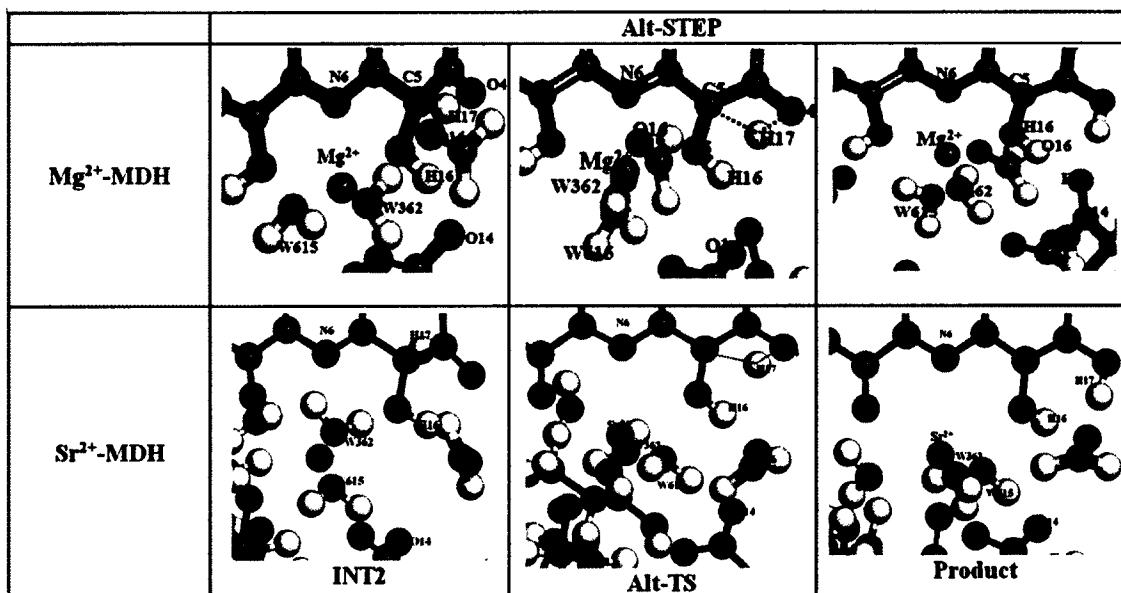


Figure 5.14: Optimized structures obtained at BLYP/DNP theory level involved in Alt-Step of the H-T mechanism for Mg²⁺-MDH and Sr²⁺-MDH.

Similarly, for Sr²⁺-MDH transition state (Alt-TS) showed an intermediate location of H17 from the C5 of PQQ to the O4 of PQQ, with H17-C5 = 1.86 Å, and the distance H17-O4 = 1.78 Å (Figure 5.14). In Figure 5.15, these distances are compared to the Ca²⁺-MDH.

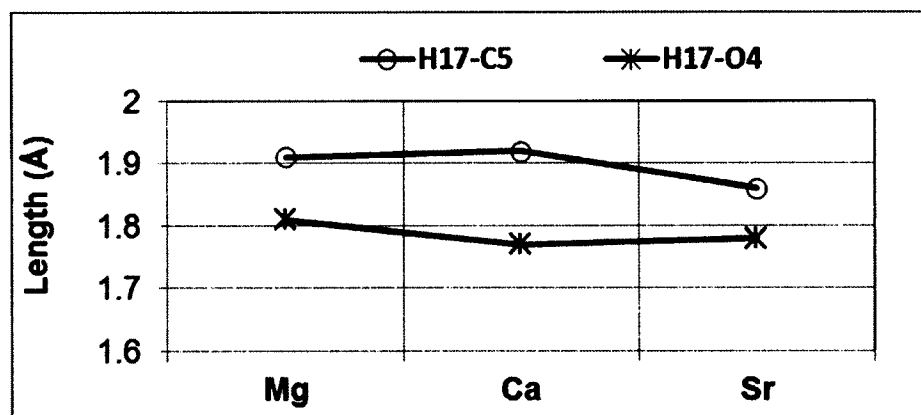


Figure 5.15: Alt-TS bond distances comparison between the Mg²⁺-MDH, Ca²⁺-MDH and Sr²⁺-MDH active site models at BLYP/DNP theory level.

For this alternate step, the free energy barrier obtained was lower for both the ion-modified MDH, showing that this step may be kinetically possible (when referred to the general kinetic requirements of an enzymatic catalytic process), as energy barriers are expected to be less than or around 18 kcal/mol. For the case Ca^{2+} -MDH, the barrier for this alternate step the reaction barrier was 0.5 kcal/mol higher than the barrier obtained for step four of classical H-T mechanism. Suggesting that ion-modified MDH enzyme active site models prefer another reaction pathway.

5.5 Conclusions

Using the generalized gradient approximation within the Density Functional Theory formalism at the BLYP/DNP theory level, methanol oxidation by a PQQ-containing MDH enzyme was investigated using Mg^{2+} and Sr^{2+} in place of Ca^{2+} in the enzyme active site. The generally accepted hydride transfer methanol oxidation mechanism by Ca^{2+} -MDH was tested for both the ion-modified MDH models. The free energy barrier for the rate limiting step (Step 1 of the H-T mechanism) for the Mg^{2+} -MDH was found to be 2.5 kcal/mol greater than that obtained for Ca^{2+} -MDH, and for Sr^{2+} -MDH, the free energy barrier was 12.9 kcal/mol lower than Ca^{2+} -MDH. This could be in accordance with kinetic and spectral investigations on Ca^{2+} and Sr^{2+} -containing Methanol Dehydrogenase by Kim *et al.* [141] who reported that Sr^{2+} -MDH is a more efficient enzyme for catalyzing methanol even though the enzymological properties were found to be similar between Ca^{2+} and Sr^{2+} -MDH. Also, the experimental activation energy values for Ca^{2+} and Sr^{2+} were in the same range, with a slight decrease in the case of Sr^{2+} -MDH, which could be attributed to an increased stability of the transition state [33]. Thus, the calculations conducted in this work imply that replacing Ca^{2+} ion with

Mg^{2+} and Sr^{2+} in the MDH active site, and testing for the H-T mechanism show that the size of the ion in the enzyme active site plays a key role in the oxidation mechanism.

Due to the distortion caused by the small size of the Mg^{2+} ion, the second proton transfer as described in the H-T methanol oxidation mechanism by Ca^{2+} -MDH seems to be unnecessary in the case of Mg^{2+} -MDH, and formaldehyde seems to be produced barrierless immediately after the second intermediate is formed. In the case Sr^{2+} -MDH, the last two steps of H-T mechanism do not seem to be possible due to the fact that formaldehyde is formed easily after that first step and PQQ reduces without the aid of Asp303.

CHAPTER 6

KINETIC MONTE CARLO STUDIES

6.1 Introduction

One of the well accepted theoretical methods which provide realistic behavior of a molecular system is Kinetic Monte Carlo (kMC) simulations, which enable us to deal with catalytic phenomena on time scales of the order of seconds or even longer, and length scales of the order of meters or more. kMC simulations were proven to be a powerful tool to give valuable information about the reaction kinetics on surfaces and have been applied to study chemical kinetics on many catalytic surfaces [142]. Due to the flexibility and robustness involved in these Monte Carlo techniques, they provide the advantage of monitoring the stochastic behavior of diffusional and kinetic properties of a catalytic surface.

As biological systems such as enzymes involve processes with differing length and time scales, kMC methods can provide information on the valuable insights of the enzyme kinetics system. These random sampling methods aid in modeling the complex process effectively by spending most of the simulations time in configuration that most favorable and neglecting those configurations that are highly improbable [116]. However, studying enzyme kinetics using kMC is not that widely recognized. Thus, in an attempt to model MDH kinetics using kMC, in this chapter, kMC calculations were performed to obtain the macroscopic rates of methanol oxidation by modified MDH enzymes and

finally the polarization curves for the methanol fed biofuel cell with MDH as an anodic catalyst were obtained.

6.2 Input Parameters

The input parameters for the kMC simulations are microscopic rates and pre-exponential factors that are obtained from DFT calculations. In order to perform these kMC simulations, the first step is building an appropriate lattice representation of the enzyme where the methanol oxidation will take place.

6.2.1 Lattice Preparation

The kMC program, CARLOS 4.1, developed by John Lukkien and A. P. J Jansen is used in this work [74, 115]. To explore the kinetics and construction of the lattice representing the enzyme active site, it is important to discuss the assumptions and boundary conditions of the systems, since the reaction mechanics are relative to these aspects. The assumptions made to describe the model and to reduce complexity are noted as follows [116]:

1. The individual substrate molecules do not interact with each other.
2. The active site particles on the lattice do not move.
3. There are no interactions between the substrate molecules and the obstacles.
4. The substrate molecules move towards the active site by the shortest available distance following the random walk motion.
5. The excluded volume condition is maintained, i.e. at any instant of time one lattice site cannot be occupied by more than one molecule of the same or different species.

A simple Michaelis-Menten equilibrium enzyme kinetics equation (Eq. 6.1) is considered [143]:



where E denotes the enzyme, S denotes the substrate (methanol), ES is the intermediate complex (enzyme-substrate), and P is the product (formaldehyde). It is considered that the reaction is diffusion limited; thus, the formation of an intermediate ES is not taken into account and the substrate is almost instantaneously converted to the product at the active site (A). Therefore, Equation (6.1) reduces to a simpler reaction between the active site (A) and the substrate (S) molecule (Eq. 6.2) [116].



Based on the above stated assumptions, further calculations were performed. Using MM simulations, the 2-D surface was determined by exploring the enzyme binding pocket and the projection of enzyme residues seen by the substrate molecules (methanol) as they approach the enzyme active site; thus reducing, in a first approximation, the complexity of the problem (Figure 6.1). A grid representing possible methanol reaction sites was mapped onto the projected biocatalyst image in a 2-D surface for a random substrate approach onto the reactive enzyme surface. A coarse graining method where the molecules are represented as beads was considered where the center of masses for all the amino acids in MDH were obtained and plotted with the active site amino acids as the center. To model enzymatic reactions, the distribution of the substrate and obstacles (amino acids that are not part of the active site) is an important aspect to consider. Hence, random sampling methods to distribute the species on the lattice have been used for enzyme kinetics modeling and they have showed that the enzyme kinetics was influenced

by aspects like obstacle density. Thus, according to the approach described by Dandala *et al.*, a biased approach is used in sampling the lattice and to investigate its effect on the kinetics of methanol oxidation by MDH [116].



Figure 6.1: Ca^{2+} -containing Methanol Dehydrogenase enzyme (**top-right**) and view of its binding pocket and active site (**left**). Projection of active site components (green) and other residues (black) according to their center of masses (and plotted as dots), onto a 2-D lattice representing the biocatalytic surface (**right**). Red and blue dots represent substrate (methanol) and product (formaldehyde) molecules [116].

6.2.2 Microscopic Rates

The microscopic energy barriers and pre-exponential factors of the reaction rates involved in methanol oxidation are required as inputs for the kMC studies. These values are obtained from Density Functional Theory (DFT) and Transition State Theory (TST). The rate constants of H-T process (Table 6.1) are given as the input at the start of each simulation and these are calculated from the activation energies obtained from the DFT calculations (Chapter 5) [49]. The free energy reaction barriers for the rate limiting step of the H-T mechanism (Step 1) were used for this study. At the start of each simulation,

the obstacle and substrate concentrations are specified and the simulation time is counted in Monte Carlo steps. The simulation is initiated with the substrate molecules (red) diffusing (making a random walk) towards the active site amino acids (green) which are distributed at the center of the lattice with the obstacles scattered (black) on it (Figure 6.1). When the substrate molecules come in contact with any one of the active site amino acids, a product (blue) is formed which also diffuses on the lattice.

Table 6.1: Input microscopic rates of the ion-modified MDH enzymes for the kMC calculations.

Model Parameter	Mg ²⁺ -MDH	Ca ²⁺ -MDH [49, 135]	Sr ²⁺ -MDH	Ba ²⁺ -MDH [49]
ΔG (kcal/mol)	22.2	19.7	6.8	10.4
Rate, r (sec ⁻¹)	1.79×10^{-3}	2.25×10^{-2}	6.43×10^7	1.48×10^5

Apart from gaining insight about the catalytic reactions taking place inside the enzyme, useful information, such as the concentration profiles of the substrate and the product with respect to time, obstacle density, reaction rate constants, and the positions of obstacles on the lattice can be obtained using this model [116]. In order to study the MDH enzyme kinetic process, two models have been built and studied. The first step is to verify that the model used follows the general enzyme kinetics principles.

6.3 Model 1

6.3.1 Model Validation

The 2D lattice model in the case of Model 1 represents only the active site amino acids as discussed earlier and shown in Figure 6.1. Enzyme kinetics is typically governed

by the rate of formation of product or the disappearance of a reactant as shown in Figure 6.2.

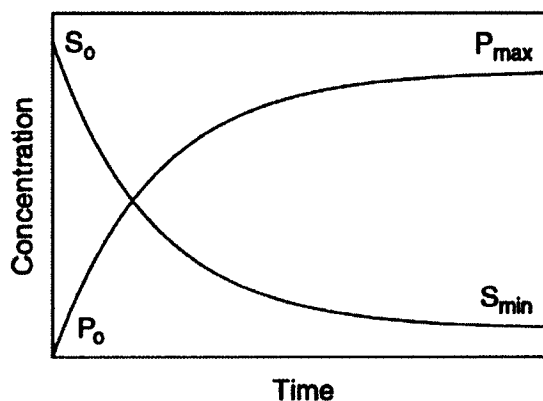


Figure 6.2 A typical progress curve for enzyme [144]

According to Zhang *et al.*, the energy generation in the MDH catalyzed biofuel cell follows a five step process. In the first step, electrons are released by the process of oxidation of methanol (substrate) by the enzyme (reaction taking place at the active site of the enzyme), and this step is considered potentially limiting. The second step involves the transfer of the electrons from the reduced enzyme to the mediator (TMPD). The next steps (Steps 3 and 4) involve the transfer of the electrons from the oxidized mediator to the cathode through an external circuit when a load is applied, and this cycle of electron transfer continues. In the final step, cathodic reaction with potassium permanganate occurs [32].

Since the first step is considered the potentially limiting step, it is important to understand thoroughly the oxidation mechanism of methanol and the enzyme kinetics behind it. The primary goal is to verify if the model (2D lattice) is representing the enzyme catalysis. In order to examine this, the progress curve for the enzyme-catalyzed reaction is generated in Figure 6.3, i.e. the rate of consumption of substrate (methanol)

and rate of formation of product (formaldehyde). It was observed that methanol concentration is reduced and the formaldehyde concentration increased, thus validating that this model follows the general kinetic behavior of an enzymatic system. From this progress curve (Figure 6.3), the reaction velocity or rate of reaction for the system can be evaluated.

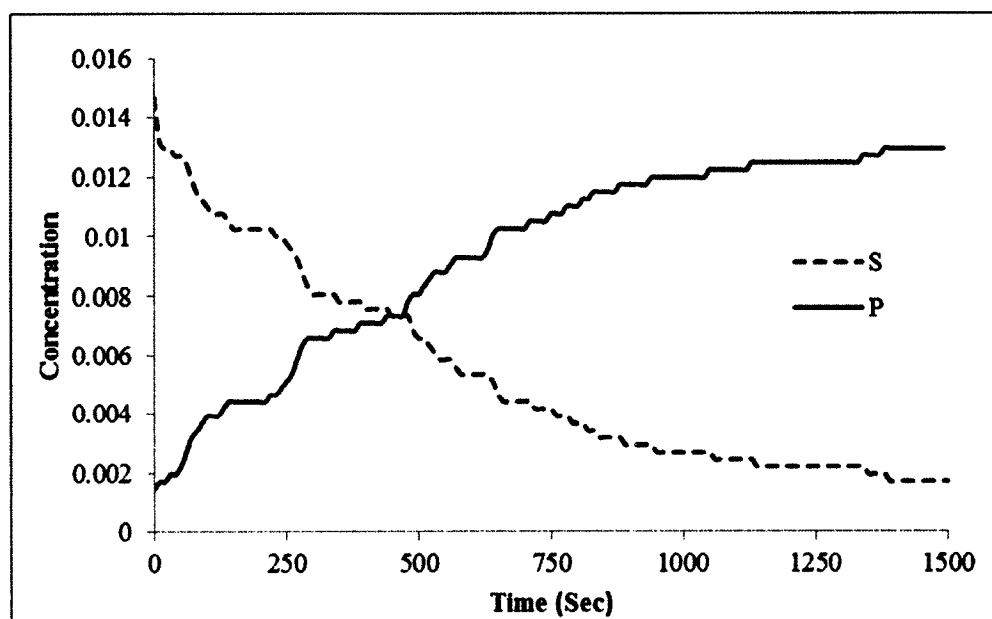


Figure 6.3: Concentration profiles of substrate and product molecules formed for MDH active site models with respect to time.

6.3.2 Effect of Obstacle Concentration

After validating this aspect, the effect of macromolecular crowding concentration on the rate of product formation was considered as shown in Figure 6.4. Earlier kMC studies conducted on enzymes have indicated that macromolecular crowding (amino acids other than the active site amino acids present in the enzyme that are not directly involved in the reaction mechanism) affect the enzyme's kinetics [145, 146]. Hence, to understand

how the other amino acids might affect the product formation, the influence of the number of amino acids (obstacle density) on the conversion of methanol molecules was investigated. This will provide useful information like the variations in the product formation rate or substrate consumption as the number of obstacle is changed.

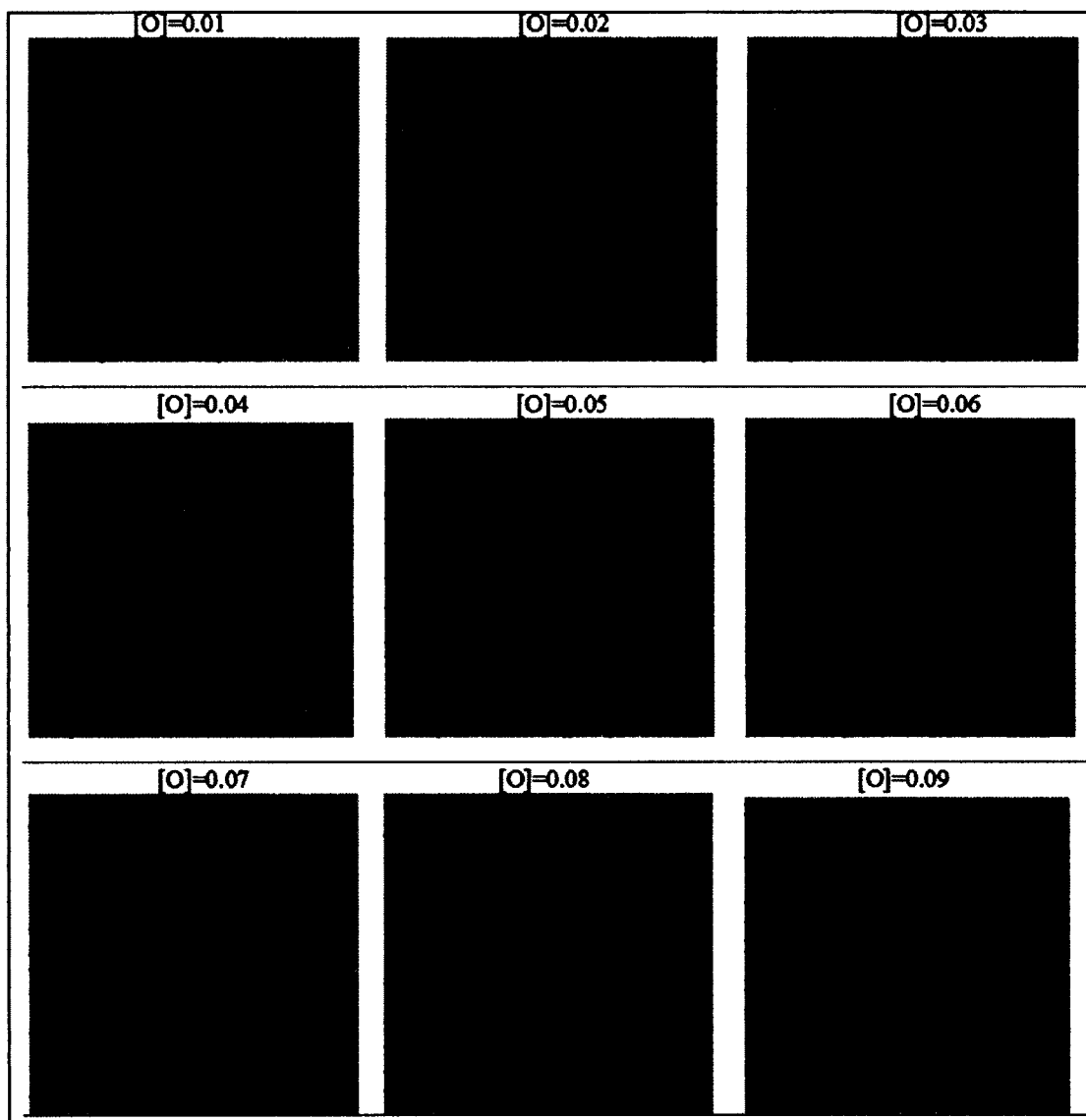


Figure 6.4: Lattice configurations showing the Substrate (Methanol molecules) as red dots and Product (Formaldehyde Molecules) as blue dots with increasing Obstacle concentration (other amino acids in MDH) for Ca^{2+} -containing MDH, and the green dots represent the active site cluster.

As observed from the simulations snapshots (Figure 6.4) for increasing obstacle concentrations (black dots [O]), i.e. the number of other amino acids in MDH, the formation of formaldehyde (product-blue dots) is reduced by 50%, implying that the amino acids around MDH (other than the active site amino acids) also play an important role for the product formation. Next, the effect of ion in the product formation was taken into account.

6.3.3 Effect of Ion

It was observed that the larger ion containing MDH (Sr^{2+} -MDH and Ba^{2+} -MDH) are more reactive than Ca^{2+} - and Mg^{2+} - containing MDH. As seen from Figure 6.5 and Figure 6.6, it can be illustrated that when a smaller ion like Mg^{2+} is present in the active site of the enzyme, the rate of product formation was decreased (less blue dots) by almost 9 times compared to the Ca^{2+} -MDH (naturally occurring MDH). At the same time when a larger ion like Ba^{2+} or Sr^{2+} are present, the concentration of the product increased (more blue dots) by 2 times when compared to Ca^{2+} -MDH. This shows that Sr^{2+} and Ba^{2+} -MDH are more reactive than the Ca^{2+} -MDH.

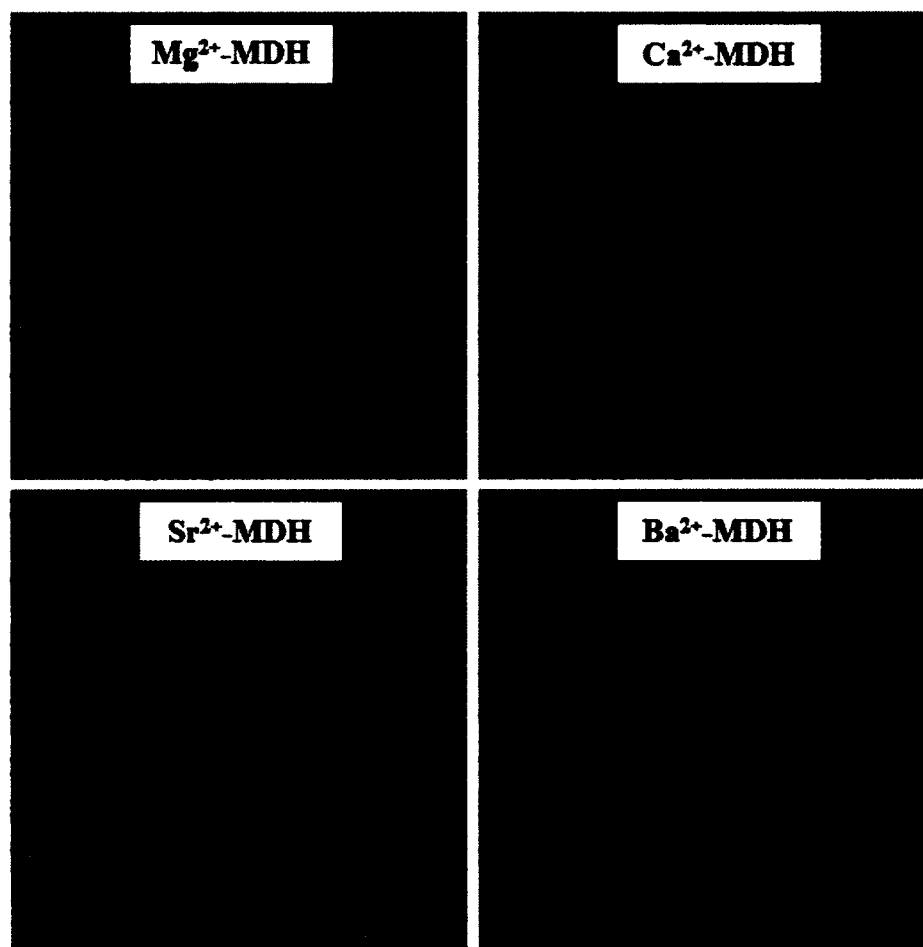


Figure 6.5: Final lattice configurations showing the effect of ion in the product formation. Green dots represent the active site amino acids and the red and blue dots represent substrate (methanol) and product (formaldehyde) molecules.

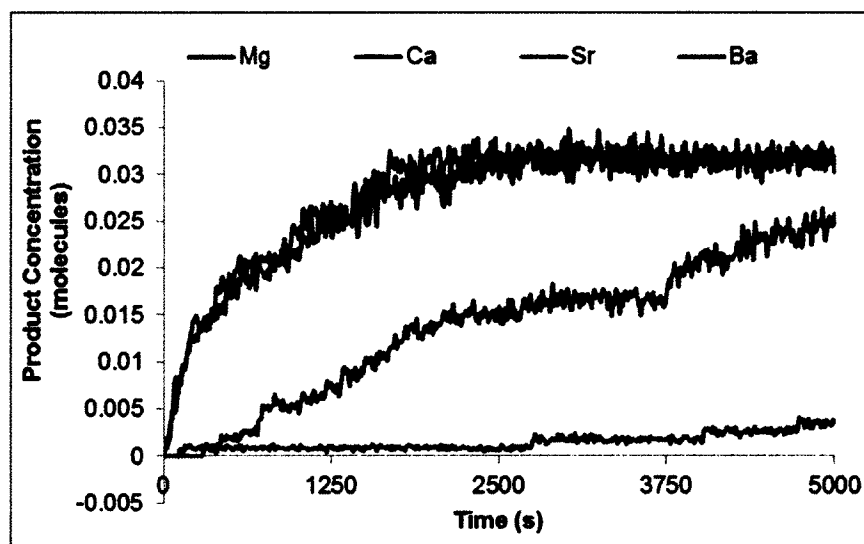


Figure 6.6: Plot showing product (Formaldehyde Molecules) formation for the different ions MDH active site models with respect to time.

It was clearly seen from the results obtained (Figure 6.4) that the rate of product formation is influenced by the presence of other amino acids. Hence, the complete enzyme lattice model (including all the amino acids) was used to evaluate macroscopic rates.

6.4 Model 2

6.4.1 Lattice Model

In order to include all the amino acids present in the enzyme, a 2D lattice model (Model 2) was built by taking the center of mass of each subunit (amino acid), and this coordinates file (xyz coordinates of the subunits) was converted to the configuration input file for Carlos 4.1 using the code provided by our collaborators. As the Carlos program requires that the 3-D enzyme structure to be displayed as a 2-D reactive surface, one of the axis's coordinates needs to be neglected. Figure 6.7 shows the full 2-D lattice models for each neglected axis.

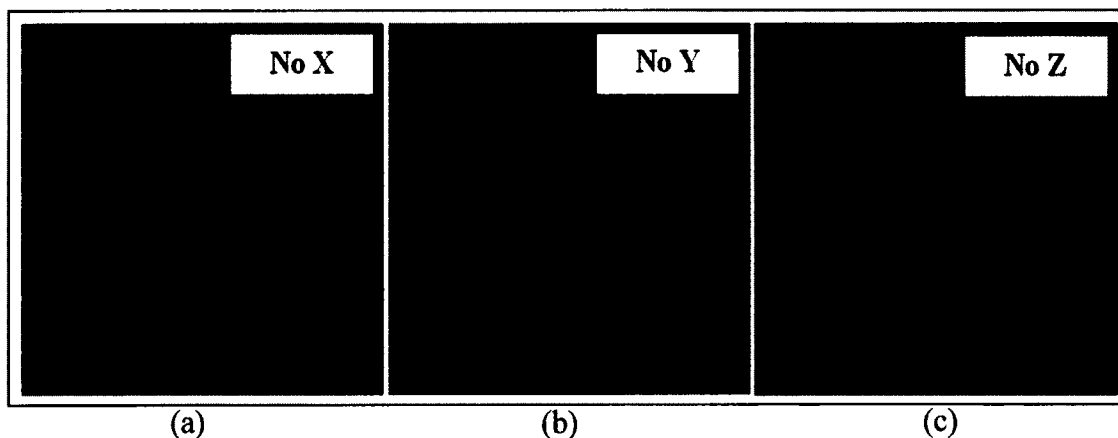


Figure 6.7: Two-dimensional enzyme structures of MDH as lattice in CARLOS program as input structure (a) X axis negated (b) Y axis negated (c) Z axis negated.

In the case of MDH, the y axis was negated so that the lattice could represent the enzyme (qualitatively) as obtained from the protein data base as shown below in Figure 6.8. For all further calculations, this lattice model (No Y lattice model) was used. In the same way as in Model 1, this model was validated by considering the concentration profiles of the product and substrate molecules.

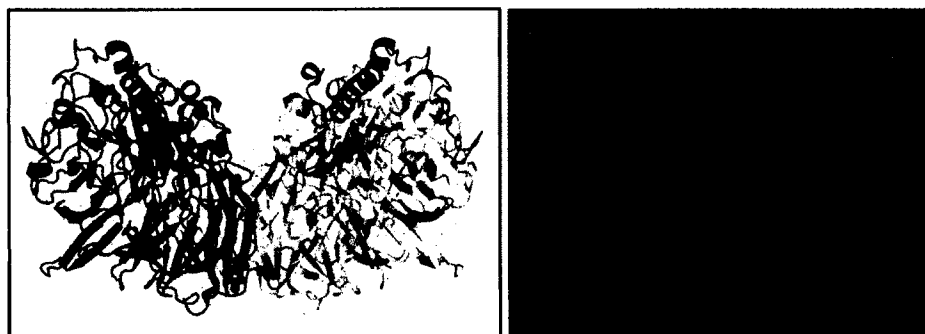


Figure 6.8: Three dimensional enzyme structure from the PDB database (left). Y-axis neglected two-dimensional enzyme structure of MDH as input structure (right).

6.4.2 Effect of Substrate Concentration

When describing biochemical reactions *in vitro* as well as in *in vivo*, V_{\max} and K_m play a major role [147]. For an enzyme to be suitable for fuel cell applications, the two main fundamental properties that are important are its turnover frequency (k_{cat}), which is the rate at which the substrate is catalyzed and the potential (driving force) necessary to achieve catalysis [6]. Values above 100 s^{-1} for k_{cat} are considered well, but for low k_{cat} values an enzyme cannot work as an effective catalyst. Another intrinsic factor is the substrate specificity, the K_m values for the substrates, both fuel and oxidant. Preferably, for a fuel cell, the concentration of substrates should be higher than K_m , which is not the case for biosensors where the substrate concentration needs to be around K_m or below [6].

For a given enzyme concentration, the rate of reaction increases with increasing substrate concentration up to a point above which any further increase in the substrate concentration produces no significant change in the reaction rate. This is because the active sites of the enzyme molecules at any given moment are virtually saturated with the substrate. For an enzyme-catalyzed reaction, the velocity (reaction rate) change with respect to the varying substrate concentration provides valuable information such as the K_m and the maximum velocity (V_{\max}). In common situations, the substrate concentration is in excess when compared to the enzyme concentration ($[S] \gg [E]$) [148]. As in this study we have considered a diffusion limited form of the MM equations, so the substrate concentration needs to be higher than the concentration of the active site ($[S] \gg [A]$) to obtain the valuable information about the MDH kinetics. Hence, for the next set of calculations, the number of substrate molecules was increased from 100 to 1200, and the

rate of formation of the product at each substrate concentration was evaluated (Figure 6.9).

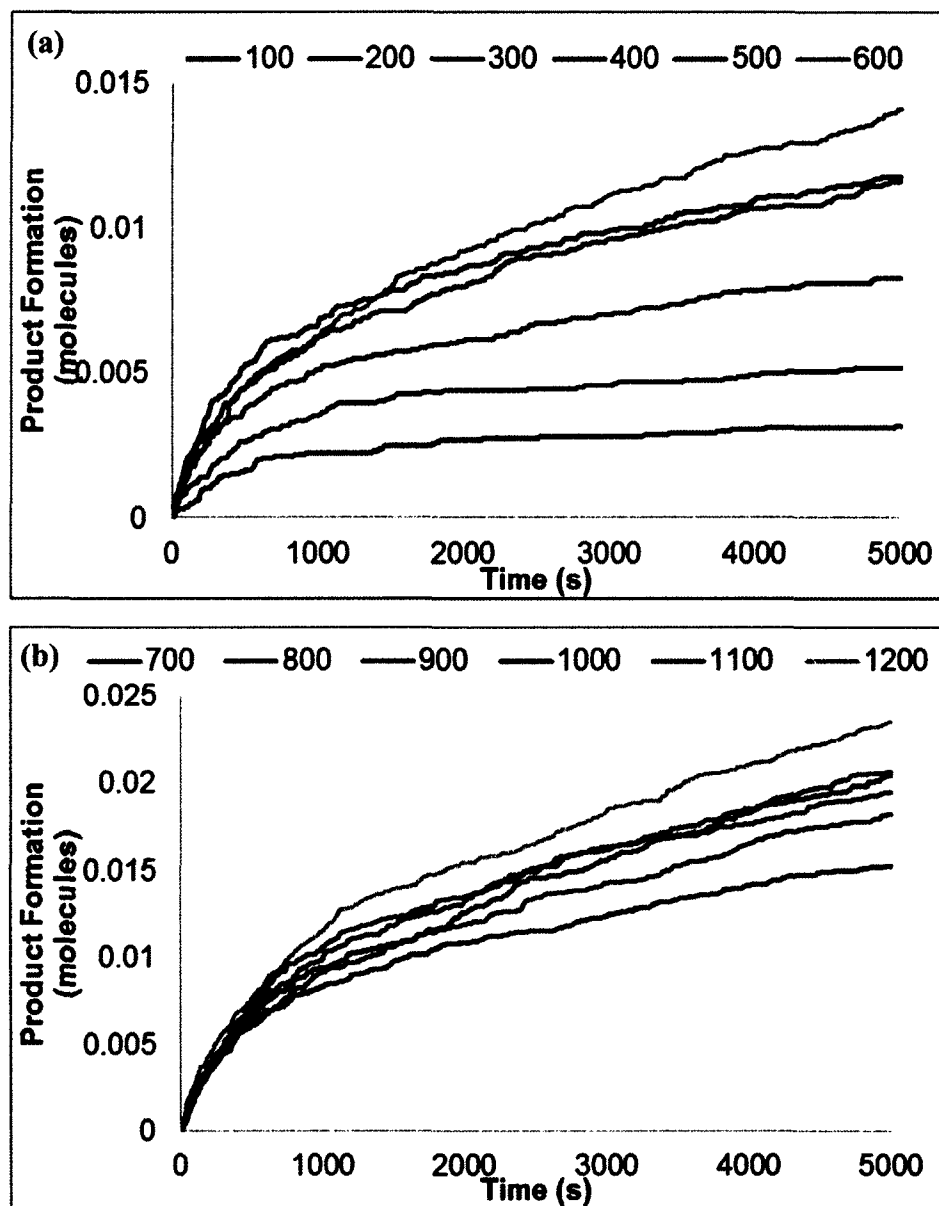


Figure 6.9: Rate of Product Formation with respect to increasing substrate concentration.

These simulations were done first for the naturally occurring MDH, i.e. Ca^{2+} -MDH, and further the replacement of Ca^{2+} in the active site of MDH was studied. In order to understand how the product formation is changing over time with respect to

increasing substrate molecules, a linear fit trend line was applied to each progress curve. In Table 6.2, the slope of each curve (reaction velocity) was recorded to show relativity to each scenario, and the R^2 value is shown to discuss the consistency of the data.

Table 6.2: Slope and R^2 value for the rate of product formation plots for increasing number of substrate molecules.

No of Substrate Molecules	Slope of Curve (10^{-7})	R^2
100	4	0.7193
200	6	0.7341
300	10	0.8735
400	20	0.8783
500	20	0.9067
600	20	0.9328
700	20	0.9024
800	30	0.9347
900	30	0.8904
1000	30	0.9546
1100	30	0.9322
1200	30	0.9399

From 100 to 700 substrate molecules, the reaction velocity is increasing with the average R^2 value being 0.8495. From 800 to 1200 substrate molecules, the reaction velocity is constant (3×10^{-6}), and the average R^2 value being 0.9303 indicates that the linear trend line association is valid for the given data set. To clearly show how the reaction rate is changing with the increasing substrate concentration, a plot of the reaction rate (slope of the curves from Figure 6.9) with respect to the substrate concentration is shown in Figure 6.10.

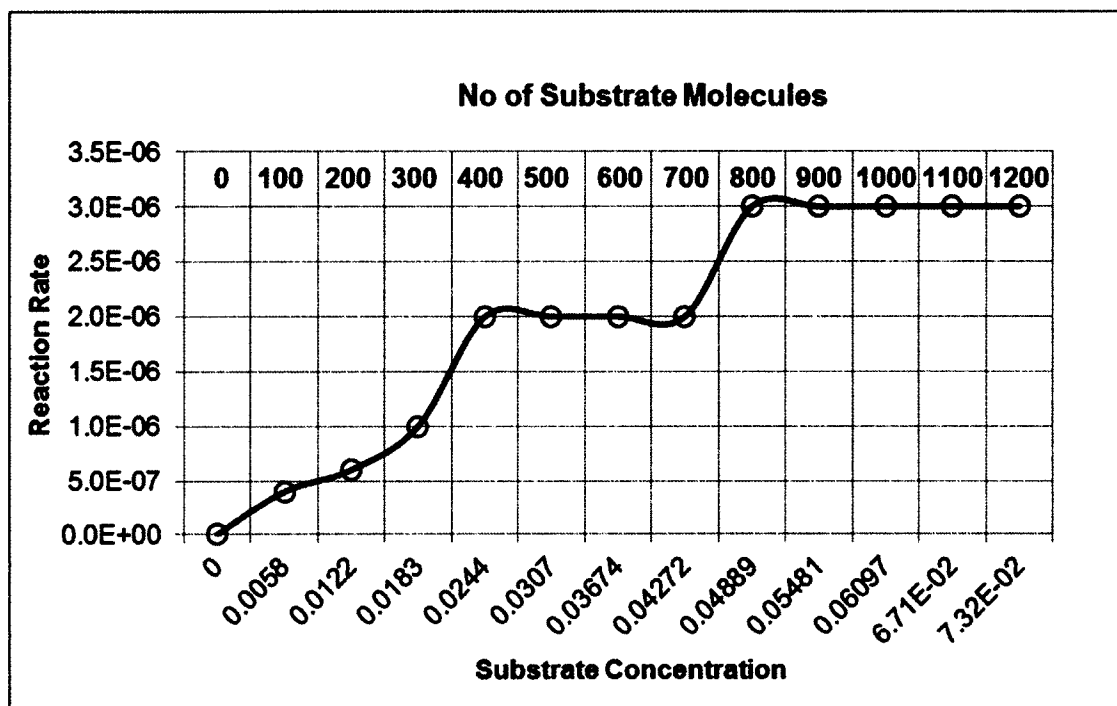


Figure 6.10: Plot showing the reaction rate with respect to number of substrate molecules.

The velocity (reaction rate) curve with respect to the substrate concentration is a rectangular hyperbola (Figure 6.10) which is the general shape of a velocity versus substrate concentration in enzyme kinetics [144]. This graph implies that at low substrate concentrations, when the velocity of the reaction changes and at high substrate concentrations, the velocity of the reaction is constant. This trend is comparable to the general enzyme kinetics behavior [144].

Hence, from this curve (Figure 6.10), for the Ca^{2+} -MDH the value of V_{\max} is 3×10^{-6} and K_m is 1.5×10^{-6} . For the case of Mg^{2+} -MDH, the value of V_{\max} is 1×10^{-6} and K_m is 0.5×10^{-6} which is less than Ca^{2+} -MDH, and in the case of Sr^{2+} and Ba^{2+} -MDH, the values of V_{\max} is 5×10^{-6} and K_m is 2.5×10^{-6} exactly 2 times higher than Ca^{2+} -MDH. This suggests that as the K_m value is higher for the case of Sr^{2+} and Ba^{2+} -MDH, the substrate molecules have a weaker affinity towards these ion-modified enzymes, and

these results are in accordance with our earlier binding energy calculations (Chapter 4) where it was established that when a smaller ion (Mg^{2+}) is present in the active site of MDH, methanol is strongly bonded, and as the size of the ion increased, the affinity towards methanol decreased.

Another point to be noted from these simulations is that at substrate concentrations above 4.89×10^{-3} (800 -1200 substrate molecules), the reaction velocity is constant. As the concentration of substrates should be higher than K_m for fuel cell applications, for further potential dependence simulations and to study the effect of the ion, the 1200 substrate molecules configuration model was considered.

6.4.3 Effect of the Ion

The effect of the ion on the reaction velocity was evaluated, and the same trend as in Model 1 was observed. The Mg^{2+} -containing MDH has a lower reaction velocity and the Sr^{2+} and Ba^{2+} -containing MDH have higher reaction velocities compared to Ca^{2+} -MDH as shown in Figure 6.11 and Figure 6.12.

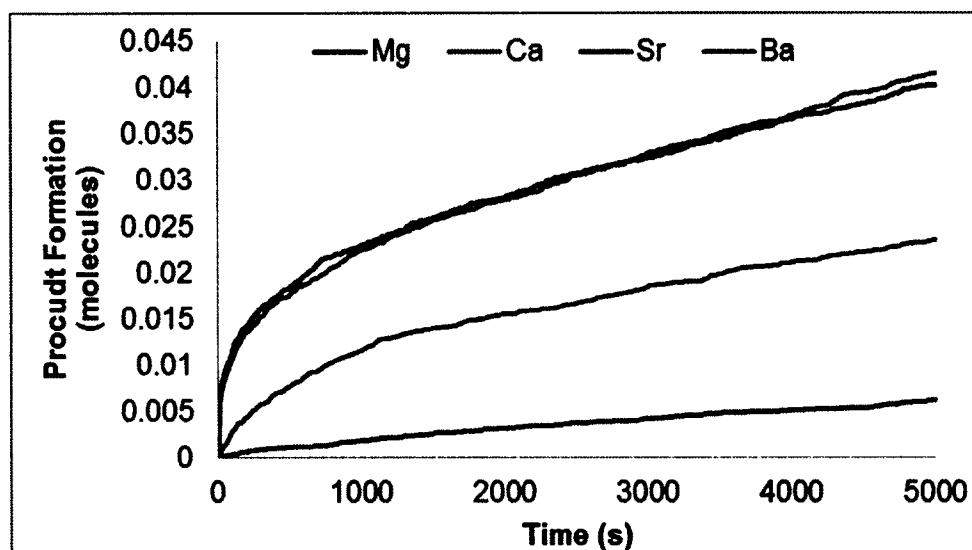


Figure 6.11: Rate of Product Formation for ion-modified MDH enzymes with respect to increasing substrate concentration.

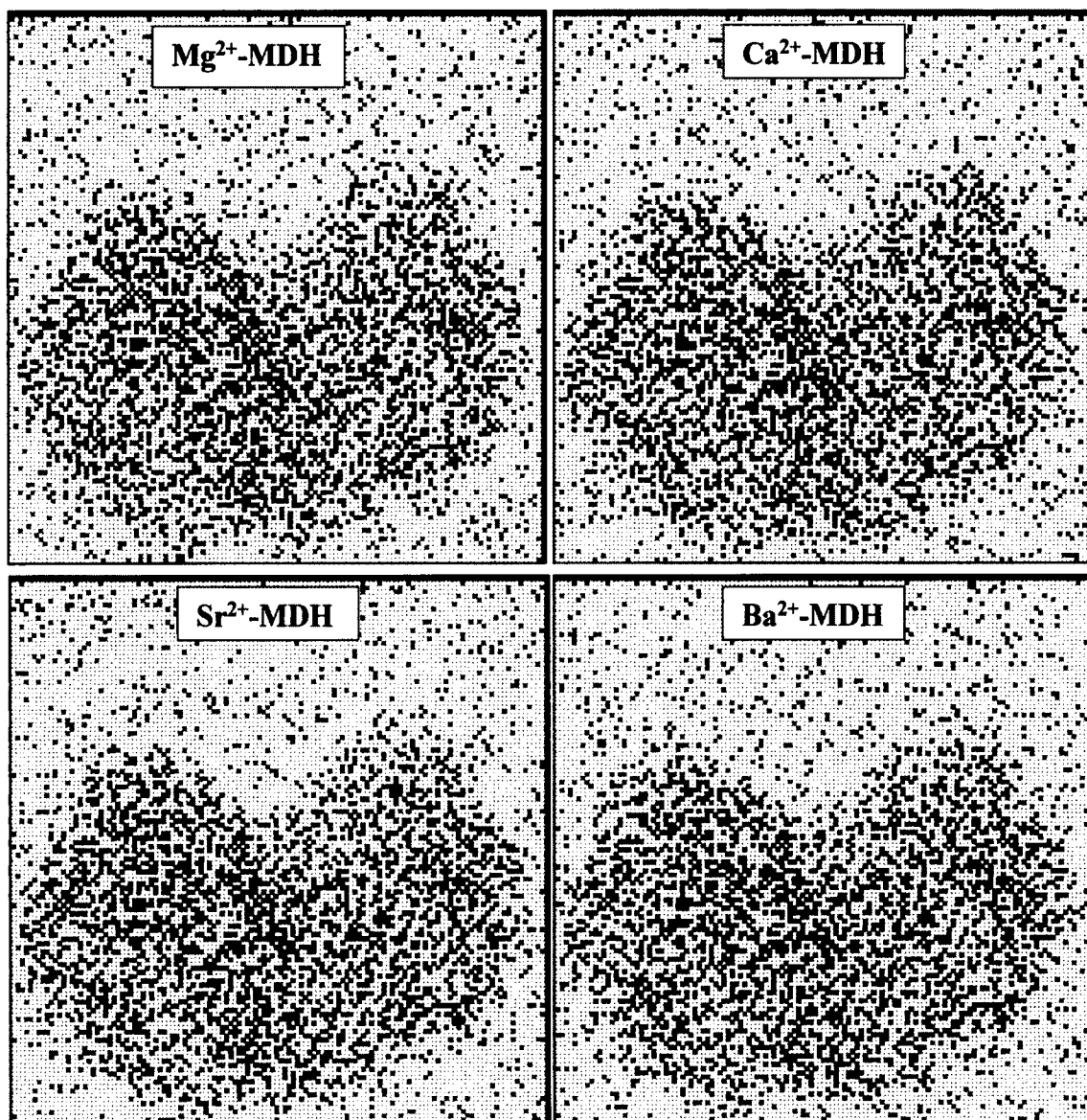


Figure 6.12: Lattice configurations showing the effect of ion in the product formation. Green dots represent the active site amino acids and the red and blue dots represent substrate (methanol) and product (formaldehyde) molecules.

These results show that the larger ion containing MDH are more reactive and have greater reaction rates, which means that the rate of production of electrons will be faster. In order to test this, the potential dependence on the reaction rates is evaluated next.

6.4.4 I-V Curves

In the event that either the reactant or product is electro-active, i.e. can either produce or consume electrons during the catalytic mechanism; the progress of the reaction can be monitored using amperometry. This concept of the bio-electrochemical reactions taking place on the surface of an electrode can be used for the generation of current for bio-sensors/fuel cell devices. Enzyme oxidation process produces electrons which are transferred to the anode where they proceed through an electrical circuit before reaching the cathode. Thus, by the catalytic activity of the enzyme, the current now flows over a potential difference and power is generated directly from the fuel [13]. It is believed that the density of the catalytic active sites and the rate of catalysis per active site (which is high for enzymes) regulate the maximum electro-catalytic current achievable at the electrodes. Therefore, the higher the rate of product formation, the greater is the electro-catalytic current possible.

As the driving force (potential) is an intrinsic property for fuel cell performance [6], the potential dependence on the reaction rates is considered in this section which will provide data to obtain the polarization curves. As mentioned in Chapter 3 (Section 3.6), the current is obtained by taking the difference between the rates of reactions for the reactions that produce electrons and those for the ones that consume electrons. From these, the polarization curves can be obtained for the fuel cell.

The current must be calculated as shown in Equation 6.3:

$$i = e_o \sum_{n=1}^{\infty} r_n , \quad \text{Eq. 6.3}$$

where i is the current, e_o is the charge of an electron ($e_o = 1.60217646 \times 10^{-19}$ C), and r is the reactions that generate or produce electrons. In our simulations, as we have

considered when the substrate molecules approach the active site, the product molecules are formed and in this process release two electrons. Two electrons are released in the methanol oxidation process where the PQQ is reduced. As in Model 2, there are two active site centers, and there will be four electrons being produced in total. Therefore, the current produced is equal to 4 times the rate of the reaction multiplied by the charge of the electron. Hence, for our system this can be rewritten as in Equation 6.4:

$$i = e_o \cdot (4r), \quad \text{Eq. 6.4}$$

where r is the reaction rate provided by the Carlos 4.1 program. The reaction rate has a stoichiometric coefficient of 4 due to the generation of 4 electrons.

The I-V curves in Figure 6.13 below show the comparison between the experimentally obtained values [32].

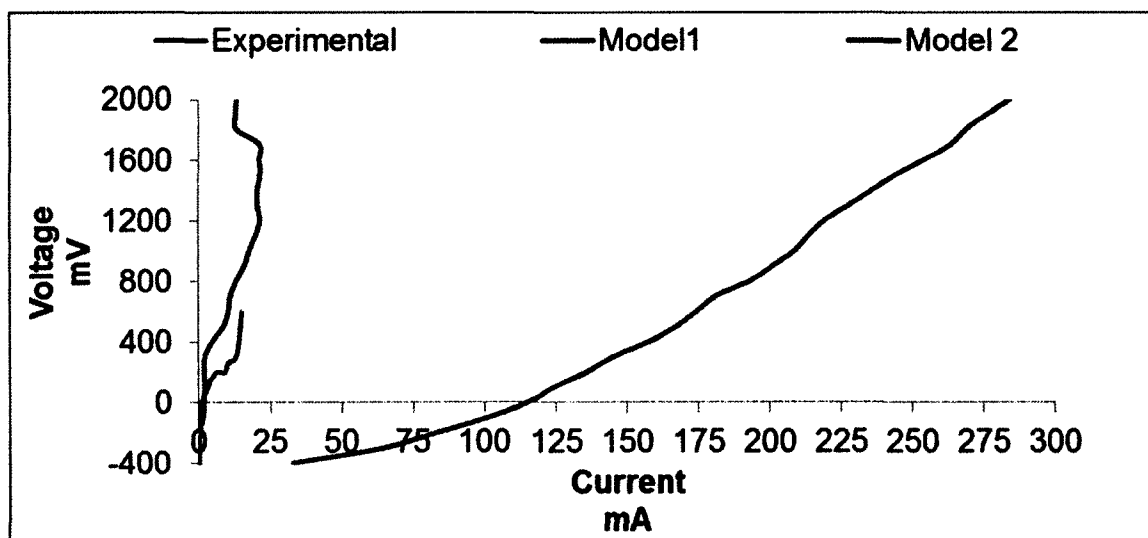


Figure 6.13: I-V curves obtained for both the models and compared to experimental obtained curve.

From the graph (Figure 6.13), it can be observed that curves obtained from our tests are not in agreement with the experimental curve. The deviation from the curve is

due to the fact that diffusion of methanol was not included in this case, and in the case of the experimental study, the electron transfer occurs via a mediator. Generally, in the case of PQQ dependent enzymes the electron transfer is considered to be direct electron transfer (DET) so in our case we did not consider the effect of a mediator during the electron transfer.

Zhang *et al.* [32] reported that the short circuit current obtained for MDH as an anode was 50 mA. In order to understand how the ion-modification affects the current, the I-V curves for the ion-modified MDH enzymes are shown in Figure 6.14 below.

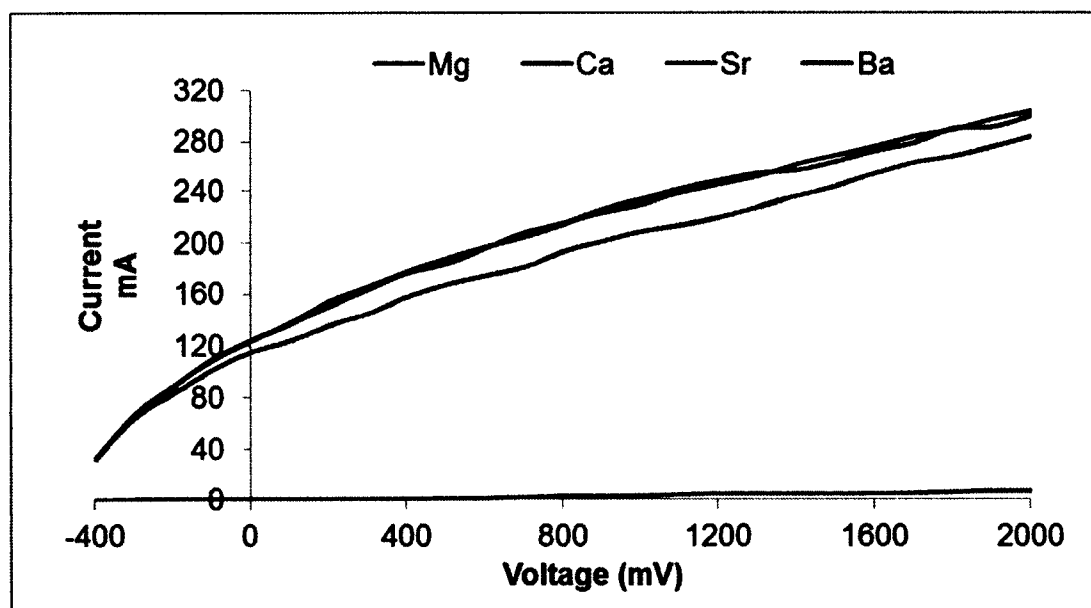


Figure 6.14: I-V curves obtained for Ion-Modified MDH enzymes.

The short circuit current for Mg^{2+} -MDH is recorded as 0.5 mA, which is below the experimental value (50 mA). In the case of Ca^{2+} -MDH, Sr^{2+} -MDH and Ba^{2+} -MDH, the short circuit currents are 115 mA and 125 mA, which are more than the experimental value, indicating that when larger ions are present in the active site of the MDH enzyme as the rate of product formation is higher. This in turn increases the production of

electrons and ultimately affects the current. This implies that modified enzymes can be more effective catalysts for fuel cell applications in agreement with experimental results [33, 68, 141].

However, there could be some limitations when a naturally occurring ion in the active site of the enzyme is replaced by other metal ions, and these factors should be taken into consideration when a bio-electrode with modified enzymes is prepared. For instance, the environment governing the working of the bio-electrodes such as the temperature and pH range can affect the functioning of the fuel cell, and it can have an impact on the current values obtained. Thus, the temperature of the system should be around room temperature and the pH range should be chosen according to the enzyme (not too acidic and too basic), so they do not deactivate or denature the enzyme. Apart from these factors, experimentally, when the ion in the active site of the enzyme is replaced, the solubility of the new ion mixture during protein purification process can be an issue. Also, it is important to consider the appropriate immobilization technique as they could affect the stability of the enzyme based biofuel cell when the ion-modifications are made as different ions can act differently during the immobilization process. Another important factor is if a mediator present electron transfer is considered, the mediator used should be chosen appropriately so that it transfers electrons from the active site of the enzyme to the electrode surface efficiently.

6.5 Conclusions

In this chapter, kinetic Monte Carlo simulations were carried out to obtain macroscopic rates which provided information about the current produced. Two 2D lattice models were considered for these calculations. From these simulations, it was

observed that macromolecular crowding plays an important role. The role of ion was also taken into account and it was observed that Sr^{2+} -MDH and Ba^{2+} -MDH have higher macroscopic reaction rates. It was witnessed that when the substrate concentration is higher than the active site concentration, the reaction velocity is constant, and this curve provided the values for V_{\max} and K_m for each MDH enzyme model. From the I-V curves, it was seen that Mg^{2+} -MDH and Ca^{2+} -MDH predict the short circuit current value below the experimental value. For the case of Sr^{2+} -MDH and Ba^{2+} -MDH, the current values were higher, therefore proving that when a larger ion is present in the active site of the MDH, the catalytic activity of the enzyme is increased.

CHAPTER 7

CONCLUSIONS AND FUTURE WORK

7.1 Conclusions

The main objective of this research was to investigate the role of ion during the oxidation of methanol by ion-modified methanol dehydrogenase enzyme. A multiscale modeling approach was applied in order to achieve the goals of this work. First, through quantum mechanical calculations (DFT), we investigated the role of the ion in the binding of methanol to the active site of MDH. After looking into the binding of methanol, the H-T methanol oxidation mechanisms for the ion-modified enzymes were tested. The results obtained from these simulations were used as inputs for kMC calculations for which a 2D MDH lattice model was built using MM simulations. kMC results provided information on the macroscopic rates for the methanol oxidation process, and the cell characteristics (I-V curves) of a methanol fed biofuel with MDH as the anode.

Therefore, analysis using various multi-scale computational techniques concludes that:

7.1.1 Binding and Orientation of Methanol

- From the binding energy calculations, it was demonstrated that the smaller ion (Mg) containing MDH has a stronger affinity towards the substrate (methanol)

with a binding energy of -1.6 eV when compared to the Sr^{2+} and Ba^{2+} - containing MDH.

- Structural investigation of ion-modified MDH active site models determined that the coordination of the ions with the selected N6, O5 and O6 atoms of the PQQ (Cofactor) molecule created a structural distortion in all three models attributed to the difference in the ionic radii of these ions with respect to the calcium ion, which is the naturally occurring ion in the MDH active site (Mg^{2+} - $\text{Ca}^{2+} = -0.27 \text{ \AA}$, Sr^{2+} - $\text{Ca}^{2+} = 0.13 \text{ \AA}$ and Ba^{2+} - $\text{Ca}^{2+} = 0.36 \text{ \AA}$).
- When testing the three active site models (3 AA, 9 AA and 13 AA), the 13 AA (Model III) active site model was the most stable as the binding energy of methanol was around 1 eV, and 0.5 eV more stable than Model I (3 AA) and Model II (9 AA). As Model III (13 AA) has the lowest binding energy in all the active site models (Mg^{2+} , Ca^{2+} , Sr^{2+} and Ba^{2+} -containing MDH), this indicated that the hydrophobic residues (Gly, Ala and Trp) side chains able a steric strain on the substrate affinity to the binding pocket of the enzyme, and provide a neutral environment to increase the catalytic power of the charged moieties, in turn aiding in the catalytic activity of the enzyme.
- From testing the effect of the nature of amino acids in the active site of MDH, it is concluded that the 3 AA model is an appropriate active site cluster model to further study the methanol oxidation mechanism as the distances with respect to the substrate (H17-O14 and H16-C5) are in the same range as in 13 AA active site model (which is the identified active site by experimental studies).

- In conclusion, the nature of the ion and the amino acids in the active site of MDH modifies the binding and orientation of methanol, and it is estimated that the methanol oxidation reaction is facilitated as the size of the ion increases.

7.1.2 Methanol Oxidation by Ion-Modified MDH Enzymes

- The size of the active site model is important in the determination of energy barriers, considering PQQ + Ion + Asp-303 + Glu-177 + Asn-261 + 3 with nearby water molecules seemed to be sufficient enough to provide accurate information.
- The calculations conducted in this work imply that replacing the Ca^{2+} ion with Mg^{2+} and Sr^{2+} in the MDH active site and testing the H-T mechanism show that the size of the ion in the enzyme active site played a key role in the oxidation mechanism.
- Diverse possible arrangements of the reactant, intermediates and product were investigated, and several optimized energy configurations along the real potential energy surface of the molecular system were found. The best configuration (lowest energy system) was considered for further calculations.
- The geometries of the reactant, intermediates and product of Mg^{2+} and Sr^{2+} containing MDH models are within the experimentally observed configurations of Ca^{2+} -MDH [39]; however structural distortion is observed by the replacement of the metal ion in the MDH active site.
- The coordination of the ions with the molecular cleft atoms N6, O5 and O6 of the PQQ are noted for the obtained minimum energy structures and compared to Ca^{2+} -MDH coordination. The bond distances of the Mg^{2+} ion to O5, O6 and N6 atoms of the PQQ has decreased by an average of 0.33 Å, and the bond distances

of the Sr^{2+} ion to O5, O6 and N6 atoms of the PQQ has increased by an average of 0.24 Å when compared to distances of the calcium ion to these atoms of PQQ. Thus, the replacement of the naturally occurring calcium ion with magnesium and strontium affects the atom coordination, creating structural distortion.

- The free energy barrier for the rate limiting step (step 1 of the H-T mechanism) for the Mg^{2+} -MDH was found to be 2.5 kcal/mol greater than that obtained for Ca^{2+} -MDH, and for Sr^{2+} -MDH the free energy barrier was 12.9 kcal/mol lower than Ca^{2+} -MDH.
- The increase in activation barrier in the case of Mg^{2+} -MDH can be due to the fact that Mg^{2+} ion could not polarize the C5-O5 bond as Sr^{2+} and Ba^{2+} [49], thus resulting in less negative charge on the oxyanion O5 of PQQ and effecting the proton abstraction process.
- Due to the distortion caused by the small size of the Mg^{2+} ion, the second proton transfer as described in the H-T methanol oxidation mechanism by Ca^{2+} -MDH seems to be unnecessary in the case of Mg^{2+} -MDH, and formaldehyde seems to be produced barrierless immediately after the second intermediate is formed. Hence, an alternate step was tested, and the barrier for this step was kinetically favorable.
- Similarly, in the case of Sr^{2+} -MDH the last two steps in the H-T mechanism were not favorable, but when tested for the alternate step, it was kinetically feasible, suggesting that ion-modified MDH enzyme active site models prefer alternate reaction pathways.

- These results show that as the binding of methanol was stronger in the case of Mg^{2+} -containing MDH, it was more difficult to oxidize the methanol or produce formaldehyde when compared to the Sr^{2+} -MDH. In the case of Sr^{2+} -containing MDH, the methanol was weakly bonded and it made producing formaldehyde easily feasible.

7.1.3 Enzyme Catalysis by kMC Simulations

- A 2D lattice model to predict the macroscopic reaction rates of the enzyme was validated by testing the rate of consumption of the substrate (methanol) and the rate of formation of the product (formaldehyde). It was observed that the methanol concentration is reduced and formaldehyde concentration is increased, thus proving that the model (2D lattice) follows the general kinetic behavior of a system.
- To understand how macromolecular crowding (the other amino acids in the enzyme) affects the product formation, the influence of increasing the number of amino acids (obstacle density) on the conversion of methanol molecules was investigated. It was determined that the formation of formaldehyde is reduced by 50%, implying that the amino acids around MDH (other than the active site amino acids) play an important role for the product formation.
- Furthermore, Model 2 that consisted of the entire enzyme amino acids was considered and validated as an appropriate lattice model to evaluate macroscopic reaction rates.
- The effect of the substrate concentrations was considered to obtain the enzyme kinetic parameters (V_{max} and K_m) which are intrinsic properties for fuel cell

applications. It was observed that when the substrate concentration is higher than the active site concentration, the reaction velocity is constant.

- From the I-V curves it was seen that Mg^{2+} -MDH predict the short circuit current value below the experimental value. For the case of Sr^{2+} -MDH and Ba^{2+} -MDH, the current values were higher and therefore, proving that when a larger ion is present in the active site of the MDH, the catalytic activity of the enzyme is increased.

In summary, when the naturally occurring ion (calcium) is replaced by other divalent ions (Mg^{2+} , Sr^{2+} and Ba^{2+}), the binding of methanol and methanol electro-oxidation process are significantly affected and in agreement with previous experimental and theoretical studies on modified MDH enzymes. This variation affects the electron transfer to the electrode. From this multi-scale study, it can be concluded that when a larger ion (Sr^{2+} or Ba^{2+}) is present in the MDH active site, the binding of the substrate is weaker, which makes methanol oxidation faster and in turn increases the production of electrons. This finally leads to more current production and hence can be a better catalyst for bio-fuel cell applications.

Even though larger ions (Sr^{2+} and Ba^{2+}) present in the MDH active size seem to be better than the naturally occurring ion (Ca^{2+}), this may not be the case for all the larger ion containing enzymes. When a larger ion is present in the active site, it means it is a weaker Lewis acid, and generally, this means it decreases the activity of the enzyme. Also, a larger ion implies the electronegativity is less, indicating that it has a lower ability to attract electrons, and thus the coordination with the surrounding amino acid group can be modified drastically and in turn affects the reactivity of the enzyme. Hence, these

points should be taken into account when replacing the native ion in the enzyme with a larger ion.

7.2 Future Work

To address enzymatic reaction mechanisms, quantum chemical methods have been used and have become a booming area of interest over the past two decades. Presently, two popular approaches are employed, namely, the cluster method or the quantum mechanics-only method (QM) that uses only a small portion of the active site of the enzyme to model the reaction mechanisms and the hybrid quantum mechanics/molecular mechanics (QM/MM) method that uses the entire enzyme as the model [149-151]. In the case of the QM/MM approaches, a small part of the system is treated quantum mechanically to describe the electronic structure of molecules and the rest of the system is treated with a molecular mechanical method that describes interactions between atoms using a forcefield [120, 138, 152].

In principle, it is believed that the QM/MM approach is more complicated than the cluster approach. It is considered that the appropriate size of the QM region has a major influence on the QM/MM results. Technically, larger QM regions yield better results. In many cases, both methods were applied to study various classes of enzymes, and similar results and conclusions have been obtained [138, 153]. For instance, it was established that the QM/MM approach is considerably faster than the QM-only approach by Ochsenfeld and co-workers [154] when they studied the convergence of isomerization energies with respect to the size of the QM region for three different proteins. In another study, different sizes of the QM regions in both QM-only and QM/MM calculations were investigated by Ryde *et al.* [155] for evaluating the reaction energies of a proton transfer

in [Ni, Fe] hydrogenase, and found that when the connection between the QM and MM parts were accurately selected, a better convergence is obtained. In another comparison study by Liao *et al.* [156] for the mechanism of tungsten-dependent acetylene hydratase, they highlight that to provide reasonable mechanistic scenarios and realistic energy profiles for enzymatic reactions, a properly designed QM model is necessary. Therefore, it is shown that QM region size plays an important part in enzyme catalysis.

In this work, the QM-only method was used to model the methanol oxidation process by MDH enzyme. In future work, the QM/MM approach can be employed to model the methanol oxidation process. To explore further, if both the approaches yield the similar results or dissimilar outcomes, QM regions with different sizes can be tested. The complete active site model (13 AA) and the 9 AA model can be considered as the QM regions and the reaction mechanisms can be studied and compared.

Another important aspect while studying the enzyme catalysis by QM approach is the electrostatic (solvation) effects which are usually modeled using a polarizable continuum technique as discussed in Chapter 3. Unlike the QM/MM method where the surroundings are accounted using a forcefield, the enzyme environment in the case of QM is considered as a homogenous polarizable medium with a dielectric constant (ϵ). Generally, a value of $\epsilon = 4$ is considered, as it is a good representation of protein surroundings. From previous studies, it is believed that as the model size grows, relative solvation effects will decrease because additional groups that provide polarization are already explicitly included in the model. It is shown that the solvation effects saturate when the model size reaches a size of ca 150-200 atoms [120].

For example, Liao *et al.* [156] investigated the effect of the active site model size for the case of decarboxylase enzymes. The size of the active site model was systematically increased from 27 to 220 atoms and five different dielectric constants ($\epsilon = 2, 4, 8, 16, \text{ and } 80$) were used. It was established that once the model reached a size of 220 atoms, the relative energies were basically the same whether the homogenous surrounding is included or not, i.e. the solvation effects saturated. In another study performed by Sevastik *et al.* [81] who explored the reaction mechanism of 4-oxalocrotonate tautomerase (4-OT) and the influence of active site cluster model size. Two different quantum chemical models consisting of 77 and 177 atoms were constructed, and to model the enzyme environment several dielectric constants ($\epsilon = 2, 4, 8, 16 \text{ and } 80$) were used. It was observed that the inclusion of solvation effects changes the reaction energies very moderately in the case of the 177 atoms model, proving that the solvation effects saturate when the model reaches a size of 150-200 atoms and critical parts of the active site are explicitly included in the quantum model. Future work could include understanding thoroughly the solvation effect on the methanol oxidation process by MDH. Active size models with an increasing number of atoms at different dielectric constants can be studied. This will provide valued information on the appropriate MDH active site model size.

Also in the future, studying the diffusion of methanol in the ion-modified MDH enzymes will provide transport properties such as diffusion coefficient. Comparing the diffusion coefficients of methanol in the ion-modified MDH enzymes will specify how fast or slow the substrate can diffuse into the enzyme and give more insight about the substrate specificity. MM and MD simulations can be performed to obtain the diffusivity

of substrate molecules into the enzyme and the diffusion coefficients obtained can be used as another input parameter for kMC calculations.

To perform its catalytic functions, it is known that the MDH enzyme prefers a basic environment. By studying a range of pH values, a premium environment for catalytic function could be determined through the examination of the effects of pH on diffusion coefficients. Also, these pH studies will also help determine which form (protonated or unprotonated) of amino acid residue should be used in the cluster model to better understand the reaction mechanism. So far the enzyme-assisted reactions were modeled as a 2-D grid for performing kMC simulations; it would be interesting to extend these simulations on a 3D lattice that would accommodate all the species of MDH in their exact positions.

REFERENCES

- [1] A. M. Kannan, V. Renugopalakrishnan, S. Filipek, P. Li, G. F. Audette, and L. Munukutla, "Bio-Batteries and Bio-Fuel Cells: Leveraging on Electronic Charge Transfer Proteins," *Journal of Nanoscience and Nanotechnology*, vol. 3, pp. 1665-1678., 2009.
- [2] E. G. Hibbert, F. Baganz, H. C. Hailes, J. M. Ward, G. J. Lye, J. M. Woodley, and P. A. Dalby, "Directed evolution of biocatalytic processes," *Biomolecular Engineering*, vol. 22, pp. 11-19, 2005.
- [3] F. Hollmann, I. W. C. E. Arends, K. Buehler, A. Schallmeyer, and B. Buhler, "Enzyme-mediated oxidations for the chemist," *Green Chemistry*, vol. 13, pp. 226-265, 2011.
- [4] C. Sissi and M. Palumbo, "Effects of magnesium and related divalent metal ions in topoisomerase structure and function," *Nucleid Acids Research*, vol. 37, pp. 702-711, 2009.
- [5] S. Sanchez and A. L. Demain, "Enzymes and Bioconversions of Industrial, Pharmaceutical, and Biotechnological Significance," *Organic Process Research & Development*, vol. 15, pp. 224-230, 2011.
- [6] J.A. Cracknell, K.A.Vincent, and F. A. Armstrong, "Enzymes as Working or Inspirational Electrocatalysts for Fuel Cells and Electrolysis," *Chemical Reviews*, vol. 108, pp. 2439-2461, 2008.
- [7] A. K. Jones, E. Sillery, S. P. J. Albracht, and F. A. Armstrong, "Direct comparison of the electrocatalytic oxidation of hydrogen by an enzyme and a platinum catalyst," *Chemical Communications*, vol. 0, pp. 866-867, 2002.
- [8] A. T. Yahiro, S. M. Lee, and D. O. Kimble, "Bioelectrochemistry: I. Enzyme utilizing bio-fuel cell studies," *Biochimica et Biophysica Acta (BBA) - Specialized Section on Biophysical Subjects*, vol. 88, pp. 375-383, 1964.
- [9] Jungbae Kim, Hongfei Jia, and P. Wang, "Challenges in biocatalysis for enzyme-based biofuel cells," *Biotechnology Advances*, vol. 24, pp. 296– 308, 2006.

- [10] L. Liu, Z. Chen, S. Yang, X. Jin, and X. Lin, "A novel inhibition biosensor constructed by layer-by-layer technique based on biospecific affinity for the determination of sulfide," *Sensors and Actuators B: Chemical*, vol. 129, pp. 218-224, 2008.
- [11] S. Suwansa-ard, P. Kanatharana, P. Asawatreratanakul, C. Limsakul, B. Wongkittisuksa, and P. Thavarungkul, "Semi disposable reactor biosensors for detecting carbamate pesticides in water," *Biosensors and Bioelectronics*, vol. 21, pp. 445-454, 2005.
- [12] H. Sakai, T. Nakagawa, Y. Tokita, T. Hatazawa, T. Ikeda, S. Tsujimura, and K. Kano, "A high-power glucose/oxygen biofuel cell operating under quiescent conditions," *Energy & Environmental Science*, vol. 2, pp. 133-138, 2009.
- [13] A.K. Sarmaa, P.Vatsyayanb, P.Goswamib, and S. D. Minteerc, "Recent advances in material science for developing enzyme electrodes," *Biosensors and Bioelectronics*, vol. 24 pp. 2313–2322, 2009.
- [14] V.Laurinavicius, J. Razumiene, B.Kurtinaitiene, I.Lapenaite, I.Bachmatova, L.Marcinkeviciene, R.Meskys, and A.Ramanavicius, "Bioelectrochemical application of some PQQ-dependent enzymes," *Bioelectrochemistry*, vol. 55, pp. 29-32, 2002.
- [15] R. A. Rincón, K. Artyushkova, M. Mojica, M. N. Germain, S. D. Minteer, and P. Atanassov, "Structure and Electrochemical Properties of Electrocatalysts for NADH Oxidation," *Electroanalysis*, vol. 22, pp. 799-806, 2010.
- [16] A.Ramanavicius and A.Ramanaviciene, "Hemoproteins in Design of Biofuel Cells," *Fuel Cells* vol. 1, pp. 25-36, 2009.
- [17] G. Davis, H. A. O. Hill, W. J. Aston, I. John Higgins, and A. P. F. Turner, "Bioelectrochemical fuel cell and sensor based on a quinoprotein, alcohol dehydrogenase," *Enzyme and Microbial Technology*, vol. 5, pp. 383-388, 1983.
- [18] P. L. Yue and K. Lowther, "Enzymatic oxidation of C1 compounds in a biochemical fuel cell," *The Chemical Engineering Journal*, vol. 33, pp. B69-B77, 1986.
- [19] J. A. Duine, "The PQQ story," *Journal of bioscience and bioengineering*, vol. 88, pp. 231–236, 1999.
- [20] I. Lapėnaitė, B. Kurtinaitienė, L. Pliuškyš, V. Laurinavičius, I. Bachmatova, L. Marcinkevičienė, and A. Ramanavičius, "Application of PQQ-GDH Based Polymeric Layers in Design of Biosensors for Detection of Heavy Metals," *Materials Science*, vol. 9, pp. 431-435, 2003.

- [21] K. J. Waldron, J. C. Rutherford, D. Ford, and N. J. Robinson, "Metalloproteins and metal sensing," *Nature*, vol. 460, pp. 823-830, 2009.
- [22] T.Dudev and C.Lim, "Effect of Carboxylate-Binding Mode on Metal Binding/Selectivity and Function in Proteins," *Accounts of Chemical Research*, vol. 40, pp. 85-93, 2007.
- [23] M.Babor, H.M. Greenblatt, M.Edelman, and V.Sobolev., "Flexibility of Metal Binding Sites in Proteins on a Database Scale," *PROTEINS:Structure, Function and Bioinformatics*, vol. 59, pp. 221-230, 2005.
- [24] Y. Lu, N. Yeung, N. Sieracki, and N. M. Marshall, "Design of functional metalloproteins," *Nature*, vol. 460, pp. 855-862, 2009.
- [25] C.Andreini, I.Bertini, G.Cavallaro, G.L. Holliday, and J. M.Thornton, "Metal ions in biological catalysis: from enzyme databases to general principles," *Journal of Biological Inorganic Chemistry*, vol. 13, pp. 1205-1218, 2008.
- [26] M. Halka and B. Nordstrom, *Alkali and Alkaline Earth Metals*, 2010.
- [27] R.Murugavel, K.Baheti, and G.Anantharaman, "Reactions of 2-Mercaptobenzoic Acid with Divalent Alkaline Earth Metal Ions:Synthesis,Spectral Studies, and Single-Crystal X-ray Structures of Calcium, Strontium, and Barium Complexes of 2,2'-Dithiobis (benzoic acid)," *Inorganic Chemistry*, vol. 40, pp. 6870-6878, 2001.
- [28] B. C.Dave, "Prospects for Methanol Production," in *Bioenergy*. Washington, DC: ASM Press, 2008.
- [29] A. Arico, S. Srinivasan, and V. Antonucci, "DMFCs: From Fundamental Aspects to Technology Development " *Fuel Cells*, vol. 1, pp. 133-161, 2001.
- [30] D.Sokic-Lazic, R. L. Arechederra, B.L.Treu, and S.D.Minteer, "Oxidation of Biofuels:Fuel Diversity and Effectiveness of Fuel Oxidation through Multiple Enzyme Cascades," *Electroanalysis*, vol. 22, pp. 757-764, 2010.
- [31] I.Ivanov, T.Vidakovic-Koch, and K.Sundmacher, "Recent Advances in Enzymatic Fuel Cells:Experiments and Modeling," *Energies*, vol. 3, pp. 803-846, 2010.
- [32] X.C. Zhang, A. Ranta, and A. Halme, "Direct methanol biocatalytic fuel cell— Considerations of restraints on electron transfer," *Journal of Biosensors and Bioelectronics*, vol. 21, pp. 2052-2057, 2006.
- [33] M. G. Goodwin and C. Anthony, "Characterization of a Novel Methanol Dehydrogenase Containing a Ba²⁺ Ion at the Active Site," *The Biochemical Journal*, vol. 318, pp. 673-679, 1996.

- [34] M.G. Goodwin, A.Avezoux, S.L. Dales, and C.Anthony., "Reconstitution of the quinoprotein methanol dehydrogenase from inactive Ca^{2+} -free enzyme with Ca^{2+} , Sr^{2+} or Ba^{2+} ," *The Biochemical Journal*, vol. 319, pp. 839-842, 1996.
- [35] A.R. Dewanti and J. A. Duine, " Ca^{2+} -assisted, direct hydride transfer, and rate-determining tautomerization of C5-reduced PQQ to PQQH₂, in the oxidation of beta-D-glucose by soluble, quinoprotein glucose dehydrogenase," *Biochemistry*, vol. 39, pp. 9384-9392, 2000.
- [36] A. R. Dewanti and J. A. Duine, "Reconstitution of membrane-integrated quinoprotein glucose dehydrogenase apoenzyme with PQQ and the holoenzyme's mechanism of action," *Biochemistry*, vol. 37, pp. 6810, 1998.
- [37] C. Anthony, *Methanol Dehydrogenase, a PQQ-Containing Quinoprotein Dehydrogenase*. New York.: Kluwer Academic/ Plenum Publishers 2000.
- [38] I. W. Richardson and C. Anthony, "Characterization of mutant forms of the quinoprotein methanol dehydrogenase lacking an essential calcium ion," *Biochemical Journal*, vol. 287, pp. 709-715, 1992.
- [39] S. Itoh, H. Kawakami, and S. Fukuzumi, "Model Studies on Calcium-Containing Quinoprotein Alcohol Dehydrogenases. Catalytic Role of Ca^{2+} for the Oxidation of Alcohols by Coenzyme PQQ (4,5 Dihydro-4,5-Dioxo-1h-Pyroolo[2,3-F]Quinoline-2,7,9-Tricarboxylic Acid)," *Biochemistry*, vol. 37, pp. 6562-6571, 1998.
- [40] P.R. Afolabi, K. Amaratunga, O. Majekodunmi, S. L. Dales, R. Gill, D. Thompson, J. B. Cooper, S. P. Wood, P. M. Goodwin, and C. Anthony, "Site-Directed Mutagenesis and XRay-Crystallography of the PQQ-Containing Quinoprotein Methanol Dehydrogenase and Its Electron Acceptor, Cytochrome CL," *Biochemistry*, vol. 40, pp. 9799-9809, 2001.
- [41] M. Ghosh, C. Anthony, K. Harlas, M. G. Goodwin, and C. C. F. Blake, "The Refined Structure of the Quinoprotein Methanol Dehydrogenase from *Methylobacterium Extorquens* at 1.94 Å," *Structure*, vol. 3, pp. 1771-1787, 1995.
- [42] S. White , G. Boyd , F. S. Mathews , Z. X. Xia , W. W. Dai , Y. S. Zhang , and V. L. Davidson, "The Active Site Structure of Calcium Containing Methanol Dehydrogenase," *Biochemistry*, vol. 32, pp. 12955-12958, 1993.
- [43] P. A. Williams, L. Coates, F. Mohammed, R. Gill, P. T. Erskine, A. Coker, S. P. Wood, C. Anthony, and J. B. Cooper, "The atomic resolution structure of methanol dehydrogenase from *Methylobacterium extorquens*," *Acta crystallographica. Section D, Biological crystallography*, vol. D61, pp. 75-79, 2005.

- [44] Z. X. Xia, Y. N. He, W. W. Dai, S. White, G. Boyd, and F. S. Mathews, "Detailed Active Site Configuration of a New Crystal Form of Methanol Dehydrogenase from *Methylophilus W3a1* at 1.9 Å Resolution," *Biochemistry*, vol. 38, pp. 1214-1220, 1999.
- [45] Z. X. Xia, Y. N. He, W. W. Dai, S. White, G. Boyd, and F. S. Mathews, "Determination of Gene sequence and Three-dimensional Structure at 2.4 Å resolution of Methanol Dehydrogenase from *Methylophilus W3A1*," *Journal of Molecular Biology*, vol. 259, pp. 480-501, 1996.
- [46] Z. X. Xia, W. W. Dai, J. P. Xiong, Z. P. Hao, V. L. Davidson, S. White, and F. S. Mathews, "The Three-Dimensional Structures of Methanol Dehydrogenase from Two Methylophilic Bacteria at 2.6 Å Resolution," *The Journal of Biological Chemistry*, vol. 267, pp. 22289-22297, 1992.
- [47] C. Anthony and P. Williams, "The Structure and Mechanism of Methanol Dehydrogenase," *Biochimica et Biophysica Acta*, vol. 1647, pp. 18-23, 2003.
- [48] M. Leopoldini, N. Russo, and M. Toscano, "The Preferred Reaction Path for the Oxidation of Methanol by PQQ-Containing Methanol Dehydrogenase: Addition–Elimination versus Hydride-Transfer Mechanism," *Chemistry*, vol. 13, pp. 2109-2117, 2007.
- [49] N. B. Idupulapati and D. S. Mainardi, "Quantum Chemical Modeling of Methanol Oxidation Mechanisms by Methanol Dehydrogenase Enzyme: Effect of Substitution of Calcium by Barium in the Active Site," *Journal of Physical Chemistry A*, vol. 114, pp. 1887, 2010.
- [50] J. Frank, S.H. van Krimpen, P.E.J. Verwiel, J.A. Jongejan, and A.C. Mulder, "On the mechanism of inhibition of methanol dehydrogenase by cyclopropane-derived inhibitors," *European Journal of Biochemistry* vol. 184, pp. 187-195, 1989.
- [51] J. Frank, M. Dijkstra, J.A. Duine, and C. Balny, "Kinetic and spectral studies on the redox forms of methanol dehydrogenase from *Hyphomicrobium X*," *European Journal of Biochemistry* vol. 174, pp. 331-338, 1988.
- [52] S. Itoh, H. Kawakami, and S. Fukuzumi, "Development of the Active Site Model for Calcium-Containing Quinoprotein Alcohol Dehydrogenases," *Journal of Molecular Catalysis B: Enzymatic*, vol. 8, pp. 85-94, 2000.
- [53] A. Oubrie, H.J. Rozeboom, K.H. Kalk, E.J. Huizinga, and B. W. Dijkstra, "Crystal structure of quinoxinoprotein alcohol dehydrogenase from *Comamonas testosteroni*; structural basis for substrate oxidation and electron transfer," *The Journal of Biological Chemistry*, vol. 277, pp. 3727-3732, 2002.

- [54] A. Oubrie, H.J. Rozeboom, K.H. Kalk, A.J. Olsthoorn, J.A. Duine, and B. W. Dijkstra, "Structure and mechanism of soluble quinoprotein glucose dehydrogenase," *The EMBO Journal*, vol. 18, pp. 5187-5194, 1999.
- [55] S. Y. Reddy, F. S. Mathews, Y. J. Zheng, and T. C. Bruice, "Quinoprotein Methanol Dehydrogenase: A Molecular Dynamics Study and Comparison with Crystal Structure," *Journal of Molecular Structure*, vol. 655, pp. 269-277, 2003.
- [56] S. Y. Reddy and T. C. Bruice, "In-Silico Studies of the Mechanism of Methanol Oxidation by Quinoprotein Methanol Dehydrogenase," *Journal of American Chemical Society*, vol. 125, pp. 8141-8150, 2003.
- [57] C. W. M. Kay, B. Mennenga, H. Görisch, and R. Bittl, "Substrate-Binding in Quinoprotein Ethanol Dehydrogenase from *Pseudomonas aeruginosa* Studied by Electron Paramagnetic Resonance at 94 GHz," *Journal of the American Chemical Society*, vol. 127, pp. 7974, 2005.
- [58] J. Li, J.-H. Gan, F. S. Mathews, and Z.-X. Xia, "The enzymatic reaction-induced configuration change of the prosthetic group PQQ of methanol dehydrogenase," *Biochemical and Biophysical Research Communications*, vol. 406, pp. 621-626, 2011.
- [59] N. B. Idupulapati and D. S. Mainardi, "A DMOL3 Study of the Methanol Addition-Elimination Oxidation Mechanism by Methanol Dehydrogenase Enzyme," *Molecular Simulation*, vol. 34, pp. 1057-1064, 2008.
- [60] A.J.J. Olsthoorn and J. A. Duine, "On the mechanism and specificity of the soluble, quinoprotein glucose dehydrogenase in the oxidation of aldose sugars.," *Biochemistry*, vol. 37, pp. 13854-13861, 1998.
- [61] O. Adachi, K. Matsushita, E. Shinagawa, and M. Ameyama, "Calcium in Quinoprotein Methanol Dehydrogenase Can Be Replaced by Strontium," *Agricultural and Biological Chemistry*, vol. 54, pp. 2833-2837, 1990.
- [62] N. B. Idupulapati and D. S. Mainardi, "Coordination and binding of ions in Ca^{2+} - and Ba^{2+} -containing methanol dehydrogenase and interactions with methanol," *Journal of Molecular Structure: THEOCHEM*, vol. 901, pp. 72, 2009.
- [63] E. T. Buurman, J. L. Boiardi, M. J. Teixeira de Mattos, and O. M. Neijssel, "The role of magnesium and calcium ions in the glucose dehydrogenase activity of *Klebsiella pneumoniae* NCTC 418," *Archives of Microbiology*, vol. 153, pp. 502-505, 1990.

- [64] T. Okajima, S. Kishishita, Y-C. Chiu, T. Murakawa, M. Kim, H. Yamaguchi, S. Hirota, S. Kuroda, and K. Tanizawa., "Reinvestigation of metal ion specificity for quinone cofactor biogenesis in bacterial copper amine oxidase," *Biochemistry*, vol. 44, pp. 12041-12048, 2005.
- [65] I.A.Topol, A.V.Nemukhin, K. Salnikow, R.E.Cachau, Y.G.Abashkin, K.S.Kasprzak, and S.K.Burt., "Quantum chemical modeling of reaction mechanism for 2-Oxoglutarate dependent enzymes: Effect of substitution of Iron by Nickel and Cobalt.," *Journal of Physical Chemistry A*, vol. 110, pp. 4223-4228, 2006.
- [66] T.Inoue, D. Irikura, N.Okazaki, S.Kinugasa, H.Matsumura, N.Uodome, M.Yamamoto, T.Kumasaka, M. Miyano, Y.Kai, and Y.Urade., "Mechanism of metal activation of human hematopoietic prostaglandin D synthase," *Nature Structural Biology*, vol. 10, pp. 291-296, 2003.
- [67] H R Horton, L A Moran, R S Ochs, J D Rawn, and K. G. Scrimgeour., *Principles of Biochemistry* Neil Patterson Publishers Prentice Hall Inc. , 1993.
- [68] T.K. Harris and V.L.Davidson, "Replacement of enzyme-bound calcium with strontium alters the kinetic properties of methanol dehydrogenase," *The Biochemical Journal*, vol. 300, pp. 175-182, 1994.
- [69] E. Garcia- Rodriguez, T. Ohshiro, T.Aibara, Y.Izumi, and J.Littlechild, "Enhancing effect of calcium and vanadium ions on thermal stability of bromoperoxidase from *Corallina pilulifera*," *Journal of Biological Inorganic Chemistry*, vol. 10, pp. 275-282, 2005.
- [70] R.Car, "Introduction to density-functional theory an ab-initio molecular dynamics," *Quantitative Structure-Activity Relationships*, vol. 21, pp. 97-104, 2002.
- [71] M. A. L. Marques and E. K. U. Gross, "TIME-DEPENDENT DENSITY FUNCTIONAL THEORY," *Annual Review of Physical Chemistry*, vol. 55, pp. 427-455, 2004.
- [72] J. W. Ponder, D. A. Case, and D. Valerie, "Force Fields for Protein Simulations," in *Advances in Protein Chemistry*, vol. Volume 66: Academic Press, 2003, pp. 27-85.
- [73] R.M.Nieminen, "From atomistic simulation towards multiscale modelling of materials," *Journal of Physics Condensed Matter*, vol. 14, pp. 2859-2876, 2002.
- [74] J. J. Lukkien, J. P. L. Segers, P. A. J. Hilbers, R. J. Gelten, and A. P. J. Jansen, "Efficient Monte Carlo methods for the simulation of catalytic surface reactions," *Physical Review E*, vol. 58, pp. 2598-2610, 1998.

- [75] J. M. Parks, P. Imhof, and J. C. Smith, "Understanding Enzyme Catalysis Using Computer Simulation," in *Encyclopedia of Catalysis*: John Wiley & Sons, Inc., 2002.
- [76] W.B.Motherwell, M.J.Bingham, and Y.Six, "Recent progress in the design and synthesis of artificial enzymes," *Tetrahedron*, vol. 57, pp. 4663-4686, 2001.
- [77] K. H. Hopmann and F. Himo, "Theoretical Study of the Full Reaction Mechanism of Human Soluble Epoxide Hydrolase," *Chemistry*, vol. 12, pp. 6898-6909, 2006.
- [78] K. H. Hopmann and F. Himo, "Quantum Chemical Modeling of the Dehalogenation Reaction of Haloalcohol Dehalogenase," *Journal of Chemical Theory and Computation*, vol. 4, pp. 1129-1137, 2008.
- [79] L. Noodleman, T. Lovell, W. Han, J. Li, and F. Himo, "Quantum Chemical Studies of Intermediates and Reaction Pathways in Selected Enzymes and Catalytic Synthetic Systems," *Chemical Review*, vol. 104, pp. 459-508, 2004.
- [80] P. Velichkova and F. Himo, "Theoretical Study of the Methyl Transfer in Guanidinoacetate Methyltransferase," *Journal of Physical Chemistry B*, vol. 110, pp. 16-19, 2006.
- [81] R. Sevastik and F. Himo, "Quantum chemical modeling of enzymatic reactions: The case of 4-oxalocrotonate tautomerase," *Bioorganic Chemistry*, vol. 35, pp. 444-457, 2007.
- [82] R. Zhen Liao, J. Yu, F. M. Raushel, and F. Himo, "Theoretical Investigation of the Reaction Mechanism of the Dinuclear Zinc Enzyme Dihydroorotase," *Chemistry - A European Journal*, vol. 14, pp. 4287-4292, 2008.
- [83] R. Cammi., B. Mennucci, and J. Tomasi, "Fast evaluation of geometries and properties of excited molecules in solution: A Tamm-Dancoff model with application to 4-dimethylaminobenzonitrile," *Journal of Physical Chemistry A*, vol. 104, pp. 5631-5637 2000.
- [84] G. S. M. Cossi, N. Rega, V. Barone, *Journal of Chemical Physics*, vol. 43, pp. 117, 2002.
- [85] Accelrys Inc., "DMOL3 User Guide ". San Diego, 2003.
- [86] B. Delley, "From Molecules to Solids with the DMol3 Approach," *Journal of Chemical Physics*, vol. 113, pp. 7756-7764, 2000.
- [87] "Material Studio Software Package," Accelrys, Ed. San Diego, CA, 2008.

- [88] A. D. Becke, "Density-functional thermochemistry III. The role of exact exchange," *Journal of Chemical Physics*, vol. 98, pp. 5648-5652, 1993.
- [89] C. Lee, W. Yang, and R. G. Parr, "Development of the Colle-Salvetti Correlation-Energy Formula into a Functional of the Electron Density," *Physical Review. B*, vol. 37, pp. 785-789, 1988.
- [90] A. D. Becke, "Density-Functional Exchange-Energy Approximation with Correct Asymptotic Behavior," *Physical Review A*, vol. 38 pp. 3098-3100, 1988.
- [91] W. Koch and M. C. Holthausen, *A Chemist's Guide to Density Functional Theory*, Second ed: Wiley-CVH, 2001.
- [92] R. M. Dreialer and E. K. U. Gross, *Density Functional Theory: An Approach to Quantum Many Body Problem*. Berlin: Springer, 1990.
- [93] C. G. Hill, *An Introduction to Chemical Engineering Kinetics & Reactor Design*. New York, 1977.
- [94] T. Xie, J. M. Bowman, K. A. Peterson, and B. Ramachandran, "Quantum Calculations of the Rate Constants for the O(3P) + HCl Reaction on new Ab Initio 3A" and 3A' Surfaces," *Journal of Chemical Physics*, vol. 119, pp. 9601-9608, 2003.
- [95] B. Ramachandran and K. A. Peterson, "Potential Energy Surfaces for the 3A" and 3A' Electronic States of the O(3P) + HCl System," *Journal of Chemical Physics*, vol. 119, pp. 9590-9600, 2003.
- [96] F. Jensen, *Introduction to Computational Chemistry*. New York: Wiley & Sons, 2002.
- [97] J. F. Stanton, A Chemist's Guide to Density Functional Theory By Wolfram Koch (German Chemical Society, Frankfurt am Main) and Max C. Holthausen (Humbolt University Berlin). Wiley-VCH: Weinheim. 2000. *Journal of the American Chemical Society*, 2001. 123(11): p. 2701-2701.
- [98] A. R. Leach, *Molecular Modeling: principles and applications*. London: Prentice Hall,, 2001.
- [99] E. lewars, *Introduction to the Theory and Applications of Molecular and Quantum Mechanics*. Norwell: Kluwer Academic Publications, 2003.
- [100] J. B. Foresman and A. Frisch, *Exploring Chemistry with Electronic Structure Methods*. Pittsburgh, PA: Gaussian Inc, 1996.

- [101] P. Hohenberg and W. Kohn, "Inhomogeneous electron gas," *Physical Review B*, vol. 136, pp. 864-871, 1964.
- [102] W. Kohn and L. J. Sham, "Self-consistent equations including exchange and correlation effects," *Physical Review A*, vol. 140, pp. 1133-1138, 1965.
- [103] J. P. Perdew, *Electronic Structure of Solids*. Berlin: Akademie Verlag, 1991.
- [104] J. P. Perdew, J. A. Chevary, S. H. Vosko, K. A. Jackson, M. R. Pederson, D. J. Singh, and C. Fiolhais, "Atoms, molecules, solids, and surfaces: applications of the generalized gradient approximation for exchange and correlation," *Physical Review B*, vol. 46, pp. 6671-6687, 1992.
- [105] Y. Wang, "Accurate and simple analytic representation of the electron-gas correlation energy," *Physical Review B*, vol. 45, pp. 13244-13249, 1992.
- [106] D. H. Jung, C. H. Lee, C. S. Kim, and D. R. Shin, "Performance of a Direct Methanol Polymer Electrolyte Fuel Cell," *Journal of Power Sources*, vol. 71, pp. 169-173, 1998.
- [107] C. J. Cramer, *Essentials of Computational Chemistry: Theories and Models*. West Sussex: Wiley & Sons, 2004.
- [108] B. Delley, "An all electron numerical method for solving the local density functional for polyatomic molecules", *Journal of Chemical Physics*, vol. 92, pp. 508-518, 1990.
- [109] Accelrys, "Materials Studio," 2006.
- [110] M.E Grillo, N. Govind, G. Fitzgerald, and K. B. Stark, "Computational Material Science with Materials Studio: Applications in Catalysis," *Lecture Notes in Physics*, vol. 642, pp. 202-227, 2004.
- [111] N. Govind, M. Petersen, G. Fitzgerald, D. King-Smith, and J. Andzelm, " A generalized synchronous transit method for transition state location " *Computational Material Science*, vol. 28, pp. 250-258, 2003.
- [112] C. S. Tsai, "Molecular Modeling: Molecular Mechanics," in *An Introduction to Computational Biochemistry*: John Wiley & Sons, Inc., 2002, pp. 285-314.
- [113] R. Perez-Aparicio, F. Alvarez, A. Arbe, L. Willner, D. Richter, P. Falus, and J. Colmenero, "Chain Dynamics of Unentangled Poly(ethylene-alt-propylene) Melts by Means of Neutron Scattering and Fully Atomistic Molecular Dynamics Simulations," *Macromolecules*, vol. 44, pp. 3129-3139, 2011.

- [114] J. Yang, Y. Ren, A.-m. Tian, and H. Sun, "COMPASS Force Field for 14 Inorganic Molecules, He, Ne, Ar, Kr, Xe, H₂, O₂, N₂, NO, CO, CO₂, NO₂, CS₂, and SO₂, in Liquid Phases," *Journal of Physical Chemistry B*, vol. 104, pp. 4951-4957, 2000.
- [115] R.M.Nieminen and A.P.J.Jansen, "Monte Carlo Simulations of surface reactions," *Applied Catalysis A:General*, vol. 160, pp. 99-123, 1997.
- [116] N.K.R.Dandala, A.P.J.Jansen, and D.S.Mainardi, "A Multi-scale Modeling Approach for Studying MDH-Catalyzed Methanol Oxidation," in *Multiscale Modeling: From Atoms to Devices*, T. C. Pedro Derosa, Ed. Florida: CRC Press Inc, 2010, pp. 91-112.
- [117] C. W. Hills, M. S. Nashner, A. I. Frenkel, J. R. Shapley, and R. G. Nuzzo, "Carbon Support Effects on Bimetallic Pt-Ru Nanoparticles Formed from Molecular Precursors," *Langmuir*, vol. 15, pp. 690-800, 1999.
- [118] F. Himo, "Catalytic Mechanism of Benzylsuccinate Synthase, a Theoretical Study," *Journal of Physical Chemistry B*, vol. 106, pp. 7688-7692, 2002.
- [119] F. Himo, "Quantum chemical modeling of enzyme active sites and reaction mechanisms," *Theoretical Chemistry Accounts*, vol. 116, pp. 232-240, 2006.
- [120] P. E. M. Siegbahn and F. Himo, "The quantum chemical cluster approach for modeling enzyme reactions," *WIREs Computational Molecular Science* vol. 1, pp. 323-336, 2011
- [121] Per E. M. Siegbahn and F. Himo, "Recent developments of the quantum chemical cluster approach for modeling enzyme reactions," *Journal of Biological Inorganic Chemistry*, vol. 14, pp. 643-651, 2009.
- [122] Shi-Lu Chen, Wei-Hai Fang, and F. Himo, "Technical aspects of quantum chemical modeling of enzymatic reactions: the case of phosphotriesterase," *Theoretical Chemistry Accounts*, vol. 120, pp. 515-522, 2008.
- [123] S. Yanagisawa, P. B.Crowley, S. J.Firbank, A. T.Lawler, D. M.Hunter, W. McFarlane, C. Li, T. Kohzuma, M. J.Banfield, and C. Dennison, " π -Interaction Tuning of the Active Site Properties of Metalloproteins," *Journal of the American Chemical Society*, vol. 130, pp. 15420-15428, 2008.
- [124] T.Lovell, F.Himo, W-G.Han, and L.Noodleman, "Density functional methods applied to metalloenzymes," *Coordination Chemistry Reviews*, vol. 238-239, pp. 211- 232, 2003.

- [125] P. Williams, L. Coates, F. Mohammed, R. Gill, P. Erskine, D. Bourgeois, S. P. Wood, C. Anthony, and J. B. Cooper, "The 1.6 Å X-ray Structure of the Unusual c-type Cytochrome, Cytochrome cL, from the Methylophilic Bacterium *Methylobacterium extorquens*," *Journal of Molecular Biology*, vol. 357, pp. 151-162, 2006.
- [126] H. Berman, K. Henrick, H. Nakamura, and J. L. Markley, "The worldwide Protein Data Bank (wwPDB): ensuring a single, uniform archive of PDB data," *Nucleic Acids Research*, vol. 35, pp. D301-3, 2007.
- [127] C. Anthony, "The quinoprotein dehydrogenases for methanol and glucose," *Archives of Biochemistry and Biophysics*, vol. 428, pp. 2-9, 2004.
- [128] Gail J. Bartlett, Craig T. Porter, Neera Borkakoti, and J. M. Thornton, "Analysis of Catalytic Residues in Enzyme Active Sites," *Journal of Molecular Biology*, vol. 324, pp. 105-121, 2002.
- [129] M. Silberstein, S. Dennis, L. Brown III, T. Kortvelyesi, K. Clodfelter, and S. Vajda, "Identification of Substrate Binding Sites in Enzymes by Computational Solvent Mapping," *Journal of Molecular Biology*, vol. 332, pp. 1095-1113, 2003.
- [130] S. Kumar, N. Kumar, and R. K. Gaur, "Amino Acid Frequency Distribution at Enzymatic Active Site," *IIOAB Journal*, vol. 2, pp. 23-30, 2011.
- [131] S. Itoh, H. Kumei, S. Nagatomo, T. Kitagawa, and S. Fukuzumi, "Effects of Metal Ions on Physicochemical Properties and Redox Reactivity of Phenolates and Phenoxy Radical: Mechanistic Insight into Hydrogen Atom Abstraction by Phenoxy radical-Metal Complexes," *Journal of the American Chemical Society*, vol. 123, pp. 2165-2175, 2001.
- [132] M. D. Toscano, K. J. Woycechowsky, and D. Hilvert, "Minimalist Active-Site Redesign: Teaching Old Enzymes New Tricks," *Angewandte Chemie*, vol. 46, pp. 3212-3236, 2007.
- [133] P. Tao, H. B. Schlegel, and D. L. Gatti, "Common basis for the mechanism of metallo and non-metallo KDO8P synthases," *Journal of Inorganic Biochemistry*, vol. 104, pp. 1267-1275, 2010.
- [134] A. L. Lehninger, "Role of Metal Ions in Enzyme Systems," *Physiological reviews*, vol. 30, pp. 393-429, 1950.
- [135] N. B. Idupulapati and D. S. Mainardi, "Methanol Electro-Oxidation by Methanol Dehydrogenase Enzymatic Catalysts: A Computational Study," in *Theory and Experiment in Electrocatalysis*, vol. 50, *Modern Aspects of Electrochemistry*, P. B. Balbuena and V. R. Subramanian, Eds.: Springer New York, 2010, pp. 243-274.

- [136] F. Himo and L. A. Eriksson, "Catalytic Mechanism of Pyruvate Formate-Lyase (PFL). A Theoretical Study," *Journal of the American Chemical Society*, vol. 120, pp. 11449, 1998.
- [137] M.H.M. Olsson, C.R.Sondergaard, M.Rostkowski, and J.H.Jensen, "PROPKA3:Consistent treatment of internal and surface residues in empirical pKa predictions," *Journal of Chemical Theory and Computation*, vol. 7, pp. 525-537, 2011.
- [138] M. W. van der Kamp and A. J. Mulholland, "Combined Quantum Mechanics/Molecular Mechanics (QM/MM) Methods in Computational Enzymology," *Biochemistry*, vol. 52, pp. 2708-2728, 2013.
- [139] Y.-J. Zheng, Z.-x. Xia, Z.-w. Chen, F. S. Mathews, and T. C. Bruice, "Catalytic mechanism of quinoprotein methanol dehydrogenase: A theoretical and x-ray crystallographic investigation," *Proceedings of the National Academy of Sciences of the United States of America*, vol. 98, pp. 432-434, 2001.
- [140] A.Sato, K.Takagi, K.Kano, N. Kato, J.A. Duine, and T. Ikeda, "Ca²⁺ stabilizes the semiquinone radical of pyrroloquinoline quinone," *The Biochemical Journal*, vol. 357, pp. 893-898, 2001.
- [141] S. W. Kim, C. S. Kim, J. S. Lee, M. J. Koh, S. S. Yang, J. A. Duine, and Y. M. Kim, "Kinetic and Spectral Investigations on Ca²⁺ and Sr²⁺-containing Methanol Dehydrogenase," *The Journal of Microbiology*, vol. 35, pp. 200-205, 1997.
- [142] C. Sendner, S. Sakong, and A. Grob, "Kinetic Monte Carlo simulations of the partial oxidation of methanol on oxygen-covered Cu (110)," *Surface Science*, vol. 600, pp. 3258-3265, 2006.
- [143] A.Cornish-Bowden, *Fundamentals of enzyme kinetics*. London: Portland Press, Ltd, 2004.
- [144] A. G. Marangoni, *Enzyme kinetics: a modern approach*. Hoboken, N.J. : Wiley-Interscience., 2003.
- [145] M. Agrawal, S. B. Santra, R. Anand, and R. Swaminathan, "Effect of macromolecular crowding on the rate of diffusion-limited enzymatic reaction," *Pramana - Journal of Physics*, vol. 7, pp. 359, 2008.
- [146] H. Berry, "Monte Carlo simulations of enzyme reactions in two dimensions: Fractal kinetics and spatial segregation," *Biophysical Journal*, vol. 83, pp. 1891, 2002.

- [147] A. M. Bersani and G. D. Acqua, "Is there anything left to say on enzyme kinetic constants and quasi-steady state approximation?," *Journal of Mathematical Chemistry*, vol. 50, pp. 335-344, 2012.
- [148] C. Baleizao and M. N. Berberan-Santos, "Enzyme kinetics with a twist," *Journal of mathematical Chemistry*, vol. 49, pp. 1949-1960, 2011.
- [149] M. J. Ramos and P. A. Fernandes, "Computational Enzymatic Catalysis," *Accounts of Chemical Research*, vol. 41, pp. 689-698, 2008.
- [150] P. E. M. Siegbahn and M. R. A. Blomberg, "Transition-Metal Systems in Biochemistry Studied by High-Accuracy Quantum Chemical Methods," *Chemical Reviews*, vol. 100, pp. 421-438, 2000.
- [151] P. E. M. Siegbahn and T. Borowski, "Modeling Enzymatic Reactions Involving Transition Metals," *Accounts of Chemical Research*, vol. 39, pp. 729-738, 2006.
- [152] H. M. Senn and W. Thiel, "QM/MM Methods for Biomolecular Systems," *Angewandte Chemie International Edition*, vol. 48, pp. 1198-1229, 2009.
- [153] R.-Z. Liao and W. Thiel, "Comparison of QM-Only and QM/MM Models for the Mechanism of Tungsten-Dependent Acetylene Hydratase," *Journal of Chemical Theory and Computation*, vol. 8, pp. 3793-3803, 2012.
- [154] C. V. Sumowski and C. Ochsenfeld, "A Convergence Study of QM/MM Isomerization Energies with the Selected Size of the QM Region for Peptidic Systems," *Journal of Physical Chemistry A*, vol. 113, pp. 11734-11741, 2009.
- [155] L. Hu, P. Soderhjelm, and U. Ryde, "On the Convergence of QM/MM Energies," *Journal of Chemical Theory and Computation*, vol. 7, pp. 761-777, 2011.
- [156] R.-Z. Liao, J.-G. Yu, and F. Himo, "Quantum Chemical Modeling of Enzymatic Reactions: The Case of Decarboxylation," *Journal of Chemical Theory and Computation*, vol. 7, pp. 1494-1501, 2011.